Signal-linear representations of colour for computer vision

A thesis
submitted in partial fulfilment
of the requirements for the Degree
of
Doctor of Philosophy
in the
University of Canterbury
by
Robert Grant

University of Canterbury
2010

Publications

1. Grant, R.N. and Green, R.D. (2006) "Chromatic variance prediction". International Conference Image and Vision Computing New Zealand, November 2006.

2. Grant, R.N. and Green, R.D. and Clark, A.J. (2007) "Hue variance prediction - an empirical estimate of the variance within the hue of an image". VISAPP 2007: Proceedings of the Second International Conference on Computer Vision Theory and Applications, Barcelona, Spain, March 8-11, 2007.

3. Grant, R.N. and Green, R.D. and Clark, A.J. (2008) "HLS Distorted colour model for enhanced colour image segmentation". International Conference Image and Vision Computing New Zealand, November 2008.

The follow paper was co-authored by me, and has information relevant to this work:

1. Clark, A. and Green, R. and Grant, R. (2007) "Image and video noise - a comparison of noise in images and video with regards to detection and removal". VISAPP 2007: Proceedings of the Second International Conference on Computer Vision Theory and Applications, Barcelona, Spain, March 8-11, 2007.

Abstract

Most cameras detect colour by using sensors that separate red, green and blue wavelengths of light which is similar to the human eye. As such most colour information available for computer vision is represented in this trichromatic colour model, Red Green Blue or RGB. However this colour model is inadequate for most applications as objects requiring analysis are subject to the reflective properties of light, causing RGB colour to change across object surfaces. Many colour models have been borrowed from other disciplines which transform the RGB colour space into dimensions which are decorrelated to the reflective properties of light.

Unfortunately signal noise is present in all acquired video, corrupting the image information. Fortunately most noise is statistically predictable, causing offsets from the true values following a Poisson distribution. When the standard deviation of a noise distribution is known, then noise can be stochastically predicted and accounted for.

However transformations inside cameras and transformations between colour models often deform the image information in ways that make the noise distributions non-uniform over the colour model. When computer vision applications need to account for non-uniform noise, wider tolerances are required overall. This results in a loss of useful information and a reduction in discriminative power.

This thesis has a focus on the linearity of signal noise distributions in colour representations which are decorrelated to the reflective properties of light. Existing colour models are described and each of their components examined with their strengths and weaknesses discussed.

The results show that the proposed Signal Linear RGB (SLRGB) colour model achieves a transformation of the RGB colour space with uniform noise distributions along all axes under changes to camera properties. This colour space maintains a signal noise with a standard deviation of one unit across the space under changes of the camera parameters: white balance, exposure and gain. Experiments demonstrated that this proposed SLRGB model consistently provided improvements to linearity over RGB when used as a basis for other colour models.

The proposed Minimum Weighted Colour Comparison (MWCC) method allows reflectively decorrelated colour models to make colour comparisons which counter the deforming effects of their coordinate systems. This was shown to provide substantial improvements to linearity tests in every case, making many colour models have a comparative noise linearity to undeformed colour models.

The proposed Planar Hue Luminance Saturation (PHLS) and Spherical Hue Luminance Saturation (SHLS) colour models are decorrelated to reflective properties of light and allow for signal linear colour comparisons. When used for pixel classification of coloured objects the PHLS and SHLS colour models used only 0.26% and 0.25% of the colour volume to classify all of the objects, with the next best using 0.88% without MWCC and 0.45% with.

The proposed Gamut Limit Invariant (GLI) colour model extends the decorrelation of reflective properties of light further by correcting for colours which are too bright and are clipped by the limits of the RGB space. When clipping occurs the properties become no longer decorrelated and shift. GLI models these changes to estimate the original values for clipped colours. The results show that this method improves decorrelation when performing pixel classification of coloured objects with varying proportions of clipped colours.

Overall, the results show that the proposed framework of colour models and methods are a significant improvement over all prior colour models in enabling the most accurate information possible for processing colour images.

Table of Contents

List of Figures

List of Tables

Chapter 1

Introduction

1.1 Thesis Overview

Computer vision is a field which is primarily concerned with the processing and extraction of information from images. At the lowest level images are collections of pixels containing colour information about a position in a scene. How these colours are represented is an important aspect of computer vision as it greatly affects what can be achieved. Historically many computer vision processes represented colour as a single dimensional scalar otherwise known as greyscale. This representation is simple to process but limits the depth of information that can be represented by a multidimensional colour space. With increasing frequency research has been making use of colour to achieve outcomes previously difficult or impossible in greyscale. Figure 1.1 shows some examples of past research using colour instead of greyscale for more robust object identification and segmentation. Figure 1.1(a) shows how colour is used in the ROBOCUP robotic soccer competition to identify various objects that are part of the game (Bruce, Balch and Veloso 2000). Without the full use of colour, identifying objects in the game would be much more difficult with many being impossible to tell apart. Figure 1.1(b) shows a colour based segmentation algorithm performing at different levels of sensitivity (Comaniciu and Meer 1997). Figure 1.1(c) shows a task that would be impossible without colour, skin region segmentation. This area of image segmentation is under heavy research as it potentially has many uses, particularly in human gesture based interaction (Lastra, Pretto, Tonello and Menegatti 2007) (Sigal, Sclaroff and Athitsos 2003) (Terrillon, Fukamachi, Akamatsu and Shirazi 2000) (Terrillon and Akamatsu 2000).

Red Green Blue (RGB) is a three dimensional colour model commonly

(a) (b)

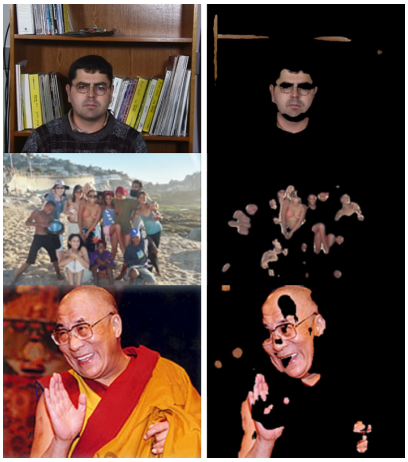

(c)

Figure 1.1: Examples of segmentation making use of colour (Bruce et al. 2000)(Comaniciu and Meer 1997)(Lastra et al. 2007).

used by image sensors, or cameras, to detect colour in a similar way to human vision. While this space increases the discriminative power possible with computer vision algorithms, common illumination effects make this data non-trivial to interpret. For this reason other colour representations are used, transforming the 3D geometry of RGB to achieve a more optimal alignment or emphasis on information that is important for the application. There are two key components that most commonly used colour models extract from the RGB colour model, the achromatic axis and the chromatic plane. The

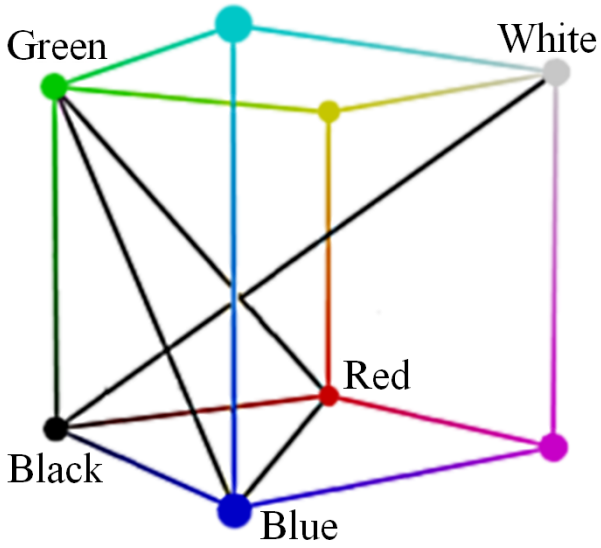

Figure 1.2: The RGB colour model with the achromatic axis shown running from black to white and the chromatic plane shown by the triangle connecting red, green and blue corners.

achromatic axis runs from black to white shown in Figure 1.2 and represents the brightness of a colour. When a colour pixel is converted to greyscale it has been transformed to a point along this line. How colours resolve to this axis depends on the colour model used. The chromatic plane is a two dimensional surface that usually runs perpendicular to the achromatic axis as shown in Figure 1.2. Reducing colours to the chromatic plane allows for simpler colour identification without brightness information. Different colour models represent the chromatic plane in different ways, varying in factors like shape, bisection angle or coordinate system. These differences can have a large effect on the success or failure of the applications using them, and selecting a colour model is a critical step in developing any computer vision application.

An often overlooked aspect of images and colour is the effect of signal noise. Signal noise is an ever present hindrance to those working with computer vision applications and reduces the reliability of systems. However it is inconsistent noise that can be even more detrimental to a system as achieving a good result is often a balance between two options. The first is to widen

the tolerances of the system so that it will still work with the noisiest data which usually results in a loss of discriminative power. For image segmentation this might mean that two distinct regions merge into one so that a noisy region does not get segmented into a large number of smaller regions around the noisy data. The second is to narrow the tolerances of the system so that enough discrimination is available to make the necessary distinctions the system needs to make to operate properly. An application might enforce restrictions on its use to avoid problems caused by narrow tolerances, such as providing a limited set of objects that work with the system. This work has a strong emphasis on achieving and maintaining linear levels of signal noise, to minimise any loss of information beyond those inherently present because of noise.

In this research the key requirements for colour models are identified and discussed, including how current models and solutions meet or fail to meet these requirements. A collection of new colour models and techniques are proposed and presented including the Signal Linear Red Green Blue (SLRGB) colour model, the Planar Hue Luminance Saturation (PHLS) colour model, the Spherical Hue Luminance Saturation (SHLS) colour model, the Minimum Weighted Colour Comparison (MWCC) and the Gamut Limit Invariance (GLI) colour model.

SLRGB is a transformation which takes RGB images from a camera and adjusts each of the dimensions to create a model with uniform signal noise. This allows statistical certainty of difference to be known when comparing any two colours.

The PHLS and SHLS colour models are two alternative polar transformations of the SLRGB space. Their polar coordinate spaces allow for shadow, shading and specular invariance to changes in light levels, while their methods of transformation, white balancing and colour comparisons using MWCC allow the spaces to be linear to signal noise along their axes.

MWCC is a method of calculating differences between colours in various chromatic plane based colour models. It can be applied to colour models to counter the distorting effects of polar coordinate systems and converging axes while making the best use of certainties.

The GLI colour model is an extension applied to PHLS and SHLS which

adds gamut limitation invariance. This allows colours which have been clipped by the limits of the camera's gamut to be estimated allowing for better colour comparisons.

The improvement these models and techniques provide are evaluated in relation to commonly used and leading models used in computer vision research.

1.2 Chapter Summary

Chapter 2: Background explores the extended background knowledge of light and colour, starting with a look at colour in physics and human biology, followed with a survey of colour representations. Signal linearity and gamut limitation research is also discussed, presenting the current extent of research in these areas.

Chapter 3: Proposed Colour Models isolates and investigates the important aspects of an optimal colour model for computer vision applications, critically evaluating measures and techniques from current work and proposing new techniques where important limitations and deficiencies are identified. The best combinations of these current and proposed techniques are proposed to solve the limitations present in other models.

Chapter 4: Experimental Methodology describes a set of experiments designed to evaluate current and proposed techniques paying particular attention to linearity using synthetic and real video.

Chapter 5: Results presents the results of the experiments described in the previous chapter. A critical analysis of these results is discussed in detail and evaluated.

Chapter 6: Conclusion summarises the results found in this research and discusses the strengths, limitations and future work planned for the proposed models and techniques.

1.3 Research Contributions

The main contributions of this thesis are:

- The Signal Linear Red Green Blue (SLRGB) colour model, exhibiting uniform noise across the space even under changes of camera settings.

- The Planar Hue Luminance Saturation (PHLS) colour model, a relatively low computational cost polar colour model invariant to shadow, shading and specular highlights, with near linear axes. The combination of some of the best elements of the HLS, HSI and nRGB colour models, this model is evaluated and is a strong improvement on other colour models. Requiring the second lowest volume of colour space for complete object classification, it is shown to have better discriminative power than any previous model.

- The Spherical Hue Luminance Saturation (SHLS) colour model, a polar colour model invariant to shadow, shading and specular highlights, with strongly linear axes. Using a spherical coordinate system, this proposed model consistently outperforms the other invariant colour models on linearity and performing strongly against less invariant models. Requiring the lowest volume of colour space for complete object classification, it is shown to have better discriminative power than any other model, using almost half as much colour space as the next best non-proposed model.

- The Minimum Weighted Colour Comparison (MWCC) technique, a method of comparing colours represented in models with converging axes. This has been shown to greatly improve linearity for comparisons in hue and purity based saturation measures, with significant reductions in the amount of colour space required to classify the test objects in all cases.

- The Gamut Limit Invariant (GLI) colour model, a novel colour model used to estimate the possible true values of a colour that has been

clipped by a limited gamut. This model has been shown to provide improvement in pixel classification when significant portions of the image exceed gamut limitations.

- A set of novel experimental methodologies that can be used to measure important aspects of colour models such as linearity, allowing comparison between colour models with different scales and limits.

Chapter 2

Background

The commonly used colour models discussed in this chapter exist in the context of the physics and cognitive perception of colour within the visible light spectrum.

2.1 Light and Colour Theory

Visible light detectable by humans and cameras consists of electromagnetic waves with wavelengths between approximately 380 and 750 nanometres. The various colours perceived can be produced by viewing specific wavelengths of visible light. Table 2.1 and Figure 2.1 show how each colour corresponds to a specific wavelength range. As the wavelength decreases from 750 nm the apparent colour shifts continuously from red through each of the colours to violet. The edges of the visible spectrum fade to black in Figure 2.1 because the light at these wavelengths becomes less visible to the human visual system and passes into the invisible infrared and ultraviolet ranges.

Table 2.1: Colours and an approximation of their corresponding wavelengths

Colour	Wavelength
Red	620-750 nm
Orange	590-620 nm
Yellow	570-590 nm
Green	495-570 nm
Blue	450-495 nm
Violet	380-450 nm

The most common sources of visible light are from incandescent sources such as the sun and fluorescent sources such as tube lighting. Incandescence

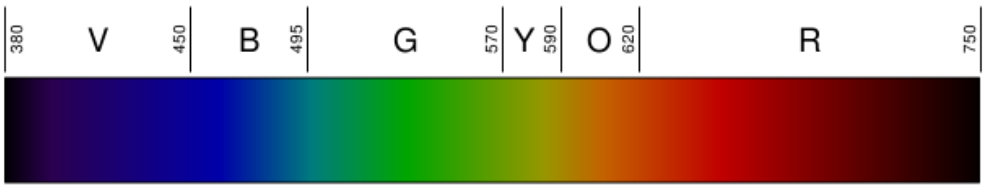

Figure 2.1: A visual representation of the visible spectrum of light.

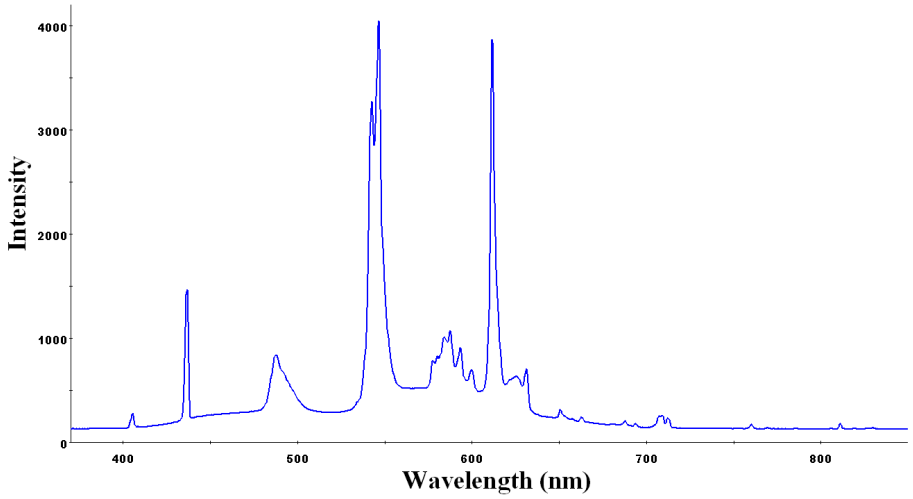

Figure 2.2: An example of a spectral distribution of a fluorescent light.

occurs when matter emits electromagnetic radiation as a result of reaching very high temperatures, while fluorescence occurs when electromagnetic waves cause phosphors to emit light in the visible range. Each of these produce a range of wavelengths which are unique to the atomic composition of the material illuminated and also, in the case of incandescence, its temperature. This is why different light sources often appear to be slightly different colours. For example the sun and tungsten light bulbs having a more reddish hue while fluorescent lights tend more towards the blue end of the visual spectrum. Figure 2.2 shows the spectral distribution of a fluorescent light source with high peaks of intensity at wavelengths corresponding to the mercury vapour and the europium and terbium phosphors. Although the human visual system perceives this as a smooth white light the spectrum is not uniformly distributed.

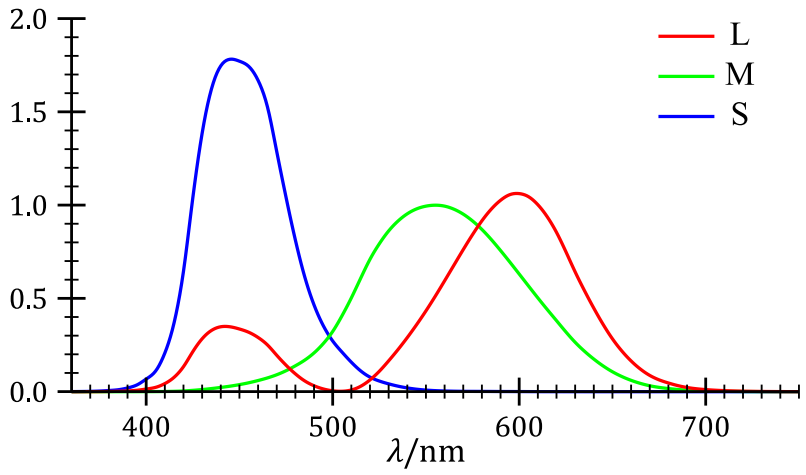

Figure 2.3: Normalised human cone response curves in the visible spectrum.

2.1.1 Human Colour Detection

Humans are unable to perceive the non-uniformity of light sources because the human eye only has three unique electromagnetic wavelength sensors called cones, or cone cells. Often denoted by long(L), medium(M) and short(S), these cones vary in sensitivity peaking at the wavelengths perceived as red, green and blue. A wavelength in between the peaks of the L and M cones for example, triggers both cones but to a lesser extent than a wavelength closer to each cone's peak. Figure 2.3 illustrates the human cone responses for the visible spectrum.

This trichromatic method of vision simplifies colour detection to a three component system, allowing multiple combinations of wavelengths at specific intensities to elicit the same response in the eye. For example, a combination of red and green wavelengths can match the perceived response from a singular yellow wavelength. Although this simplification results in a large loss of information which was present in a spectral distribution, it is sufficient for biologically important distinctions between objects in the environment while reducing cognitive load.

The International Commission on Illumination defined a colour space to match the cone responses of the human eye called the CIE 1931 XYZ colour space (CIE 1932). These tristimulus values X, Y and Z describe the amounts

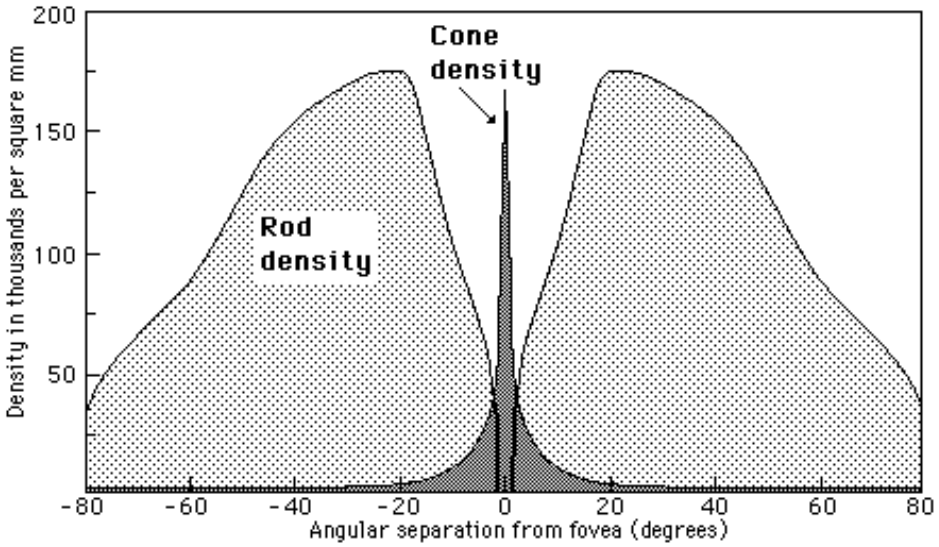

Figure 2.4: Distribution of rods and cones on the retina (`http://hyperphysics.phy-astr.gsu.edu/hbase/vision/rodcone.html`).

or intensities of these primary wavelengths that can be mixed to produce the same colour sensation in the eye.

The human eye has a fourth light sensor referred to as a rod cell. These rods are much more sensitive to light than the cones and have a wider spectral range which allows them to detect light at much lower intensities than the cone cells. The density of rods on the retina is much higher away from the centre of vision where cone density drops off, as shown in Figure 2.4. Rod cells are predominantly used for low light vision and peripheral vision as they provide an extended view of the scene but do not provide colour information. As this research is concerned with colour vision the monochromatic detection using rod cells is not relevant.

2.1.2 Human Colour Perception

While cones detect colour as three discrete wavelength intensities, colour is cognitively perceived much differently. This is most apparent when the colour created by mixing red and violet wavelengths is considered. The range of perceived colours between red and violet cannot be created by the use of a single wavelength of light and are known as non spectral colours. This demonstrates

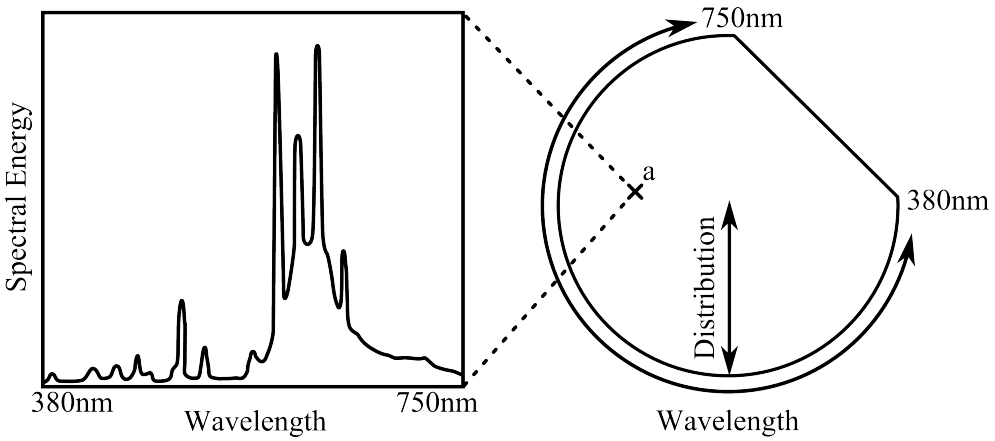

Figure 2.5: Shows how a given spectral distribution can result in a colour response in the circular perceptual system.

the fact that the human perception of colour "wraps around" to connect the opposite ends of the linear visible spectrum thus creating colours that do not exist as a pure singular wavelength of light. This enables an extra dimension of colour to be perceived, the measure of how wavelengths are distributed across the visible spectrum. For example an evenly distributed array of wavelengths equally triggers the L, M and S cones and consequently these are perceived as colourless, such as white or a shade of grey. Because of this the wavelength distribution is equivalent to the purity or saturation of the colour. Figure 2.5 shows how a spectral distribution might be perceived in this circular perceptual system. This forms a three dimensional perceptual model of colour comprising of average wavelength (hue), distribution of wavelengths (saturation) and spectral energy of visible wavelengths (luminance). These colour dimensions are decorrelated to the properties of light reflection, allowing for better perception of continuous surfaces and discrete objects under reflective variation.

Other perceptual models have been proposed such as Opponent Colour Processes (Buck, Knight and Bechtold 2000). This theory asserts that the L, M and S signals are transformed before they are sent to the brain. The transformed signals are:

- L + M signifying the overall brightness of the light, as S cones do not

have a very large contribution to the perception of brightness.

- L - M to determine the relative difference between red and green responses.

- (L + M) - S which provides a signal representing the difference between blue and yellow responses.

This colour theory proposes the four colour primaries of red, green, blue and yellow. Support for this conclusion is based on the assertion that each of these four colours cannot be perceived as mixtures of any other two colours. For example orange could be described as a reddish yellow, but blue could not be described as a greenish purple.

2.1.3 Light and Matter Interaction

Previous sections have described how different distributions of visible light are detected and perceived in the brain. In this section the interactions of light and matter are discussed, specifically dealing with reflection. Reflection is the effect occurring when light bounces off a material's surface, with the material usually absorbing some of the light in the process. Because different materials reflect individual wavelengths differently, the wavelengths reflected can help identify and distinguish between materials. This is important in vision as generally the colour of the object illuminated is of more interest than the colour of the light.

Reflection from most common objects and surfaces can be estimated by the dichromatic reflection model (Shafer 1992). This model describes the two common reflection types; diffuse and specular reflections. The main difference is that diffuse reflections cause illumination light to be altered by surface properties while specular reflections do not. Unlike specular reflections, diffuse reflections contain information about materials. Dichromatic

reflection is modelled by the following equations, where λ is light wavelength:

$$I_k = \sigma_d D_k + \sigma_s S_k \tag{2.1}$$

$$D_k = \int E(\lambda) R(\lambda) C_k(\lambda) d\lambda \tag{2.2}$$

$$S_k = \int E(\lambda) C_k(\lambda) d\lambda \tag{2.3}$$

The factors σ_d and σ_s describe the amount of shading and specular reflection respectively which depends on geometric properties of the reflection. D_k and S_k represent the diffuse and specular reflections respectively for $k = R, G, B$. $E(\lambda)$ represents the spectral power distribution of the incident light while $C_k(\lambda)$ is the spectral sensitivity of each of the red, green or blue sensors, together representing the light that would be detected if the incident light were to be directly detected by the sensor.

Equation 2.3 shows how specular reflection is independent of a surface's colour properties. Conversely equation 2.2 shows how diffuse reflection includes the factor $R(\lambda)$ which represents the spectral reflectance properties of the surface. Most illumination invariants use this model of illumination either included in the colour representation, used explicitly (Matas, Marik and Kittler 1994)(Shashua 1997)(Zickler, Mallick, Kriegman and Belhumeur 2006) or using a diagonal matrix (Finlayson 1995)(Barnard, Finlayson and Funt 1996).

2.1.4 Metamers

Metamers are colours that are detected as equal but actually have different spectral distributions. Metamerism in human vision is a result of the loss of information due to having only three unique wavelength detectors in the eye. When two different spectral distributions cause an identical response in the L, M and S cones in the human eye they cannot be told apart. While this is a limitation on the perceptive ability of materials, it also allows the duplication of colours in nature without needing to use the same material. This is the basis of how image reproduction works. With computer and television displays, red, green and blue light is used in combination to trigger similar cone responses as real world objects mimicking normal vision.

Metamers are often illumination dependent. This is because different light sources often have very different spectral distributions themselves. When illuminated with one source two materials may be detected as the same colour, but illuminated with a different source they appear completely different. An example of this is when metamers are viewed under fluorescent lighting. The high peaks of specific wavelengths can produce very different responses if a material's reflectance pattern coincides with any of these wavelength peaks. As a result of this it can sometimes be impossible to exactly match two identical materials under different lighting conditions with a trichromatic system.

2.1.5 Artificial Detection

Most modern imaging devices such as cameras and scanners mimic the way the eye works to build their representations of the world. This is especially true of colour because these devices are used specifically to capture images of real world objects for the purpose of redisplaying them as close to their original appearance as possible. By utilising trichromatic techniques for capture, displaying these images is simple and each combination of three primary colours creates the appearance of a unique colour. Figure 2.6 shows a cross section of the CIE XYZ colour model based on human cone cell response overlaid by the sRGB colour space, a standardised space based on the red, green and blue primaries.

The most common method that cameras use to capture images in colour is through the use of the Bayer pattern filter array shown in Figure 2.7. These colour filters block electronic photo receptive cells, such as CCD or CMOS based sensors, allowing only light of specific wavelengths to pass through and be detected. The resulting image is then demosaiced to produce a complete coherent colour image. This process closely mirrors the processes described in Section 2.1.1, because usually only an image display is required. That is, the colour model is left relatively intact since the computer is effectively "forwarding" the image for human visual detection. However, when image processing and computer vision becomes a priority, other colour representations often become necessary to aid analysis, analogous with the cognitive models of colour constructed in the brain.

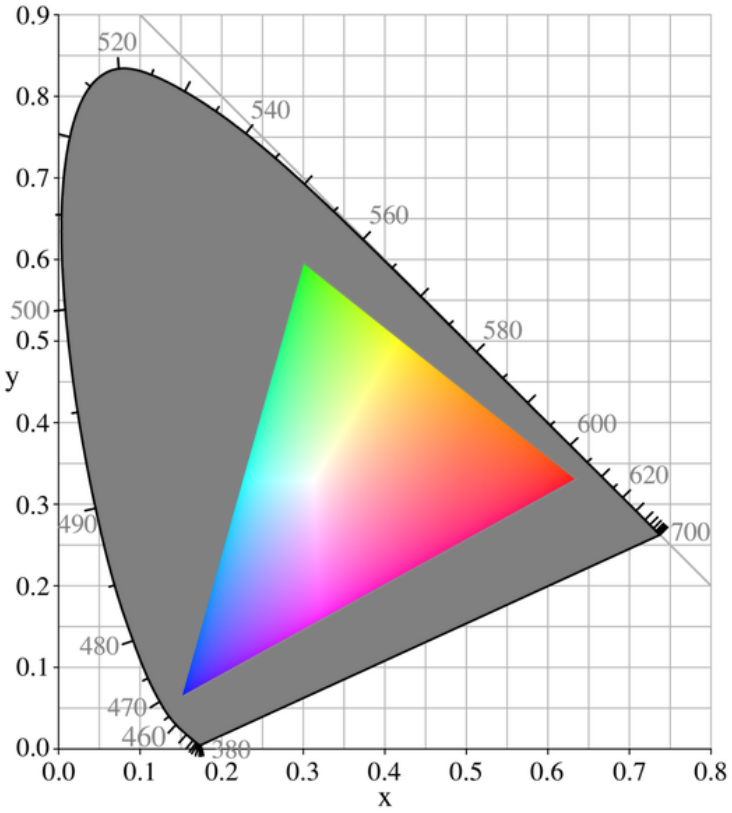

Figure 2.6: The sRGB colour space fits inside the range of colours a human is capable of seeing.

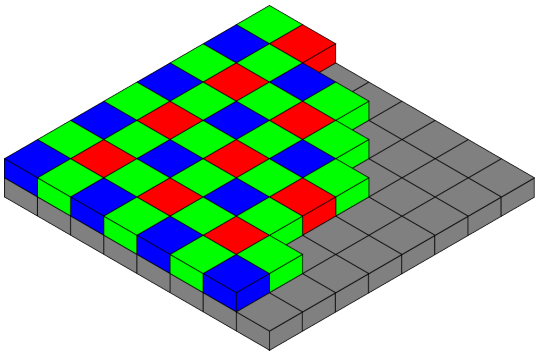

Figure 2.7: The Bayer pattern of filters is commonly used to capture images in colour.

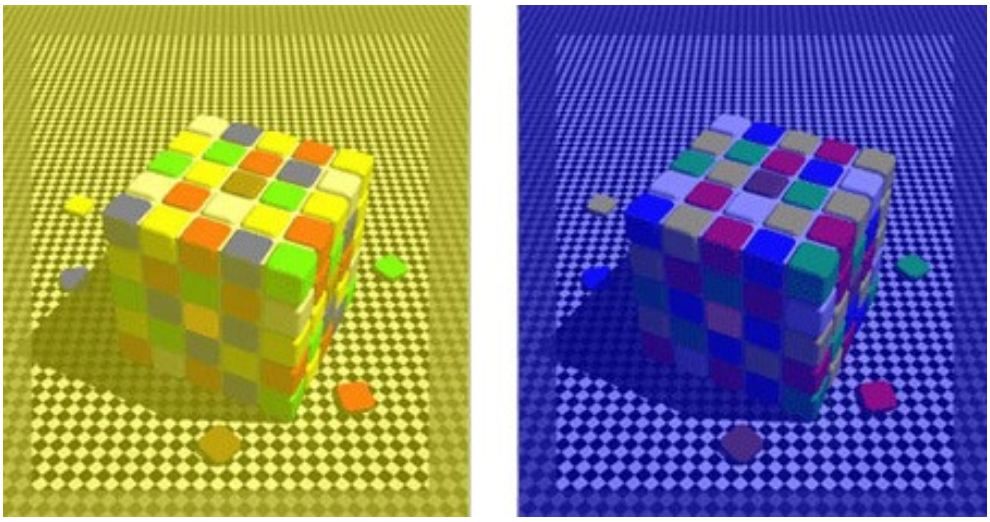

Figure 2.8: Illustration of local colour constancy. Top facing blue squares in the left image are exactly the same colour as the top facing yellow squares in the right image despite appearing different colours.

2.2 Colour Constancy

Common light sources such as sunlight, tungsten light and fluorescent light all have different spectral distributions and as such appear as different colours. Light which reflects off matter is a combination of properties of the light source and the reflectance properties of the matter. This results in significant differences in the detected colour of the same object under different light sources.

Colour constancy describes the ability of a vision system to adjust for changes in illumination colour so that colours detected from reflection remain consistent. Human vision does this using techniques which are not fully understood (Arend and Reeves 1986)(Brainard and Wandell 1986)(Blackwell and Buchsbaum 1988). Figure 2.8 shows how even in relatively small local regions under coloured illumination, colours can still be detected and identified. The top facing blue tiles from the yellow lit image are actually identical in colour to the top facing yellow tiles in the blue lit image, but are perceived as different colours.

In photography the correction of the effects of coloured illumination is called white balancing. This transformation produces an image which ap-

pears to be taken under a neutral light from one taken in the presence of a coloured illuminant. There are two main reasons why white balancing is particularly important in computer vision. First, it provides a way to more accurately correlate objects between scenes which have different types of light sources. Second, the identification of the light colour allows for detection of and invariance to specular reflection as described in Section 2.1.3 by the dichromatic reflection model. This is because specular reflection creates an additive colour shift along a vector parallel to the light source colour vector. The following sections discuss some common methods used for white balancing in digital imaging.

2.2.1 Colour Temperature

Colour temperature is a method of modelling the colour of an illuminant by estimating it as a black body radiator. An ideal black body absorbs all wavelengths of the electromagnetic spectrum therefore appearing completely black. However as a black body increases in temperature, electromagnetic radiation is emitted, eventually entering the visible spectrum in the red wavelengths. An example of a low temperature emitter is the fire from a match, the red/orange glow can be modelled as black body radiation at a temperature of approximately 1700 Kelvin. As the temperature of the black body increases the dominant colour of the light shifts towards a more even distribution, then passing onto a primarily blue colour cast. Figure 2.9 shows how common illuminants relate to the black body estimation of illumination colour.

By restricting estimated illumination colour to positions along the curve shown in Figure 2.10, most illumination types can be accurately modelled in a computationally simplistic way. Many digital cameras have the capability to set colour temperatures or use pre-set modes such as “daylight” or “indoor” options which utilise this principle. Most computer displays also use this paradigm to allow for easy selection of a colour balance that will better match the surrounding environment. Colour temperature is often used in computer vision because it restricts the set of possible illumination colours leaving less room for error and reducing complexity (Marchant and Onyango 2000)(Qian,

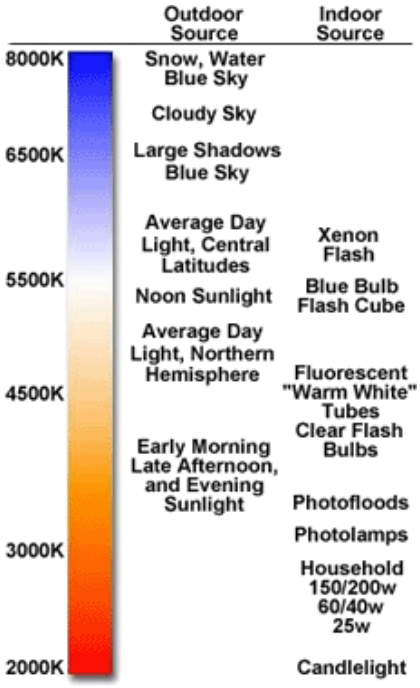

Figure 2.9: Colour temperatures in the Kelvin scale (`http://www.better-photographs.com/colour-temperature.html`).

Toker and Bencuya 1997), however this is only accurate if every light source fits the black body model.

2.2.2 Unconstrained White Balance

When the colour of an illuminant cannot be predicted by a black body model, less constrained methods must be used. The two most popular methods of calculating an arbitrary white vector are the Grey World and the Retinex assumptions.

The Grey World method assumes that there will be an even distribution of colours in a scene and that the colour of the light source can be found by calculating the average of all of the image's pixels (Lam, Au and Wong 2004a)(Lam, Au and Wong 2004b)(Lin 2006). This method is generally stable but performs badly when used on images with large regions of a similar colour which are common. The Retinex method assumes that there will be an object within the image that reflects all of the red, green and blue light

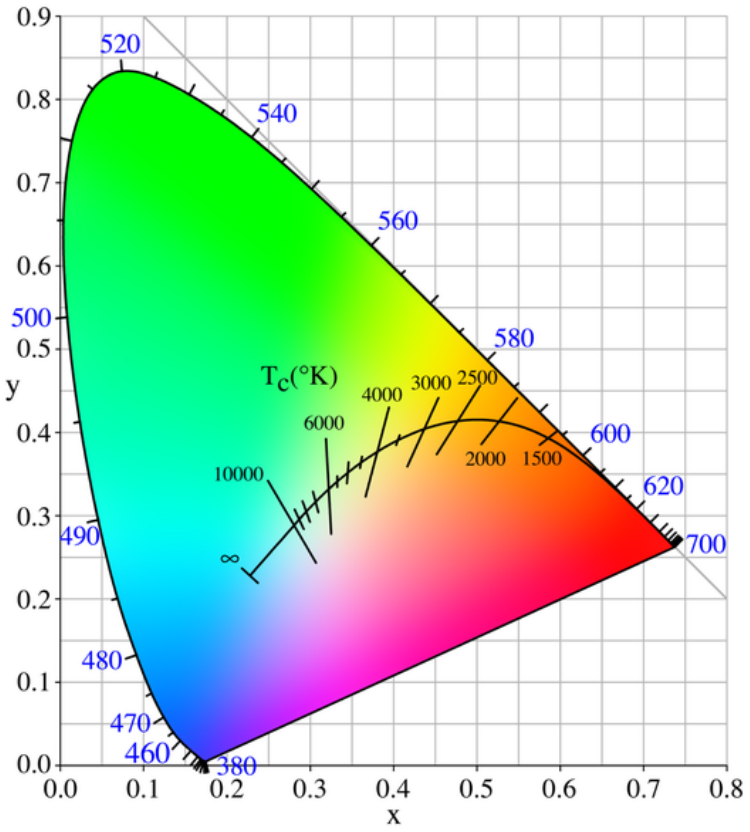

Figure 2.10: The path of black body radiation in chrominance space.

from the light source. Since objects do not reflect more light than they received then the maximum of each of the colour channels will determine the colour of the light source (Brainard and Wandell 1986)(Finlayson, Hordley and Drew 2002b)(Barnard and Funt 1999). Retinex has weaknesses in images where overexposure is present as maximum values are limited by the detection capabilities of the camera.

Other methods combine these methods mathematically (Lam 2005)(Rizzi, Gatta and Marini 2002) or blur the image to simulate Grey World while performing Retinex as normal (Gijsenij and Gevers 2007a). Some methods optimise the results by constraining the possible values (Barnard et al. 1996) or limiting which parts of the image can be used for calculation (Gijsenij and Gevers 2007b)(van de Weijer, Gevers and Geusebroek 2005).

There are many more methods used to estimate the colour of the illumination source, however this is not a primary concern of this research. Agarwal, Abidi, Koschan and Abidi (2006) and Hordley (2006) provide thorough reviews of existing methods used to estimate image illumination colour.

2.3 Colour Representation

Different representations of colour, also known as colour models or colour spaces, have been proposed and defined over time to ease the use and manipulation of colour in various fields. The following sections cover currently used colour models and where applicable, computer vision applications which utilise them.

2.3.1 Trichromatic models

Trichromatic colour models mix different proportions of three primary colours, either additively or subtractively, to create a wide gamut of colours. These create metamers of the colours humans detect in their environment. Because the human vision system is also trichromatic, three primaries are all that is needed to represent any colour within the range of their gamut.

Red Green Blue (RGB) is an additive colour model designed to allow the reproduction of a myriad of different colours by using varying levels of red, green and blue light. The additive nature of the space means that colours

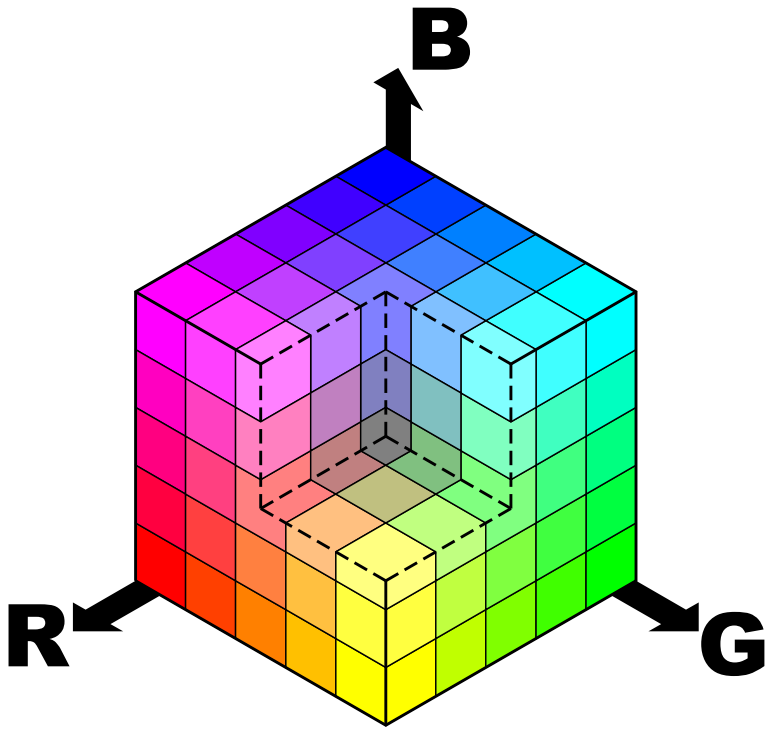

Figure 2.11: The RGB colour model.

are blended constructively, each primary colour adding together to create a more intense light. This forms a positive three dimensional space with the three axes increasing in intensity, as shown in Figure 2.11. The colour space has no inherent upper limits for the axes. However, when represented digitally it is limited by the range of sensor and display devices and the range of the numbering primitives used to store it. This colour model is used in various devices including televisions, computer monitors, digital cameras and scanners. It is a particularly good technique for image display as the primaries are similar to the primary wavelengths detected by the human eye, making reproduction of a large proportion of our visual gamut possible with minimal complexity as discussed previously. The raw data received from cameras remains in the RGB space as there is often no need to convert it to anything else between receiving and displaying the images.

Despite its advantages in image capture and display, the RGB colour spaces is unsuitable for many computer vision applications. Although the colour model represents the levels of red, green and blue illumination in much

the same way as the eye does (Geusebroek, van den Boomgaard, Smeulders and Dev 2000), the lack of invariance to reflection effects can have negative effects in computer vision. The RGB values taken from differently shaded areas of an object of uniform material tend to change simultaneously in ways that can make it difficult to determine whether they belong to the same object. There are colour models which try to alleviate this problem by separating luminance (brightness) from chromatic information while some approaches use vectors within the space to represent these invariants (Evans and Liu 2006).

The CMYK(cyan, magenta, yellow, key black) colour space is a subtractive colour space used in the printing process. Semi-transparent inks filter the light that reflects off the printed surface, destructively mixing the colours. Although four inks are used, it is essentially a trichromatic colour model as key black is used for practical reasons such as print quality and cost reduction.

The sRGB colour space is a standardised definition of the RGB colour space with specific device independent primaries and gamma curve. It was created in 1996 by Hewlett-Packard and Microsoft so that consistency could be maintained for colours between different monitors and printers, especially with the diversity of display devices present on the Internet. It is often used as an intermediary colour model because when used, devices need not know about each other's colour properties to convert between them (Finlayson, Hordley and Drew 2002a).

The CIE XYZ colour model mentioned in Section 2.1.1 is an example of another trichromatic model. The colour model has three primaries X, Y and Z which were formulated to align closely to human light detection. The

following formulae convert sRGB colours into CIE XYZ tristimulus values:

$$r = \begin{cases} R/12.92 & R \leq 0.04045 \\ ((R + 0.055)/1.055)^{2.4} & R > 0.04045 \end{cases} \tag{2.4}$$

$$g = \begin{cases} G/12.92 & G \leq 0.04045 \\ ((G + 0.055)/1.055)^{2.4} & G > 0.04045 \end{cases} \tag{2.5}$$

$$b = \begin{cases} B/12.92 & B \leq 0.04045 \\ ((B + 0.055)/1.055)^{2.4} & B > 0.04045 \end{cases} \tag{2.6}$$

$$\begin{bmatrix} X \\ Y \\ Z \end{bmatrix} = \begin{bmatrix} 0.4124564 & 0.3575761 & 0.1804375 \\ 0.2126729 & 0.7151522 & 0.0721750 \\ 0.0193339 & 0.1191920 & 0.9503041 \end{bmatrix} \begin{bmatrix} r \\ g \\ b \end{bmatrix} \tag{2.7}$$

Because of the dissimilarity between trichromatic models and the perception of colour, various axes have been fitted to trichromatic spaces to mimic these perceptual notions. The colour models presented in Sections 2.3.2 and 2.3.3 all divide the RGB or CIE XYZ colour spaces into two distinct parts:

- **Achromatic axis** is the one dimensional measure of the brightness of the detected light. Different approaches to this measure can represent anything from total spectral power to perceived brightness.

- **The chromatic plane** is the two dimensional space containing information regarding spectral distributions. Variations along this plane cause changes in perceived hue and saturation. Some colour spaces represent this in Cartesian coordinates while others use a polar coordinate system.

There are two ways in which chromatic planes are calculated in common colour models. These are described as purity based and chroma based. The coordinate space of a purity based model's chromatic plane increases in scale as luminance increases, while a chroma based plane maintains consistent scale independent of luminance. This is illustrated in Figure 2.12 where the size of the intersecting triangles represent the chromatic planes coordinate space at each point along the achromatic axis. The left image shows a purity based chromatic plane, growing as the distance from the origin increases, while the

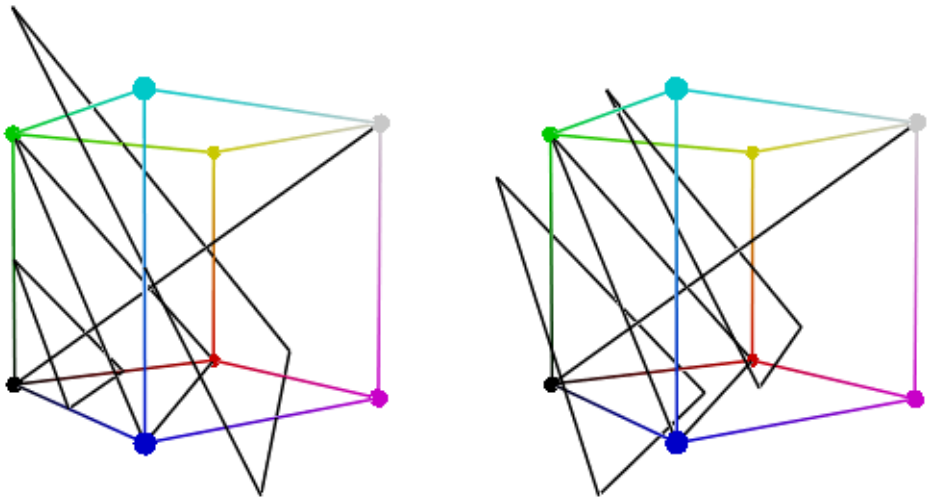

Figure 2.12: Comparison of a purity based(left) and a chroma based(right) chromatic plane.

right image shows a chroma based plane, remaining equally sized at every luminance.

This gives each method particular advantages over the other. Purity based models maintain consistent chromatic plane coordinates on object colours at varying shades, allowing for illumination invariance to shadows and shading. This can be found empirically or by using the equations 2.1-2.3 to model illumination changes to surfaces. Chroma based models on the other hand are subject to a more uniform noise distribution, not being dependent on luminance with regards to noise but shift chromatic plane coordinates with changes in light levels. Much of the reason for isolating the chromatic information from a trichromatic colour model is to allow for better illumination invariance. Despite this, often chroma based models are selected over purity based models because of their stability with regards to noise, unfortunately this means that a lot of information is being thrown away (Hanbury 2008). Chroma based models also have the property in that they reduce in range as their luminance measure decreases. This is because darker colours have a lower maximum chroma, for example, black can only ever have a chroma value of zero.

2.3.2 Cartesian chromatic models

The following section presents a summary of colour models that describe the chromatic plane in two dimensional Cartesian space.

YUV

YUV is a colour model commonly used for video signal transmission. It was designed as a replacement for black and white video transmissions, carrying the colour information separately for two distinct reasons. The first was so the new signal would still be decodable on older black and white televisions without modification and not require a separate transmission. The second reason was so that the colour signal could operate at a reduced bandwidth from the brightness information. This is because the human visual system is significantly more sensitive to differences in brightness than colour. By separating colour from illumination, YUV allows for a reduction of the colour information to lower the signal bandwidth requirements, which is not possible in RGB without also reducing the quality of the brightness information.

The YUV colour model uses a measure of luminance closely aligned with the human perception of brightness. Which means that blue has a significantly lower contribution to the luminance than red or green. The chromatic plane in this space consists of two components, U and V, which approximate to a blue-yellow axis and a red-cyan axis respectively. Figure 2.13 shows a cross section of this plane at $Y = 0.5$. YUV has a chroma based chromatic plane which means as Y decreases the possible ranges of U and V are reduced. YUV is often implemented at a hardware level for data transmission and is often used because it allows access to a colour model with a chromatic plane without the overhead of conversion (Bruce et al. 2000). The following formulae describe the conversion from RGB to YUV:

$$Y = W_R R + W_G G + W_B B \tag{2.8}$$

$$U = U_{Max} \frac{B - Y}{1 - W_B} \tag{2.9}$$

$$V = V_{Max} \frac{R - Y}{1 - W_R} \tag{2.10}$$

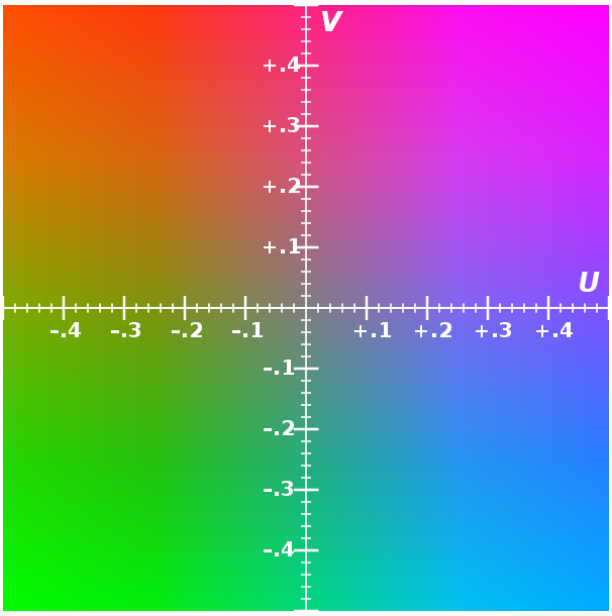

Figure 2.13: The UV plane at Y = 0.5.

These constants are used which define the relationship between the YUV and RGB colour models:

$$W_R = 0.299 \tag{2.11}$$

$$W_B = 0.114 \tag{2.12}$$

$$W_G = 1 - W_R - W_B = 0.587 \tag{2.13}$$

$$U_{Max} = 0.436 \tag{2.14}$$

$$V_{Max} = 0.615 \tag{2.15}$$

Variations of the space include YIQ, YPbPr and YCbCr, which are primarily application specific variations.

CIE Lab and Luv

As discussed in Section 2.1.1 the CIE XYZ colour model attempted to describe cone signal responses in human vision, however the space did not reflect human perception of colour very well. In 1976 two similar colour models were adopted by the International Commission on Illumination(CIE)

called CIE Lab and CIE Luv. These were designed to closely match the perceptual differences that humans experience between colours (Sharma and Trussell 1997)(Chen, Chien and Wang 2004)(Guo, Guo and Liu 2005)(Liu and Chou 2007). Because of this design, they are well suited for vision applications which require the detection of biologically significant differences in colour or when generating colours with respect to human viewing. Later, addenda were added to address inconsistencies in colour differencing especially with relation to human chromatic adaptation (Hill, Roger and Vorhagen 1997)(Luo, Cui and Rigg 2001)(Sharma, Wu and Dalal 2005).

CIE Lab and CIE Luv are extensively used in physical colour matching as when correctly calibrated they provide a device independent colour space. These colour spaces have chroma based chromatic planes because they are designed to match human perceptual differences. Since the human eye has lower sensitivity at low light levels the space reduces in size to keep perceptual differences consistent. Equations 2.16–2.32 show the calculation of Lab and Luv colour coordinates from the X, Y and Z tristimulus values calculated in equations 2.4–2.7. The terms X_r, Y_r and Z_r refer to reference white, which is the XYZ tristimulus values of the illuminant used.

$$x_r = \frac{X}{X_r} \tag{2.16}$$

$$y_r = \frac{Y}{Y_r} \tag{2.17}$$

$$z_r = \frac{Z}{Z_r} \tag{2.18}$$

$$f_x = \begin{cases} \sqrt[3]{x_r} & x_r > 0.008856 \\ \frac{903.3x_r+16}{116} & x_r \leq 0.008856 \end{cases} \tag{2.19}$$

$$f_y = \begin{cases} \sqrt[3]{y_r} & y_r > 0.008856 \\ \frac{903.3y_r+16}{116} & y_r \leq 0.008856 \end{cases} \tag{2.20}$$

$$f_z = \begin{cases} \sqrt[3]{z_r} & z_r > 0.008856 \\ \frac{903.3z_r+16}{116} & z_r \leq 0.008856 \end{cases} \tag{2.21}$$

$$L = 116 f_y - 16 \tag{2.22}$$
$$a = 500(f_x - f_y) \tag{2.23}$$
$$b = 200(f_y - f_z) \tag{2.24}$$

$$y_r = \frac{Y}{Y_r} \tag{2.25}$$
$$u' = \frac{4X}{X + 15Y + 3Z} \tag{2.26}$$
$$v' = \frac{9Y}{X + 15Y + 3Z} \tag{2.27}$$
$$u'_r = \frac{4X_r}{X_r + 15Y_r + 3Z_r} \tag{2.28}$$
$$v'_r = \frac{9Y_r}{X_r + 15Y_r + 3Z_r} \tag{2.29}$$

$$L = \begin{cases} 116\sqrt[3]{y_r} - 16 & y_r > 0.008856 \\ 903.3 y_r & y_r \leq 0.008856 \end{cases} \tag{2.30}$$
$$u = 13L(u' - u'_r) \tag{2.31}$$
$$v = 13L(v' - v'_r) \tag{2.32}$$

In both Lab and Luv the L component refers to the luminance of a given colour, while $\{a, b\}$ and $\{u, v\}$ are the respective coordinates on the chromatic planes of Lab and Luv.

xyY

The xyY model is a normalisation of the CIE XYZ colour model and the normalised x and y components describe any colour independent of light intensity. This provides some illumination invariance as the chromatic plane is purity based. The colour space is calculated from the CIE XYZ tristimulus values calculated in equations 2.4–2.7 as follows:

$$x = \frac{X}{X+Y+Z} \tag{2.33}$$

$$y = \frac{Y}{X+Y+Z} \tag{2.34}$$

$$Y = Y \tag{2.35}$$

Normalised RGB

Normalised RGB (sometimes referred to as *nRGB*, *rg* or not explicitly named) is widely used in computer vision for its simplicity and shadow/shading invariant properties (Berwick and Lee 1998)(Barnard 1999)(Barnard and Finlayson 2000). In a similar way to how xyY is a derivation of the CIE XYZ colour space, nRGB normalises the components of the RGB colour space, transforming the data to a purity based colour model. Although luminance is not explicitly measured, the sum of the RGB red, green and blue components can be used and also allows for conversion back to RGB if required. Additionally only two components are necessary to describe any unique coordinate on the chromatic plane, so often the normalised blue component is dropped. However when differencing colours in nRGB the third component is required if linearity is needed across the space. The colour space is calculated from RGB coordinates as follows:

$$r = \frac{R}{R+G+B} \tag{2.36}$$

$$g = \frac{G}{R+G+B} \tag{2.37}$$

$$b = \frac{B}{R+G+B} = 1 - r - g \tag{2.38}$$

Opponent

The opponent colour model was designed using the concept of the opponent colour processes that happen in the eye, as discussed in Section 2.1.2. The first two components o_1 and o_2 correspond to the red-green response and the blue-yellow response respectively. The last component o_3 corresponds to the

luminance. The opponent colour model is effectively a rotation of the RGB colour model so that the chromatic plane sits parallel with two of the axes. Through the use of an RGB white vector $\{\alpha, \beta, \gamma\}$ the space can be white balanced by rotation such that the o_3 axis is aligned to the white vector. Because it is simply a rotation in Cartesian space the chromatic plane is chroma based. The colour space is calculated from RGB as follows (van de Weijer, Gevers and Smeulders 2006):

$$o_1 = \frac{\beta R - \alpha G}{\sqrt{\alpha^2 + \beta^2}} \tag{2.39}$$

$$o_2 = \frac{\alpha\gamma R + \beta\gamma G - (\alpha^2 + \beta^2)B}{\sqrt{(\alpha^2 + \beta^2 + \gamma^2)(\alpha^2 + \beta^2)}} \tag{2.40}$$

$$o_3 = \frac{\alpha R + \beta G + \gamma B}{\sqrt{\alpha^2 + \beta^2 + \gamma^2}} \tag{2.41}$$

Spherical

The spherical colour space transforms the Cartesian coordinates of RGB to a spherical coordinate system with an origin at $RGB = \{0, 0, 0\}$. In this model radius r is equivalent to luminance measured using the Euclidean distance from the origin, rather than the distance along a common vector. This results in a spherical chromatic plane centred at the origin. θ and φ describe the chromatic plane as two angles, which could be loosely described as the angle between red-green and between blue-yellow. Because the chromatic plane is represented as angles from the origin it is a purity based plane/curve, being the same range no matter what the luminance. The colour space is calculated from RGB as follows (van de Weijer et al. 2006):

$$r = \sqrt{R^2 + G^2 + B^2} \tag{2.42}$$

$$\theta = \arctan\left(\frac{G}{R}\right) \tag{2.43}$$

$$\varphi = \arcsin\left(\frac{\sqrt{R^2 + G^2}}{\sqrt{R^2 + G^2 + B^2}}\right) \tag{2.44}$$

2.3.3 Polar chromatic models

As discussed in Section 2.1.2, human perception of colour can be seen as circular. A dimension approximating to the average wavelength can be calculated as a modular or circular dimension, connecting the higher wavelengths to the lower wavelengths through the non-spectral colours. The concept of saturation was also discussed which related to the distribution of individual wavelengths. These measures can be replicated on the chromatic plane by using a polar coordinate system with the origin at white.

As previously mentioned, polar chromatic models also fall into two categories; purity based and chroma based. Unlike previously, this categorisation only affects one of the dimensions, *saturation*, with the names *purity* and *chroma* used to distinguish between the distinct types of saturation. Saturation was previously described as representing the distribution of wavelengths in a colour, however this meaning does not always hold true and is often used to describe chroma based measures also. For this reason the term *saturation* is from this point on used to refer to any radial distance measure on the chromatic plane. The following sections cover existing polar colour models and the different approaches they take.

Munsell

The Munsell colour system was one of the first colour models to separate colour into the three perceptual dimensions of hue, brightness and chroma. It was created in the early 20th century by Professor Albert H. Munsell as a way of ordering colour based on human perception. The colour positions were determined by experimental data from human participants' responses to various colours (Glenn and Killian 1940)(Kelly, Gibson and Nickerson 1943). Because the model used was polar and based on human visual data, the perceived differences in hue, brightness and chroma, could be analysed and it was found that the space had an irregular shape. Figure 2.14 shows how this colour space is arranged, the shape and extent varying across the space.

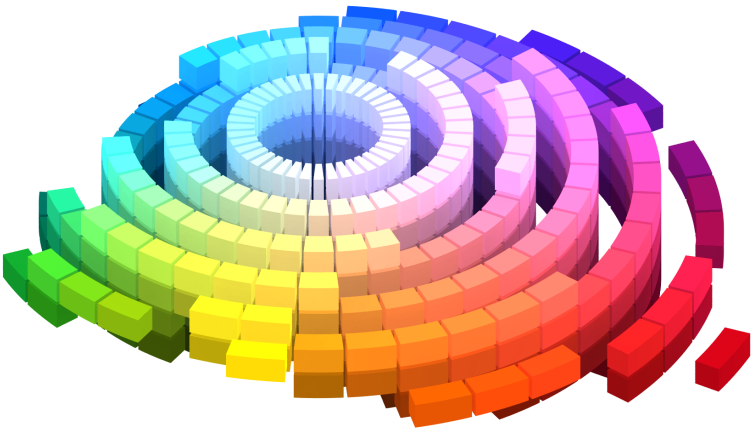

Figure 2.14: The Munsell colour system represented in 3D (`http://en.wikipedia.org/wiki/Munsell_color_system`).

LCH_{lab} and LCH_{luv}

The LCH_{lab} and LCH_{luv} colour spaces are polar derivatives of the CIE Lab and Luv colour spaces respectively. The C component represents chroma which is measured as the radial distance from the centre of the polar chromatic plane. In LCH_{luv} purity can be computed to better allow for illumination invariance to form the variant LSH_{luv}. A similar calculation can be made in LCH_{lab} although this does not strictly correlate with the purity response but gives an approximation of it.

$$L_{lab} = L \tag{2.45}$$

$$C_{lab} = \sqrt{a^2 + b^2} \tag{2.46}$$

$$H_{lab} = \arctan(b/a) \tag{2.47}$$

$$L_{luv} = L \tag{2.48}$$

$$C_{luv} = \sqrt{u^2 + v^2} \tag{2.49}$$

$$H_{luv} = \arctan(v/u) \tag{2.50}$$

$$S_{luv} = \frac{C}{L} = 13\sqrt{(u' - u'_r)^2 + (v' - v'_r)^2} \tag{2.51}$$

Lindbloom[1] describes the problems faced when using Lab for substituting colours which are out of the gamut of the destination colour model. Often when using a hue angle derived from a space such as Lab or Luv there is an apparent shift in perceived hue when reducing chroma. This is because Lab and Luv were not designed for the perception of hue, but were focused on achieving perceptual uniformity across the entire space.

The Munsell colour system was designed so that the hue measure matches the human perception of hue closely. Figure 2.15 shows how the Lab and Luv polar measures of hue compare to the Munsell system's measure. Some areas of the colour spaces curve across hue more than others. Lindbloom created the Uniform Perceptual Lab(UP Lab) colour space to address these problems. Figure 2.16 shows the difference between regular Lab space and the proposed UP Lab space, the angular hue measure being equal to that of the Munsell space.

HLS and HSV

The Hue Luminance Saturation (HLS) and the Hue Saturation Value (HSV) colour models are transformations of the RGB colour model designed to be more intuitive to a user. The colour models are primarily used for colour selection in computer programs as they simplify the manipulation of colours compared to RGB. Both of these colour models have been utilised often in computer vision applications as they lend themselves particularly well when dealing with colour and are simple to calculate and use (Demarty and Beucher 1998)(Sigal et al. 2003). The colour models are effective when working with

[1] `http://www.brucelindbloom.com/index.html?UPLab.html`, August 2010.

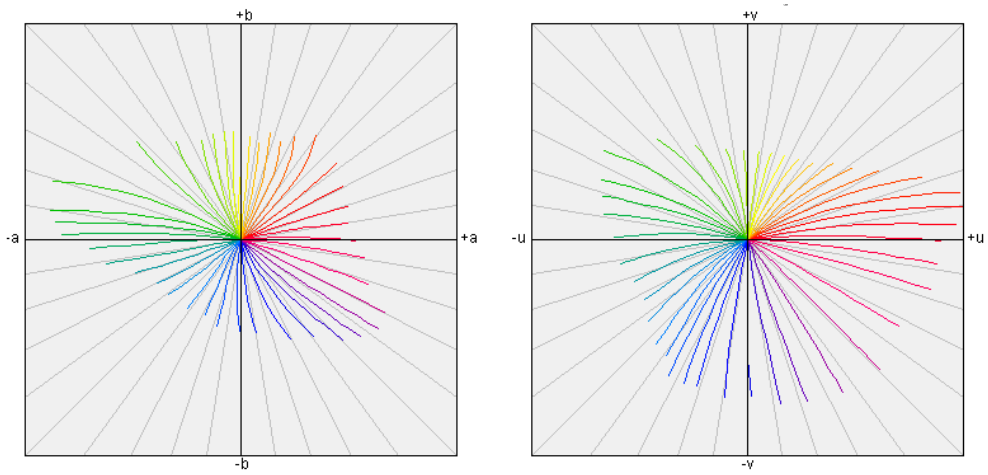

Figure 2.15: A comparison of the Munsell hue radials in CIE Lab(left) and in CIE Luv(right).

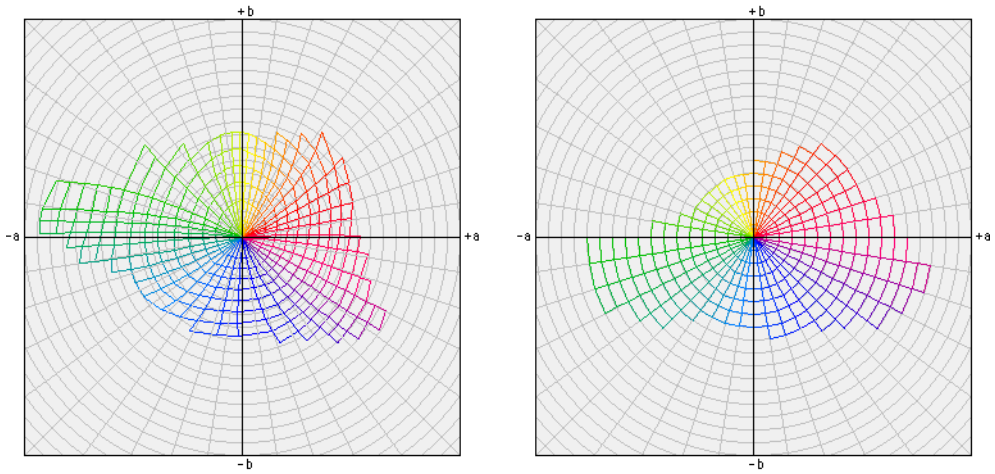

Figure 2.16: A comparison of the Munsell colour system in CIE Lab(left) and in Uniform Perceptual Lab(right).

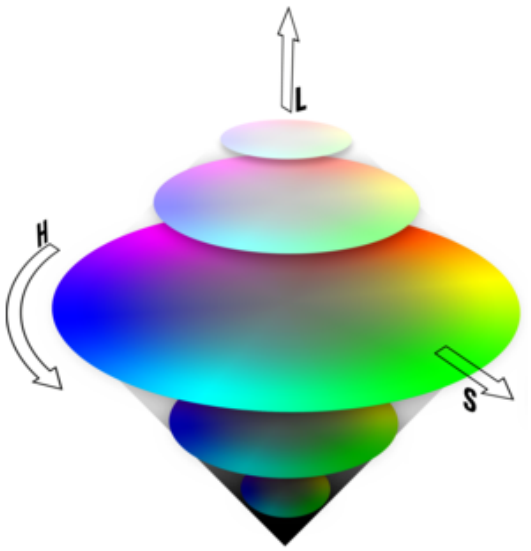

Figure 2.17: The HLS colour model (`http://en.wikipedia.org/wiki/HLS_color_space`).

highly saturated objects but can have unsatisfactory results when nearing the achromatic axis.

The HLS colour model can be visualised as a double-cone solid as shown in Figure 2.17. As luminance approaches the maximum or minimum values, the chromatic plane shrinks making it a variation of a purity based colour space. In the following equations *max* is the maximum of the red, green and blue components, while *min* represents the minimum of these values. To convert from an RGB colour into HLS the following equations can be used:

$$H = \begin{cases} 0^\circ & \max = \min \\ (60^\circ \frac{G-B}{\max - \min}) \mod 360^\circ & \max = R \\ 60^\circ \frac{B-R}{\max - \min} + 120^\circ & \max = G \\ 60^\circ \frac{R-G}{\max - \min} + 240^\circ & \max = B \end{cases} \tag{2.52}$$

$$L = \frac{1}{2}(\max + \min) \tag{2.53}$$

$$S = \begin{cases} 0 & \max = \min \\ \frac{\max - \min}{\max + \min} = \frac{\max - \min}{2L} & L \leq \frac{1}{2} \\ \frac{\max - \min}{2 - (\max + \min)} = \frac{\max - \min}{2 - 2L} & L > \frac{1}{2} \end{cases} \tag{2.54}$$

The HSV colour model differs from HLS with the luminance measure (Value) no longer ranging from black to white in all cases. In this model white is only achieved by both a high luminance measure and a reduced saturation. While this has some limitations it also makes the colour model simpler to calculate which makes it popular to use in computer vision applications (Femiani and Razdan 2009)(Erbay, Turgay and Akar 2011). Hue remains calculated in the same way while saturation and value are calculated as follows:

$$S = \begin{cases} 0 & \max = 0 \\ \frac{\max - \min}{\max} = 1 - \frac{\min}{\max} & \text{otherwise} \end{cases} \tag{2.55}$$

$$V = \max \tag{2.56}$$

Because HLS and HSV are models often used interchangeably it is often considered that they are very similar or would produce similar results. However because of fundamental differences in their calculation of saturation and luminance, they can have very different properties when compared. In this work both models are used for comparison during experimentation because of these differences to give a more thorough evaluation.

GLHS is a generalisation of the HLS family of colour models including HLS, HSV, HSB, etc. (Levkowitz and Herman 1993). Equations 2.57–2.62 can be used with a given set of weights w_{max}, w_{mid} and w_{min} to duplicate any of HLS family while adding potentially many more useful variations.

$$L = w_{max}max + w_{mid}mid + w_{min}min \tag{2.57}$$

$$k = \begin{cases} 0 & \text{if } r > g \geq b \\ 1 & \text{if } g > r \geq b \\ 2 & \text{if } g \geq b > r \\ 3 & \text{if } b \geq g > r \\ 4 & \text{if } b > r \geq g \\ 5 & \text{if } r \geq b > g \\ undefined & \text{if } r = g = b \end{cases} \tag{2.58}$$

$$f = \begin{cases} (mid - min)/(max - min) & \text{if } k \text{ even} \\ (max - mid)/(max - min) & \text{if } k \text{ odd} \end{cases} \tag{2.59}$$

$$H = (k + f)60 \tag{2.60}$$

$$L_q = (w_{mid}\frac{mid - min}{max - min} + w_{max})M \tag{2.61}$$

$$S = \begin{cases} \frac{L-min}{L} & \text{if } L \leq L_q \\ \frac{max-L}{M-L} & \text{if } L > L_q \end{cases} \tag{2.62}$$

For example by using the weight values of $w_{max} = \frac{1}{2}$, $w_{mid} = 0$ and $w_{min} = \frac{1}{2}$ with the equations calculates colours in the HLS colour space. *mid* is additionally defined as the middle value of the red, green and blue components.

Many believe that it is incorrect to represent saturation as a purity measure, a fraction ranging from 0 to 1 at all levels of luminance. Hanbury (2002) proposes the IHLS colour model, primarily differing in the calculation of saturation, as the proportion of the distance from the achromatic axis and the maximum distance from the axis that is possible at the given hue, effectively using a measure of chroma instead of purity. This means that the maximum possible saturation for a colour at a luminance of 0.25 is 0.5. This is claimed to be of benefit as it helps decouple luminance from saturation and also means that now distances between colours are more uniform as the space tapers as colours get harder to distinguish apart. The problem with this argument is that in calculating saturation in this way the true result is a more highly coupled space. The usual aim when using HLS to represent

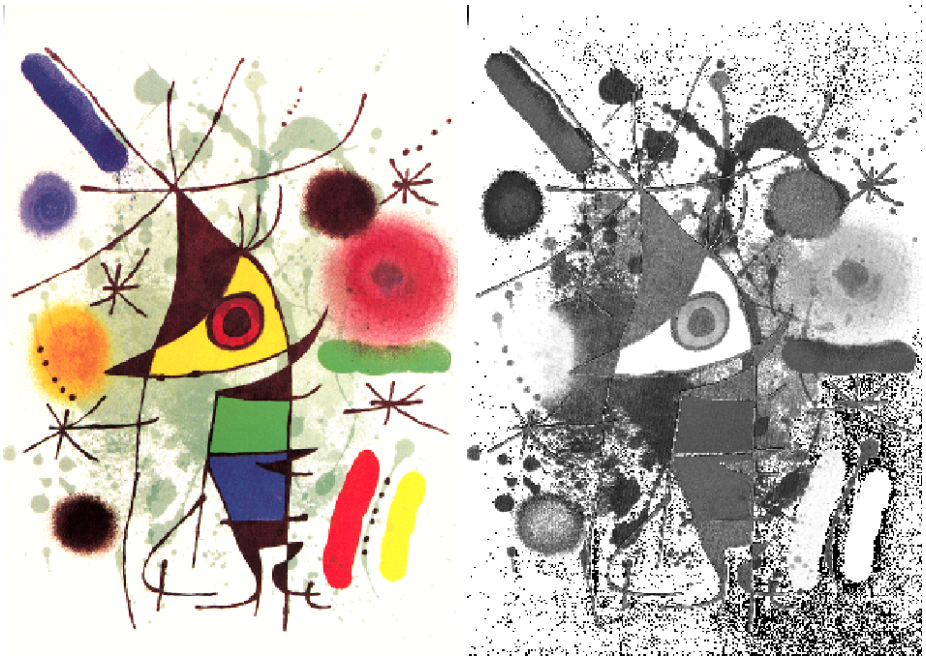

(a) (b)

Figure 2.18: (a) "Le Chanteur" by Joan Mirò, (b) the saturation channel of the HLS colour model(Hanbury 2002).

colours is to have independent axes which represent important features of light when trying to interpret a scene.

Luminance is the intensity or power of the light while saturation is representative of wavelength distribution, i.e. an even distribution of visible wavelengths has zero saturation, while a highly wavelength biased distribution will have a high saturation. When looking at a physical scene it is useful to note that an evenly coloured matte object should not change in saturation regardless of shadowing or reduction in light. By using a chroma based saturation measure uniformly coloured objects shift in saturation as luminance varies, confounding changes in colour purity with changes in light levels. What does reduce, is the sensitivity to changes in hue and saturation at these light levels and this needs to be taken into account when working with colours at these levels.

Hanbury and Serra (2001) discuss how to apply mathematical morphologies to colour images using the HLS colour space. They propose three ap-

proaches which involve different orderings of the dimensions for the erode and dilate operators. In all equations two HLS colours are compared, $i = \{H_i, L_i, S_i\}$ and $j = \{H_j, L_j, S_j\}$ and the $\div$ symbol is used to denote the smallest angular difference between two angles on a unit circle ($0° \leq \theta < 360°$) and is defined as:

$$a_1 \div a_2 = \begin{cases} |a_1 - a_2| & if \quad |a_1 - a_2| \leq 180° \\ 360° - |a_1 - a_2| & if \quad |a_1 - a_2| \geq 180° \end{cases} \tag{2.63}$$

Where the a_1 and a_2 are the two angles being compared. The three ordering approaches are as follows:

Luminance-centric This approach prioritises luminance ahead of saturation and hue with the ordering defined as:

$$c_i > c_j \; if \begin{cases} L_i > L_j \\ or \\ L_i = L_j \; and \; S_i < S_j \\ or \\ L_i = L_j \; and \; S_i = S_j \; and \; H_i \div H_0 < H_j \div H_0 \end{cases} \tag{2.64}$$

This approach is almost a regular greyscale order as the times when $L_i = L_j$ will be few and random as to not have a consistent effect. Hanbury and Serra state that the use of $H_i \div H_0 < H_j \div H_0$ to order hues is not an ideal one but is not important as it will have a negligible effect on the results.

Saturation-centric This approach prioritises saturation ahead of luminance and hue with the ordering defined as:

$$c_i > c_j \; if \begin{cases} S_i > S_j \\ or \\ S_i = S_j \; and \; |L_i - 0.5| < |L_j - 0.5| \\ or \\ S_i = S_j \; and \; |L_i - 0.5| = |L_j - 0.5| \; and \; H_i \div H_0 < H_j \div H_0 \end{cases} \tag{2.65}$$

Once again, in this approach hue is an afterthought and not often used. More interestingly this saturation-centric approach allows dilation of pure colours

onto weak colours or vice versa for erosion.

Hue-centric This approach prioritises hue over luminance and saturation and also reduces weighting to low saturation hues. This allows ordering to favour stronger colours when using a hue-centric approach. The following equation recalculates H_i as the number of degrees relative to the origin H_0.

$$H_i \rightarrow \begin{cases} H_i - H_0 & if \quad H_i - H_0 \geq 0 \\ 360^\circ + (H_i - H_0) & if \quad H_i - H_0 < 0 \end{cases} \tag{2.66}$$

This is followed by the calculation of $H_i^{'}$ which is the number of degrees from the origin weighted by saturation. This is to reduce the effect of unsaturated colours taking possible precedence over highly saturated but slightly further from the origin hue.

$$H_i^{'} = \begin{cases} sup[H_i, 90^\circ(1 - S_i)] & if \quad 0^\circ \leq H_i \leq 90^\circ \\ inf[H_i, 90^\circ(1 + S_i)] & if \quad 90^\circ < H_i \leq 180^\circ \\ sup[H_i, 90^\circ(3 - S_i)] & if \quad 180^\circ < H_i \leq 270^\circ \\ inf[H_i, 90^\circ(3 + S_i)] & if \quad 270^\circ < H_i < 360^\circ \end{cases} \tag{2.67}$$

It should be also noted that this approach only works when using the double-cone version of the HLS space which has a shrinking range. In this model the full saturation range (0.0 - 1.0) only exists at a luminance of 0.5. At luminance values of 0.25 and 0.75 the maximum saturation is halved to 0.5. This means that saturation and luminance are now highly correlated and a change in observed surface brightness results in a change in both luminance and saturation. Finally the ordering equation shows how this weighted hue value is used.

$$c_i > c_j \; if \begin{cases} H_i^{'} \div 0^\circ < H_j^{'} \div 0^\circ \\ or \\ H_i^{'} \div 0^\circ < H_j^{'} \div 0^\circ \; and \; |L_i - 0.5| < |L_j - 0.5| \\ or \\ H_i^{'} \div 0^\circ < H_j^{'} \div 0^\circ \; and \; |L_i - 0.5| = |L_j - 0.5| \; and \; S_i > S_j \end{cases} \tag{2.68}$$

While this approach works when morphology is needed on highly saturated

colours it is focused on this and does not always work as desired.

HSI

The HSI colour model while closely related to the HLS family has the distinctive difference of being a chroma based space. It can also be derived from the opponent colour space described in Section 2.3.2 which means that using the white vector the model can have the achromatic axis rotated if the white balance is not correct. The space is a cylindrical coordinate system applied to the opponent colour space from the equations 2.39–2.41 as follows (van de Weijer et al. 2006):

$$H = \arctan\left(\frac{o_1}{o_2}\right) \tag{2.69}$$

$$S = \sqrt{o_1^2 + o_2^2} \tag{2.70}$$

$$I = o_3 \tag{2.71}$$

Lambert and Carron (1999) presents a similar transform instead calculated from a variant of the YUV colour space.

2.3.4 Derivative models

Derivative models measure relationships between colours as opposed to the properties of the colour itself. Geusebroek et al. (2000) presented work on enabling colour to be treated in a similar manner as intensity. They say that currently this does not take place as colour is more often taken at pixel value. When working with a greyscale image, a single pixel's value is meaningless, it is the values surrounding the pixel that give it context and meaning. The same is true of colours but it is harder to detect. When looking for a specifically coloured object, the approach often taken is to find pixels that fit the believed colour of the object. But due to illumination effects absolute colour values are highly unreliable. Human vision uses neighbouring colours and various other techniques to maintain stable colouring of objects so that the colour of an object can be recognised even if viewed under an

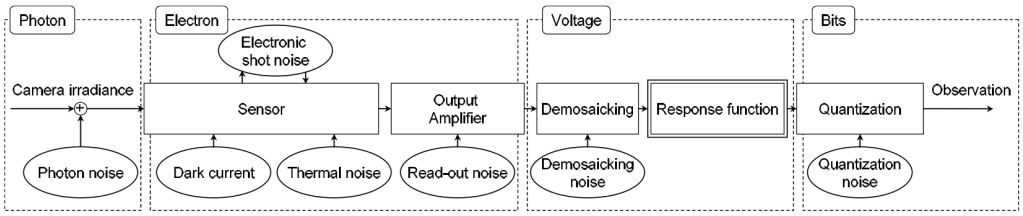

Figure 2.19: The imaging process including sources of noise in digital cameras (Matsushita and Lin 2007).

illuminant which skews scene colours. Their work attempts to use Gaussian Mixture Models to create images which can be used to find edges caused by specific phenomena. Using this method they can produce edge maps which only include object edges and no edges caused by shadowing or specular artefacts. The approach produces good results but is limited by having a derivative model of the scene. This limits the applicability of the model to only edge based problems. This is also the case for other derivative colour models such as quasi-invariants (van de Weijer et al. 2006) and $m_1 m_2 m_3$ (Gevers and Smeulders 1999), while useful sometimes they lack the generality of the other colour models.

2.4 Colour Signal Linearity

When processing computer vision algorithms using video from image sensors, signal noise causes scene colours to shift unpredictably by usually small amounts. While this noise is completely random it does have a statistically stable distribution conforming to Poisson law (Alter, Matsushita and Tang 2006)(Matsushita and Lin 2007). This noise distribution is often relative to the radiometric response of the camera, however because of the imaging process between image capture and image retrieval, this noise distribution often varies across the image. Figure 2.19 shows the imaging process common in digital cameras and the sources of noise. Matsushita and Lin (2007) describe these noise sources in detail and state that they all have symmetric Poisson distributions. It is however because of asymmetric transformations to the image that these distributions lose uniformity.

By finding the radiometric response function, the noise distributions can

be predicted allowing for certainties to be estimated whenever trying to determine if two colour responses could have originated from the same incident light. There have been various approaches to determining the correct radiometric response including varying the scene illumination (Shafique and Shah 2004), using probabilistic intensity similarity (Takamatsu and Matsushita 2008) or image noise variance (Takamatsu, Matsushita and Ikeuchi 2008). These approaches operate by analysing video data to determine response. However single image methods have been proposed in greyscale (Lin and Zhang 2005) and colour (Lin, Gu, Yamazaki and Shum 2004).

Figure 2.20 shows the benefits of noise estimation with edge detection performed on an image ignoring signal noise and accounting for it. The image on the bottom clearly shows an overall reduction in noise and clearer edges, while the centre image shows some areas are high in noise while edges are lost. No new image data has been acquired to obtain the result on the right. Simply by knowing and accounting for signal noise correctly, less information is wasted by the edge detection algorithm.

Signal linearity is essential in any computer vision application to obtain the most information about a scene, although currently this has not been done in an illumination invariant colour space.

2.5 Gamut Limitations

When working with colour it is also important to consider the limitations of the image capture device being used. Different cameras have various properties when it comes to the range of colours they are able to capture. This especially becomes an issue when converting between colour representations as many colour models have limits which can cause clipping. There is a large body of research concerning how best to clip these gamuts during conversion (Yang and Kwok 2000) or to change the scale of the colour models so that one converted gamut will fit within the other (Zeng 2005). The opposite process is also considered when converting an image of a smaller gamut into a larger one. While no transformation is necessary, some research looks at enhancing the original image to make better use of the wider gamut (Anderson, Garcia and Gupta 2007). Figure 2.21 shows an image taken of an outdoor scene with

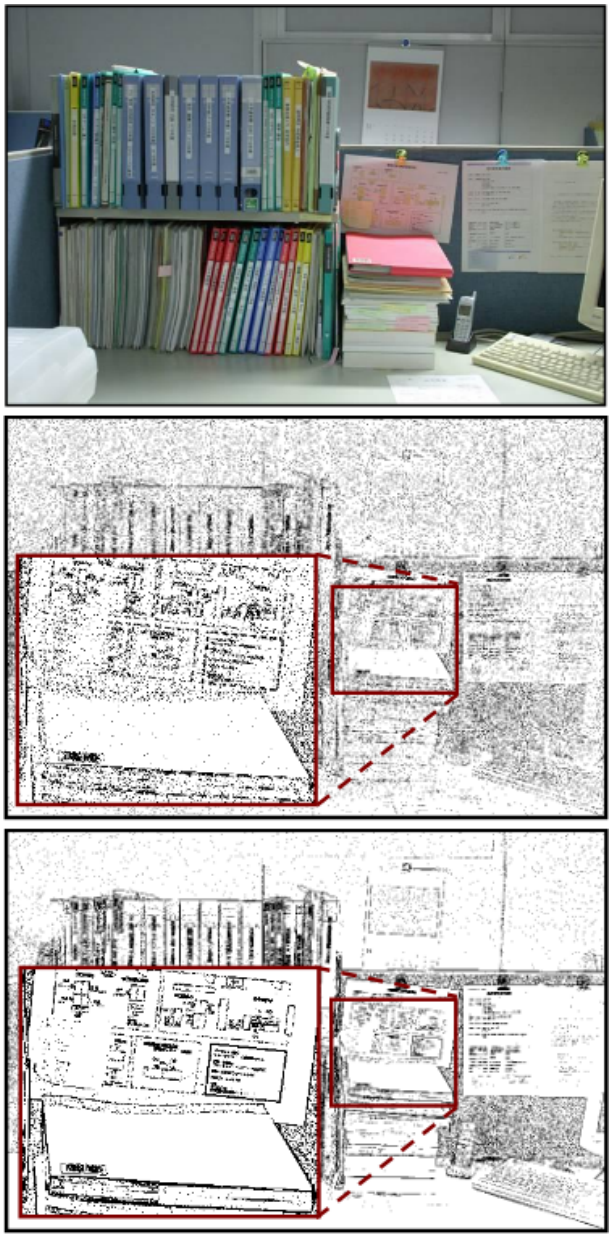

Figure 2.20: Edge detection using a Laplacian performed on an image (top) using two different measures of intensity difference; a standard difference (centre) and a linearised approach (bottom) with small region enlarged to better identify the differences (Takamatsu and Matsushita 2008).

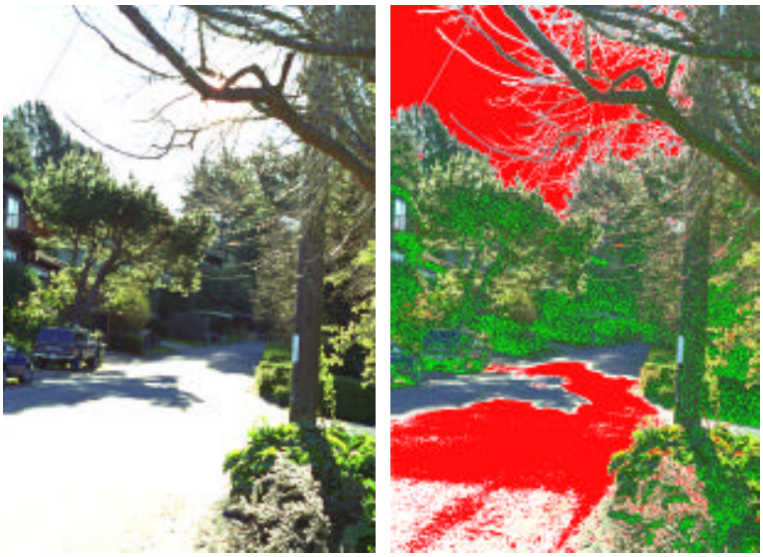

Figure 2.21: An image with out of gamut regions, red regions show pixels that are too bright or too dim and green shows pixels that cannot display the full colour (Larson 1998).

a high dynamic range. The image on the left shows what can happen when a wider gamut image is converted into a narrower colour space. The image on the right indicates the regions of the image that could not be properly represented in a smaller colour space, with red regions denoting areas where the pixel colours are too bright or too dim for the gamut, and green showing pixels which have a reduced colour saturation.

For illumination invariant computer vision, clipping between different colour spaces is not a common issue. When processing an image the data is important and display is just a representation of the internal state of the data. Conversions that clip important information from the data are not used where possible.

However there is one situation which can be seen as a form of gamut clipping, in image acquisition. This is the process whereby light received by the camera is clipped by the detection limits of the camera sensors. When colours are too bright for a pixel sensor, clipping occurs naturally as the maximum level is reached. Gamut clipping can also happen inside the camera when converting the image from the raw detected format into a more

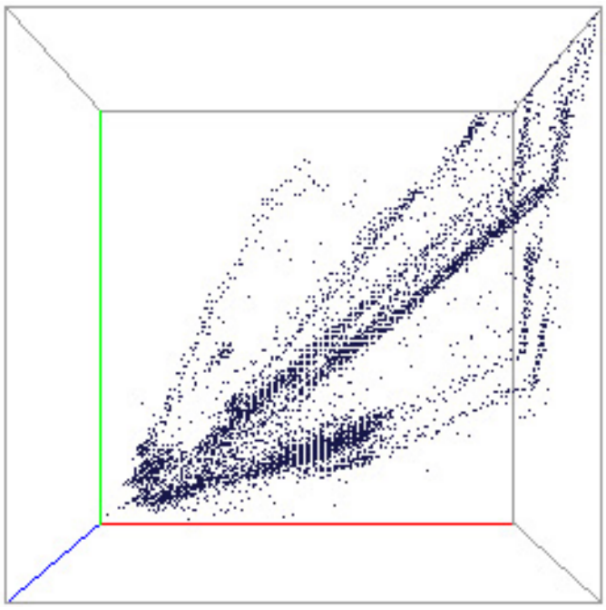

Figure 2.22: An RGB point cloud showing what happens when colours exceed the limits of the camera (Omer and Werman 2003).

compact colour model for transmission. The clipping causes a shift in the colour detected on an object making illumination invariant colour models ineffective. Omer and Werman (2003) recognised this shift in colour was caused by reaching these limits and proposed a method of tracking colour paths through RGB space so that these shifts did not effect them, shown in Figure 2.22. While this approach is invariant to shadow and shading, it has a weakness when specular reflections are present and cause the colour of an object to no longer conform to a line in colour space, making narrow paths hard to define.

Chapter 3

Proposed Colour Models

3.1 Problem Summary

In the previous chapter a comprehensive list of colour models used in various applications was presented. Most of these models are actively used in the field of computer vision despite often being designed for other purposes. Many commonly used colour models provide distinct advantages for certain applications and are not as useful when used elsewhere. Because most colour models were not designed with computer vision as their primary purpose they lack focus on the features that are the most important in this domain. The major requirements of a computer vision representation of colour are:

- **Linear colour comparisons** is the requirement that all comparisons between two colours have equal certainty in relation to signal noise.

- **Decorrelated dimensions** is the requirement that the dimensions of the colour space are decorrelated to object reflectance properties of light.

3.2 Signal Linearity

When using colour for classification, linearity in the space can be extremely important. This allows the difference between two colours to be of uniform certainty across the colour space. There are two distinct classes of linearity referred to in literature, perceptual linearity and signal linearity.

Perceptual linearity is concerned with how a colour difference is perceived to humans. This means that the distance between any two colours in this space will have the same human perceived difference as another two colours

at the same distance. Models such as CIE Lab and Luv were designed to achieve this kind of linearity. While these models achieve this in most cases, human colour perception shifts depending on a variety of conditions, such as neighbouring coloured regions, making it difficult to get an accurate and consistent result. These issues are not relevant for cameras as they capture images in a two dimensional array of pixels which are independent of each other.

Signal linearity is related to signal noise present when capturing images. Effects such as heat, background radiation and electromagnetic interference result in signal noise that is random and unavoidable. The statistical measures of this noise on a given colour can determine the range and probability of which physical colour could have caused the observed response in the camera. As such two colours can have a probability calculated which describes the likelihood that the two colours were the result of the same signal. Signal linearity is concerned with linearising the noise level across the signal range, allowing any two signals to be compared across the range with identical reliabilities.

In computer vision it is often necessary to decide which of these forms of linearity is required. While it is debatable which is ideal, this research postulates that signal linearity is more important for most applications. If a camera determines that two colours have a low probability of being caused by an identical signal then they are likely to have been caused by reflections from materials with different properties. A perceptually linear space however could determine two colours as significantly different when statistically there is no significant difference between the two, and their differing colours may be a product of noise. The reverse of this is also possible, when two significantly different source signals are considered to be perceptually indistinguishable.

When data is received by a camera it undergoes a process of digitisation which results in quantisation loss. To reduce the effect of this on image quality, image information is often manipulated within the camera before digitisation is performed. This manipulation process is designed to enhance the image for viewing purposes, reducing the need for image manipulation post digitisation. Unfortunately this often means that signal noise is delinearised and the final RGB image is not linear with respect to perception or

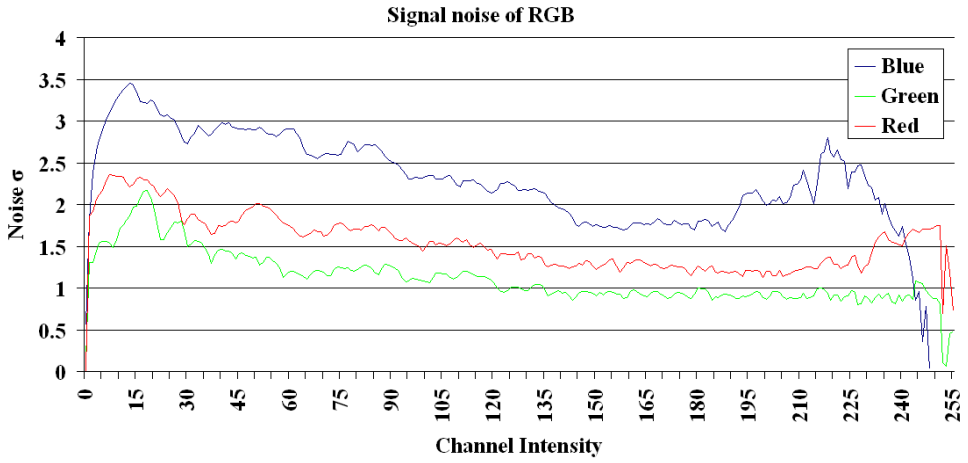

Figure 3.1: The standard deviation for each colour channel at each intensity.

signal noise. Figure 3.1 shows the measured signal standard deviation of the red, green and blue channels of a Logitech QuickCam Pro camera under fixed camera settings. This measure represents the noise present in the signal, not to be confused with the signal-to-noise ratio which in this case would be the ratio between the channel intensity and the noise shown in the graph. This noise is measured by statistically analysing pixel data over multiple frames of a stationary camera viewing a static scene, extracting the standard deviation as noise and the mean as channel intensity. Clear curves can be seen in this data, while each channel itself has a different level of noise. The differences in noise between the channels are as expected as the human eye is the least sensitive to the blue range of wavelengths and the most sensitive to greens, when white balanced this causes the increased blue signal noise.

3.2.1 Proposed Signal Linear RGB

There are many methods for measuring signal noise and achieving linearity as outlined in section 2.4. This research is not concerned with finding an optimal method of single channel linearisation but rather in representing linear colour spaces. Because every camera will be different and may require different approaches to achieving a signal linear space, an all encompassing conversion to the Signal Linear RGB model cannot be defined. Just as each

imaging device that is compatible with the standardised sRGB colour model has a unique transformation to the space, each camera device would require a unique transformation into Signal Linear RGB. However a number of requirements can be defined which will facilitate the creation of the space. The space should have:

- an even distribution of noise across the entire space.
- a noise distribution of one standard deviation per one colour space unit in each of the colour channels.
- equal colour ratios for all colours of equal colour ratio in the original space.

There are a few important points to note when linearising in the RGB colour space. Firstly, measured noise levels are affected by proximity to the boundaries of each channel as shown in figure 3.1. This is caused by the limits imposed on the distribution of noise at the bounds of the colour channel, reducing the size of the standard deviation calculated. As such, when modelling the linearisation curve, these steep declines in signal noise should not be included in the model. Secondly, the channels should be scaled first to match their signal levels to give each channel equal certainty, which is especially important when later converting to a decorrelated colour model. The same linearisation model needs to be applied to all three channels. Because the ratios between the channels are what describe object colours, if these relationships are altered then colours will shift across detected objects dependent on the channel intensity. Once all three channels have a linear distribution individually, each channel can be uniformly altered so that all three channels have equal levels of noise. This alters the colour ratios of objects but keeps them consistent over the object itself. Figure 3.2 shows the signal noise from the Logitech QuickCam Pro after linearisation. The signal noise standard deviation now sits at around 1 for each of the colour channels allowing any two colours in this space to be compared with a standard certainty. Real channel intensity measurements will never be perfectly linear, as demonstrated on the graph. There are spikes and dips in the noise

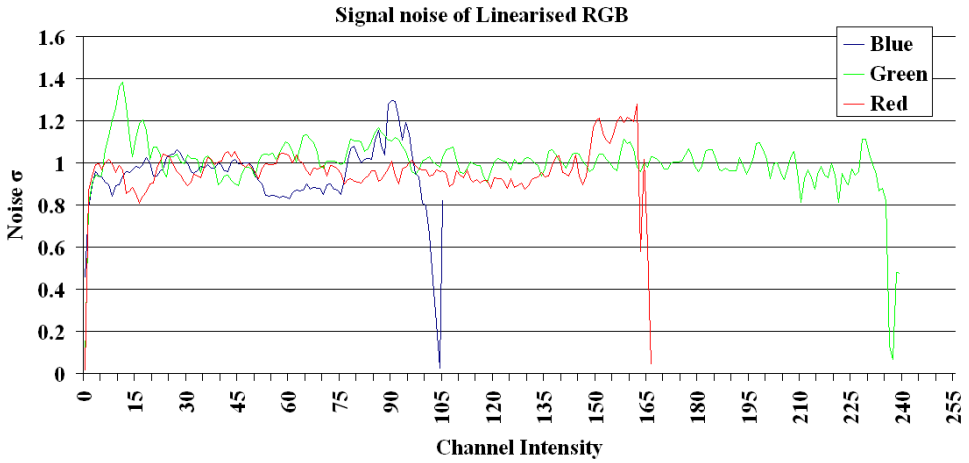

Figure 3.2: The standard deviation for each colour channel at each intensity after linearisation.

levels which follow no consistent pattern, correcting for each would actually reduce the usefulness of the resultant model. This is because of the third of the three criteria, i.e. equal colour ratios. This means that all three colour channels have to be transformed with consistent ratios of each other. If they do not then object colours will shift with intensity changes. The method used to acquire the data shown in figures 3.1 and 3.2 is described in section 4.2.

Additionally, camera settings such as white balance, exposure and gain can affect the level of noise present in the captured image. By modelling these properties when performing linearisation, adjustments can be made to the camera settings to optimise the range of the camera for the environment, while still maintaining a uniform noise distribution with a standard deviation of one unit. Even automatic settings can be used if the camera hardware allows access to this information during capture. Chapter 4 discusses in detail how to measure these criteria quantitatively so that different possible methods of transforming to the Signal Linear RGB colour model can be directly compared.

3.3 Luminance

There are three distinct methods for calculating the luminance of a given RGB colour.

The first is commonly known as *luma* or the perceptual sensation of brightness. Luma measures are used in the colour models CIE XYZ, YUV, CIE Lab, CIE Luv, xyY and Munsell, and is commonly used in greyscale conversions. The transformation to luma does not preserve signal linearity as it scales the red, green and blue channels based on perceptive sensitivities.

The second method is usually called *intensity* and is simply an additive measure of spectral power. Colours of equal intensity lie on a plane perpendicular to the achromatic axis when viewed in the RGB space. The measure is not explicitly included in normalised RGB, but is often used in conjunction with it as it is the factor that relates the normalised values back into the RGB cube. The Opponent colour model and HSI also use a variant of intensity with the added advantage of white balancing without compromising linearity. In this case the space rotates and all spatial relationships between colours are preserved. Often the average of the three colour components is used instead of the total, this really only serves to keep the calculated intensity value at the same scale and is conceptually no different from the additive total.

The last main method of measuring luminance is by finding the Euclidean distance between the colour and black $\{0, 0, 0\}$. This is used in the spherical model and has the advantage of remaining linear to signal noise and is invariant to rotational white balancing. When viewing colours of equal Euclidean luminance in the RGB space they lie on a sphere centred around the origin.

The HLS colour model and the HSV colour model both selectively exclude one or two colour channels from the luminance calculation. This results in a luminance channel that remains linear, but lacks the same descriptive power of all inclusive measures. Since both of these methods exclude some illumination information they are not ideal for illumination invariance. Figure 3.3 shows a comparison between the planes of equal luminance using each of these measures shown in RGB.

Since both intensity and Euclidean distance measures of luminance have

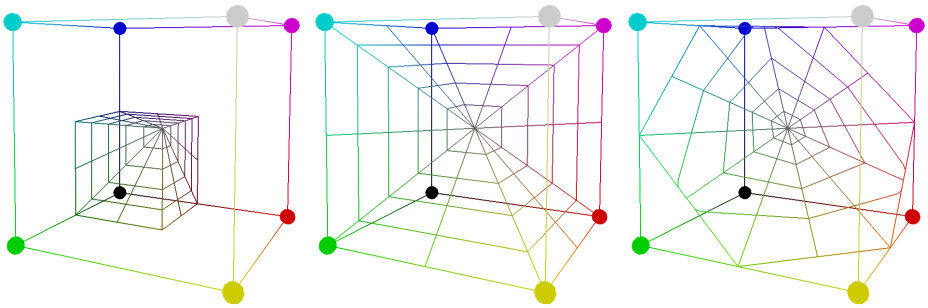

(a) (b) (c)

Figure 3.3: A view of three chromatic planes in the RGB cube at a luminance of 50%, (a) HSV, (b) HLS, (c) Additive.

properties required by the proposed ideal colour model, variations using each will be used and evaluated to determine which method is the best for an illumination invariant signal linear colour model. Luminance is the property which is inherently removed when illumination invariance is required, but it cannot be ignored altogether. Shifts in object brightness due to shading or shadow cause colour changes along an object specific vector which intersects the origin/true black. While both measures are linear they measure luminance along different angles. The Euclidean distance measure calculates the distance along the same vector as the illumination changes, meaning that changes in object illumination may be measured with better certainty and more meaning using this method.

3.4 Hue

Unlike luminance and saturation, hue has relatively little difference in calculated values across colour models. The notable exceptions to this are the LCH_{lab}, LCH_{luv} and LSH_{luv} colour spaces which have very different results for the hue value because they are calculated from very different colour models.

The hue calculation of the HLS and HSV colour models is an estimation of angle around the achromatic axis. This method has a speed advantage over the other methods as it does not require the use of computationally expensive square root and inverse trigonometric functions. The speed increase comes at a cost to accuracy and as such is not always ideal. Hanbury (Hanbury 2002)

compares the hue estimate method to an accurate trigonometric method of hue calculation, finding that these estimations cause inaccuracies visible when viewed as a histogram. Trigonometric hue is a calculation of the angle made between the colour and an origin colour (usually red) on the chromatic plane.

One feature missing from both the estimated hue and the trigonometric hue calculations is white balance. While traditionally these methods would scale the red, green and blue channels to correct for illumination colour, this is no longer ideal when signal linearity needs to be maintained. White balance is important when specular highlights are observed as these cause a shift on the chromatic plane towards the colour of the light source. If the colour model has been adjusted correctly with respect to the illumination colour then every object in the scene will maintain the same hue regardless of specular highlights, making the hue shadow, shading and specular invariant. However, once the pixels are over exposed with the reflected light these colours end up as white and indistinguishable from any other over exposed pixels. The HSI colour model calculates hue from the opponent colour model which allows for white balance adjustments through linearity preserving rotation of the entire space.

In addition to these hue measures from prior research, two new measures of hue are proposed in this thesis, *planar hue* and *spherical hue* which are presented in the following sections. Also a weighting scheme is proposed and presented which allows for almost linear comparisons for angular measures.

3.4.1 Proposed Planar Hue

Planar hue is similar to the IHLS method (Hanbury 2002) but allows for linearity preserving white balance. Rather than a rotation, this method skews the space which allows it to maintain linearity without expensive rotation operations. The first step is to transform a Signal Linear RGB colour or original RGB colour $\{I_r, I_g, I_b\}$ into a vector between the normalised colour and normalised white. This forms a chromatic plane similar to normalised RGB but with the origin shifted to the specified white vector $\{W_r, W_g, W_b\}$.

$$V_{\{r,g,b\}} = \frac{I_{\{r,g,b\}}}{I_r + I_g + I_b} - \frac{W_{\{r,g,b\}}}{W_r + W_g + W_b} \tag{3.1}$$

Using this intermediate space the white balanced hue can be found using the following equations:

$$\theta = \arccos\left(\frac{2V_r - V_g - V_b}{\sqrt{6(V_r^2 + V_g^2 + V_b^2)}}\right) \tag{3.2}$$

$$H = \begin{cases} 360^\circ - \theta & \text{if } V_b > V_g \\ \theta & \text{otherwise} \end{cases} \tag{3.3}$$

3.4.2 Proposed Spherical Hue

The second proposed method, spherical hue, is a variation of the HSI hue calculation but reduces colour shifts caused by rotating the space in one step. It does this by first rotating the RGB space so the achromatic axis matches $r = g = b$ using Rodrigues' rotation formula, where $w = \{w_r, w_g, w_b\}$ (white vector), $c = \{1, 1, 1\}$ (centre vector), $I = \{I_r, I_g, I_b\}$ (colour vector) and z (calculated axis of rotation):

$$\theta = \arccos(\bar{w} \cdot \bar{c}) \tag{3.4}$$

$$z = w \times c \tag{3.5}$$

$$V = I\cos\theta + (\bar{z} \times I)\sin\theta + \bar{z}(\bar{z} \cdot I)(1 - \cos\theta) \tag{3.6}$$

The space is then rotated again using the opponent model transformation with no white balance factors:

$$o_x = \frac{V_r - V_g}{\sqrt{2}} \tag{3.7}$$

$$o_y = \frac{V_r + V_g - 2V_b}{\sqrt{6}} \tag{3.8}$$

$$o_z = \frac{V_r + V_g + V_b}{\sqrt{3}} \tag{3.9}$$

This step can also be calculated using Rodrigues' rotation formula a second time. At this point hue can be calculated in the same way as in the HSI colour model:

$$H = \arctan\left(\frac{o_x}{o_y}\right) \tag{3.10}$$

Spherical hue can increase the correlation between the same object under different light sources, although neither Spherical or HSI hue achieves this as well as white balance via scaling but, as previously stated, this breaks the signal linearity of the space. Additionally the original part of this rotation method of applying white balance can be applied to any of the previous hue methods mentioned. The space $\{V_r, V_g, V_b\}$ can be used in place of the original red, green and blue components in previous methods to calculate a white balanced hue.

3.4.3 Proposed Hue Weighting

The problem with using hue as a measure is that linearity is inherently lost in the transformation from a Cartesian space to a polar one. Figure 3.4 shows how the scale within the polar space changes in relation to the distance from the origin. The Cartesian space however is equally spaced across every part of the chromatic plane. The closer the colours are to the origin of the polar space the greater effect signal noise has on the angle.

One possible way to solve this problem is to use arc distances instead of angles to measure hue. Unfortunately this would result in colours which have the same hue angle and differing saturation values that no longer have the same hue. The proposed solution is to use a comparison weight when comparing two hues which best approximates the colour shift in the hue dimension proportional to the actual shift in the linearised RGB space. This weight can be calculated for each hue value as a distance from the centre of the origin of the polar chromatic plane multiplied by the luminance value. When two hues (a_h, b_h) are compared, the minimum of the two weights (a_{hw}, b_{hw}) is used as a factor as shown in the following equation where $\div$ again denotes an angular difference and δ_h is the calculated difference between hues:

$$\delta_h = (a_h \div b_h) \min(a_{hw}, b_{hw}) \tag{3.11}$$

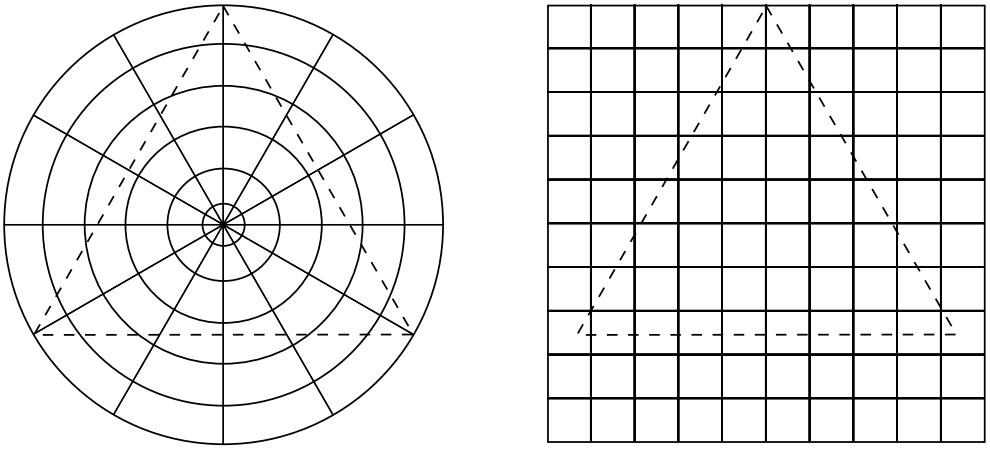

Figure 3.4: A comparison of the polar coordinate space and the Cartesian coordinate spaces on the chromatic plane.

The minimum is used because this represents the best certainty available when comparing the hues. To illustrate, Figure 3.5 shows two colours a and b on the chromatic plane with certainties shown as solid circles. When a_h and b_h are compared using a_w then both hues are well outside their range of certainty (a and b' in the illustration). However when these hues are compared using the minimum weight b_w these points are within range and determined to be of indistinguishable hues (a' and b in the illustration). The second comparison (a' and b) is determined to be the more correct of the two when the certainty of b is extended from the origin, the hue a lies within range to match.

Any previous measure of colour can make use of this technique and by itself it greatly improves certainty when comparing colours along the hue dimension. The weight used will depend on the space. In chroma based models the chroma value is ideal to use as the weight. In purity based models the luminance multiplied by the purity is required to compensate for the change in scale.

3.5 Saturation

The saturation component has the most variations of all of the decorrelated components between colour models. As previously discussed the component

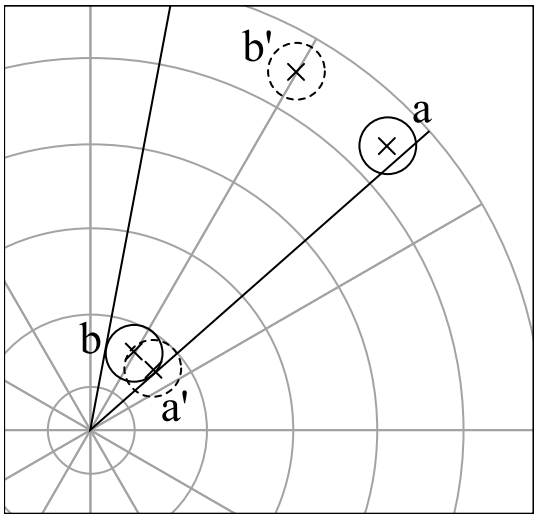

Figure 3.5: Two colours a and b have their hue components compared on the chromatic plane with their certainties represented by circles around each point.

itself is usually classed as either a measure of chroma or purity, with each having distinct advantages.

Chroma is a measure which describes the apparent difference between a colour and a grey of the same intensity. It can be useful because it models how in low light an object's colour is less distinctive from other colours under the same light level. This preserves spatial linearity under changes in brightness which means noise does not increase on the chromatic plane as it approaches black. Unfortunately this also means that shadowing and shading affects the chroma of an object causing shifts in object chroma which are correlated to brightness. Hanbury (2008) favours the chroma method over purity as it remains uncorrelated to brightness with respect to noise but fails to acknowledge that the chroma measure is not invariant to shadows and shading on real world objects. Figure 3.6(a) shows how the chroma axis is square with respect to a cross section of the original RGB space at an individual hue. This means that under linear noise the axis is uniformly sized regardless of the level of luminance.

Purity consists of an axis emanating from the origin which keeps it consistent under object illumination changes. However because of the shrink-

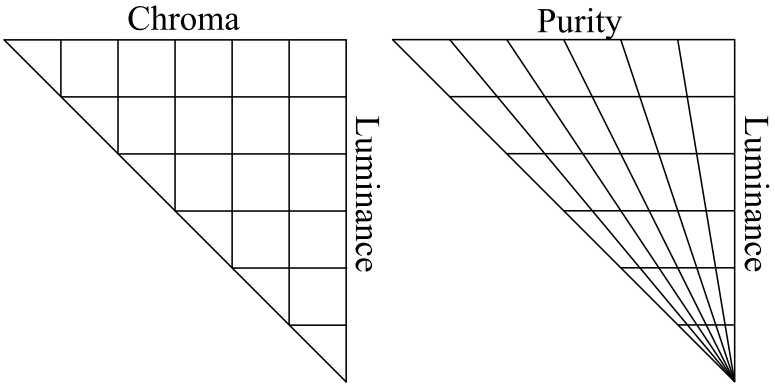

Figure 3.6: A cross section of two polar colour spaces at an individual hue.

ing space near the origin, signal noise is magnified when dealing with dark colours. Figure 3.6(b) illustrates how the purity axis shrinks as luminance decreases. This is similar to the human perception of colour saturation which is invariant to illumination level. An object has the same perceived saturation regardless of whether it is illuminated under bright sunlight or a dim tungsten light. The notable exception to this in humans is when the light level drops to below the sensitivity level of the cone cells and the rod cells are primarily used, creating an unsaturated view of the environment.

When calculating polar coordinates for the chromatic plane, different formulations often result in different shapes of the chromatic plane. Figures 3.7(a) and 3.7(b) show the limits of the plane when a direct geometric measure is used. The hexagonal shape and the triangular shape are a result of the compression of the RGB space into chroma and purity respectively. The chroma measure used in the HSI colour model and the L2 measure presented by Hanbury and Serra (2003) both produce hexagonal shaped limits in the chromatic plane. There are currently no known purity measures that produce a triangular shaped chromatic plane, however the non-polar normalised RGB space has a triangular chromatic plane which could be derived into a triangular purity based measure.

Figure 3.7(c) shows the limits of a spaces which are circular in shape. This type of saturation can be referred to as being relative to its own limits at any given hue. This means that a saturation measure can vary between

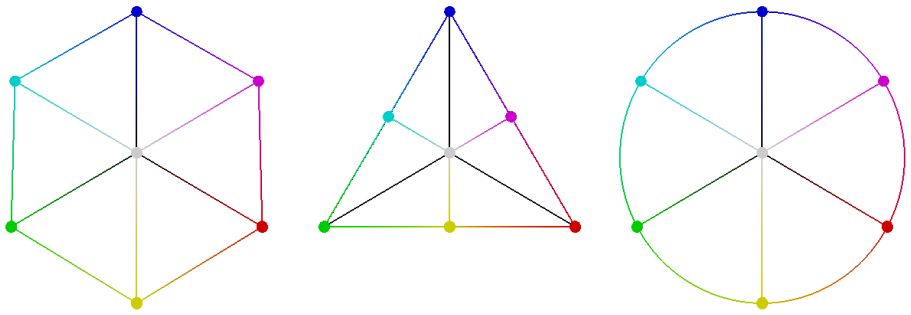

(a) (b) (c)

Figure 3.7: The saturation measure effects the shape of the chromatic plane.

0% and 100% at any given hue, which is used by the HLS and HSV colour models. However, once luminance exceeds 50% of the maximum in HLS, saturation becomes relative to the maximum saturation possible within the upper limits of the RGB space. This distortion of the top half of the space changes the meaning of saturation because highly unsaturated colours with a high luminance will have a higher than normal saturation making it unrelated to colour purity. The reason HLS was designed this way was so that every possible HLS coordinate would correspond to a real RGB colour, making it impossible for a user selecting colours in an application to select an invalid colour. Likewise this is also the reason a circular chromatic plane is used to calculate the saturation in both HLS and HSV. When maintaining signal linearity this is not ideal because the expansion of the triangular chromatic plane to the circular one stretches the secondary colours, causing periodic shifts in linearity. The max-min measure of saturation proposed by Hanbury and Serra (2003) is a circular measure of chroma. This method is the same as HLS and HSV saturation calculation but without the luminance normalisation.

Table 3.1 shows a comparison of the current saturation techniques in terms of previously mentioned properties. In the table *Direct* references both the hexagonal and triangular measures as these are both direct measures, using geometric chromatic distances rather than using a proportion of the maximum at that colour which would be *Circular*. An ideal measure for most computer vision tasks would be a direct purity measure but as shown there

are no current measures which fit both categories.

Table 3.1: Comparison of saturation measures.

Measure	Purity	Chroma	Direct	Circular
HLS	✓			✓
HSV	✓			✓
HSI		✓	✓	
Max-Min		✓		✓
L2 norm		✓	✓	
Ideal	✓		✓	

To fill this missing *Ideal* slot, two new measures of saturation are proposed, *planar saturation* and *spherical saturation* which are presented in the following sections. Also a weighting scheme is proposed and presented for purity measures which allows for almost linear comparisons to counter the noise experienced when luminance is low. Note that the following two measures of saturation coincide with the two proposed measures of hue.

3.5.1 Proposed Planar Saturation

Planar saturation is unlike any previous method of measuring purity because it is calculated based on a linear direct measure and additionally can adjust for white balance. It is a linear measure of distance between a normalised colour and the normalised white point. This forms a triangular measure of saturation centred around the white point. Using equation 3.1 from the planar hue calculation a white balanced normalised RGB space is calculated. From this, the measure of saturation is the length of the resulting vector $V_{\{r,g,b\}}$ calculated by:

$$S = \sqrt{V_r^2 + V_g^2 + V_b^2} \tag{3.12}$$

3.5.2 Proposed Spherical Saturation

Spherical saturation measures the purity as the angle made between the colour vector $I_{\{r,g,b\}}$ and the white vector $w_{\{r,g,b\}}$. This causes a triangular chromatic plane with curved edges as pictured in figure 3.8. The advantage

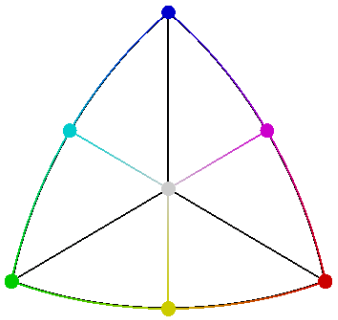

Figure 3.8: The proposed spherical saturation measure has a curved triangular chromatic plane.

of this space is that the saturation measure is perpendicular with the illumination path of an object within the space. This means the saturation will have a better measure of saturation noise within a single object.

Spherical saturation can be calculated in two distinct ways. The first uses the normalised dot product between the colour vector and the white vector. And the second calculates the angle based on the proposed rotated opponent space calculated in equations 3.4–3.9. Both are shown below:

$$S = \arccos\left(\frac{I \cdot w}{|I||w|}\right) = \arccos\left(\frac{o_z}{|o|}\right) \tag{3.13}$$

3.5.3 Proposed Saturation Weighting

The chroma measure has a distinct advantage over purity because it maintains signal linearity regardless of the luminance. But since chroma does not model illumination shifts on objects purity is better suited in most cases. This problem was previously illustrated in Figure 3.6. To overcome this non-linearity, a similar weighting system to hue weighting can be employed when performing purity comparisons.

The difference between a chroma measure and a purity measure is often simply a normalisation using the luminance measure of the accompanying space. This luminance measure can therefore be used as the weight for each

saturation and applied at the time of comparison as follows:

$$\delta_s = (a_s - b_s)\min(a_{sw}, b_{sw}) \tag{3.14}$$

By using the minimum weight again we compare the saturations at the best certainty available. This method means that a dark part of the image has a low certainty and as such could match a wider range of bright colours. Not enough information is provided by dark colours to reliably exclude them from a large range of matches, but other features such as proximity could be used to improve classification later.

For the proposed methods, planar saturation and spherical saturation the weights used are the additive luminance and euclidean luminance respectively.

3.6 Gamut Limitation

Most digital colour models have distinct limits on their axes. In 24-bit RGB each colour channel has a range of 0 to 255 given by the range of a byte. While larger representations are used in high dynamic range cameras such limits will still be present on the camera itself. A camera exposes a light sensitive surface to a scene for a given time known as the exposure time. The sensitivity of the surface and the amount of light in the scene will determine how long the exposure time will need to be to achieve sufficient information. But because the exposure time is selected for the entire scene, and different regions will receive different amounts of light, over exposed regions or pixels can occur even under ideal settings.

In general the colour of an object consists of a unique ratio $I_r : I_g : I_b$, this is the basis which allows us to calculate the chromatic plane and produce invariance to shadow and shading. Because colours are limited by the size of the colour space available to the camera, clipping occurs which alters the colour recorded. Once one of the colour components becomes over saturated (that is, it reaches the upper limit of the channel), the colour ratio changes as one of these components is fixed, i.e. $R_{\text{lim}} : I_g : I_b$ contains the limit of the red channel R_{lim}, a constant, which means the ratio is constantly chang-

ing as luminance changes. These colours are called out of gamut colours because their true values lie outside of the colour gamut of the RGB space. When trying to classify coloured pixels as belonging to a specific object, an out of gamut colour often will not match the original description of the object. When working in a polar chromatic space this results in a reduction in saturation and in many cases a shift in hue. As hue is shadow, shading and specular invariant, a shift in this measure is highly detrimental to most vision applications. Likewise when two of the recorded channels become over saturated then only one of the remaining channels retains any of the properties of the original colour. Finally if all three channels are over saturated then all of the chromatic information is lost. While there is extensive research of how to clip a colour gamut correctly when moving between media with differently shaped gamuts, the reverse operation is often overlooked as information which has been lost and cannot be recovered. This problem has lead to the creation of the Gamut Limit Invariant (GLI) colour model proposed in this thesis.

3.6.1 Proposed Gamut Limit Invariant Colour Model

The proposed GLI colour model works as an addition to the Planar and Spherical HLS models as well as other compatible models. It provides extra information that aids comparisons with potentially gamut clipped colours. However colours that have been clipped by the limitations of the gamut are unable to be determined exactly. GLI can be used to calculate whether the observed clipped colour could have occurred from a colour of the same hue as the unclipped colour it is compared with. If matched then a corrected saturation value is calculated for the clipped colour, to be used with the matched hue for regular colour comparison.

The GLI colour estimation puts the most importance on hue as it is shadow, shading and specular invariant. This makes it generally the most stable and important colour component across object surfaces. This is especially true of out of gamut colours as many are the result of high intensity specular reflections. Figure 3.9 illustrates how GLI estimation works viewed from the chromatic plane, with w as the white point, a as the apex or point

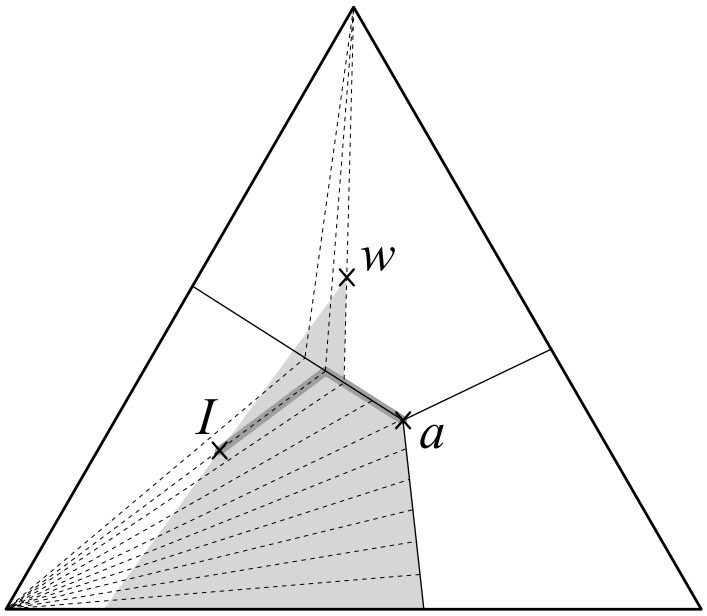

Figure 3.9: The chromatic plane with GLI matching, the light grey area denotes the region of identical hue while the dark grey line shows the path of identical saturation and hue.

of highest possible luminance and I as our "within gamut colour". The chromatic plane is split into three regions extending from the apex. These regions denote which of the three colour channels (red, green and blue) would reach or have reached their limit. The light grey area in the illustration shows all of the possible "at-limit" colours that could have resulted from a colour with the same hue as I. The darker grey line shows all of the possible "at-limit" colours that could have resulted from a colour with the same hue and saturation as I. Note that this dark grey line extends from the point I along a path directly away from the external corner of the region. Once a barrier between regions is reached then it follows from this point to the apex point. The dotted lines are lines of equal saturation and where they intersect with the hue of I will be the estimated saturation.

3.6.2 GLI Definition

There are two main sets of data involved in the GLI colour model; global data and pixel data. Global data needs only to be calculated once per image and

depending on the properties of the camera and scene, often only needs to be computed when the camera or illumination properties change. Alternately pixel data, as the name suggests, is calculated for every pixel in the image and for every new frame of an image sequence. While pixel data is at the core of the GLI colour model, the global data represents the space specific constants used when calculating colour differences.

Global data First, three constants are defined, R_{lim}, G_{lim} and B_{lim}, which are the limits of the linearised RGB model. If linearisation is not required these are often $R = G = B = 255$ in 24bit RGB. These three values form the apex of the colour space, at the point $a = \{R_{lim}, G_{lim}, B_{lim}\}$. Next the white vector is defined as the point $w = \{W_r, W_g, W_b\}$. Finally the corner points of the chromatic plane are defined as $\hat{r} = \{1, 0, 0\}$, $\hat{g} = \{0, 1, 0\}$ and $\hat{b} = \{0, 0, 1\}$.

With this set of five key points we can begin calculating important information about their relative positions. To make the GLI colour model independent of the base colour model, these relative positions are calculated using the conversion formulae of the base model. In this way three symbolic functions are defined f_h, f_l and f_s which calculate the hue, luminance and saturation respectively in the base model. The input to these functions is first the colour being converted and second the white vector to calculate these relative to. To ease understanding of these terms in later formulae, they all use the notation $x_y^z = f_y(x, z)$ where x is the colour to be converted, y is the component calculated (one of h, l and s) and z is the white vector. While GLI is largely base model independent, it cannot be used with chroma based colour models such as HSI or any models that use channel scaling to apply white balance.

The first six values define the hues and saturations of the three corner

points of the chromatic plane.

$$\hat{r}_h^w = f_h(\hat{r}, w) \tag{3.15}$$
$$\hat{g}_h^w = f_h(\hat{g}, w) \tag{3.16}$$
$$\hat{b}_h^w = f_h(\hat{b}, w) \tag{3.17}$$

$$\hat{r}_s^w = f_s(\hat{r}, w) \tag{3.18}$$
$$\hat{g}_s^w = f_s(\hat{g}, w) \tag{3.19}$$
$$\hat{b}_s^w = f_s(\hat{b}, w) \tag{3.20}$$

The next three values define the hue angles of white when balanced by each of the three corner points of the chromatic plane.

$$w_h^{\hat{r}} = f_h(w, \hat{r}) \tag{3.21}$$
$$w_h^{\hat{g}} = f_h(w, \hat{g}) \tag{3.22}$$
$$w_h^{\hat{b}} = f_h(w, \hat{b}) \tag{3.23}$$

The final three values define the hue angles of the apex when balanced by each of the three corner points of the chromatic plane.

$$a_h^{\hat{r}} = f_h(a, \hat{r}) \tag{3.24}$$
$$a_h^{\hat{g}} = f_h(a, \hat{g}) \tag{3.25}$$
$$a_h^{\hat{b}} = f_h(a, \hat{b}) \tag{3.26}$$

Pixel data For each colour pixel $I = \{I_r, I_g, I_b\}$, the GLI colour model first calculates the following four booleans, which define significant regions of the RGB space that the pixel's colour exists within:

$$I_{mr} = \begin{cases} 1 & \text{if } \frac{I_r}{I_r+I_g} \geq \frac{R_{lim}}{R_{lim}+G_{lim}} \text{ and } \frac{I_b}{I_b+I_r} \leq \frac{B_{lim}}{B_{lim}+R_{lim}} \\ 0 & \text{otherwise} \end{cases} \tag{3.27}$$

$$I_{mg} = \begin{cases} 1 & \text{if } \frac{I_g}{I_g+I_b} \geq \frac{G_{lim}}{G_{lim}+B_{lim}} \text{ and } \frac{I_r}{I_r+I_g} \leq \frac{R_{lim}}{R_{lim}+G_{lim}} \\ 0 & \text{otherwise} \end{cases} \tag{3.28}$$

$$I_{mb} = \begin{cases} 1 & \text{if } \frac{I_b}{I_b+I_r} \geq \frac{B_{lim}}{B_{lim}+R_{lim}} \text{ and } \frac{I_g}{I_g+I_b} \leq \frac{G_{lim}}{G_{lim}+B_{lim}} \\ 0 & \text{otherwise} \end{cases} \tag{3.29}$$

The final boolean determines whether or not the current colour has any channels at the upper limits of the colour gamut:

$$I_{ml} = \begin{cases} 1 & \text{if } I_r = R_{lim} \text{ or } I_g = G_{lim} \text{ or } I_b = B_{lim} \\ 0 & \text{otherwise} \end{cases} \tag{3.30}$$

Using these we can determine various properties of the colour. For example, if $I_{mr} = 1$ and $I_{ml} = 1$ then we know that the colour has reached the maximum value for the red channel. Likewise, if $I_{mr} = 1$, $I_{mg} = 1$ and $I_{ml} = 1$ then we know that both the red and green channels have reached their respective maximums. Together these four booleans determine whether a comparison between two colours should use the GLI tier 1, tier 2, tier 3 or use the standard comparison methods for the accompanying space.

Finally three angles are calculated for the colour relative to the corners of the chromatic plane. These angles are calculated using the hue calculation of the base colour model, white balanced to the three corner points $\hat{r}$, $\hat{g}$ and $\hat{b}$.

$$I_h^{\hat{r}} = f_h(I, \hat{r}) \tag{3.31}$$

$$I_h^{\hat{g}} = f_h(I, \hat{g}) \tag{3.32}$$

$$I_h^{\hat{b}} = f_h(I, \hat{b}) \tag{3.33}$$

Calculating and storing all three of these angles is unnecessary because only the angles based on the regions the colour belongs to need to be stored. In most cases only one angle is stored, but in cases where a colour has maximum values for two colour channels then a second angle is required. The following

equations outline the logic to determine which two angles need to be stored:

$$\theta_1 = \begin{cases} I_h^{\hat{r}} & \text{if } I_{mr} = 1 \\ I_h^{\hat{g}} & \text{if } I_{mg} = 1 \\ I_h^{\hat{b}} & \text{if } I_{mb} = 1 \end{cases} \tag{3.34}$$

$$\theta_2 = \begin{cases} I_h^{\hat{g}} & \text{if } I_{mr} I_{mg} (1 - I_{mb}) I_{ml} = 1 \\ I_h^{\hat{b}} & \text{if } (I_{mr} + I_{mg}) I_{mb} I_{ml} = 1 \\ 0 & \text{otherwise} \end{cases} \tag{3.35}$$

3.6.3 GLI Colour Difference

Given two colours, α and β, we first determine which tier calculations are required:

$$T_\alpha = (\alpha_{mr} + \alpha_{mg} + \alpha_{mb})\alpha_{ml} \tag{3.36}$$

$$T_\beta = (\beta_{mr} + \beta_{mg} + \beta_{mb})\beta_{ml} \tag{3.37}$$

The maximum of the two T values provides the tier at which comparisons should be made. If both values are zero then neither of the colours have been clipped by the limited gamut and standard colour comparisons for the source colour space can be used. The colour with the maximum T value is also defined as the "at-limit" colour L for comparative purposes, with the other being defined as I as follows:

$$L = \begin{cases} \beta & \text{if } T_\alpha < T_\beta \\ \alpha & \text{otherwise} \end{cases} \tag{3.38}$$

$$I = \begin{cases} \alpha & \text{if } T_\alpha < T_\beta \\ \beta & \text{otherwise} \end{cases} \tag{3.39}$$

Tier 1 The first step of tier 1 is to determine the sector of interest. This is determined by which colour channel has been over saturated and caused a possible colour shift. The following substitutes $\hat{x}$ for the sector for all

following equations:

$$\hat{x} = \begin{cases} \hat{r} & \text{if } L_{mr} = 1 \\ \hat{g} & \text{if } L_{mg} = 1 \\ \hat{b} & \text{if } L_{mb} = 1 \end{cases} \tag{3.40}$$

This is followed by two checks between the colours to ensure that it is possible for the clipped colour L to have resulted from an unclipped colour of the same hue as I. The conditions asserted in equation 3.41 checks that both colours lie on the same side of the vector made between w and $\hat{x}$. While the conditions asserted in equation 3.42 completes the comparison to determine whether L can result from the same hue as I.

$$\frac{\hat{x}_h^w \div I_h^w}{|\hat{x}_h^w \div I_h^w|} = \frac{\hat{x}_h^w \div L_h^w}{|\hat{x}_h^w \div L_h^w|} \tag{3.41}$$

$$|\hat{x}_h^w \div I_h^w| \leq |\hat{x}_h^w \div L_h^w| \tag{3.42}$$

If either of these assertions fail then I and L are compared in the standard method for the colour model and no extra information can be derived. However the colour L does lie within the region of equal hue then a new saturation and hue can be determined for L as follows:

$$L_s^{w'} = \frac{\sin(|w_h^{\hat{x}} \div L_h^{\hat{x}}|)\hat{x}_s^w}{\sin(180^\circ - |w_h^{\hat{x}} \div L_h^{\hat{x}}| - |\hat{x}_h^w \div I_h^w|)} \tag{3.43}$$

$$L_h^{w'} = I_h^w \tag{3.44}$$

This final result can then be compared using the standard comparative method of the base colour space, comparing the colours I and L' invariant to gamut clipping. Figure 3.10 illustrates how these calculations fit together on the chromatic plane, with $\theta^\Delta = |w_h^{\hat{x}} \div L_h^{\hat{x}}|$ and $h^\Delta = |\hat{x}_h^w \div I_h^w|$.

Tier 2 The second tier is used when one of the colours being compared has been clipped on two of the colour channels. In this case the region of interest is determined by I as follows:

$$\hat{x} = \begin{cases} \hat{r} & \text{if } I_{mr} = 1 \\ \hat{g} & \text{if } I_{mg} = 1 \\ \hat{b} & \text{if } I_{mb} = 1 \end{cases} \tag{3.45}$$

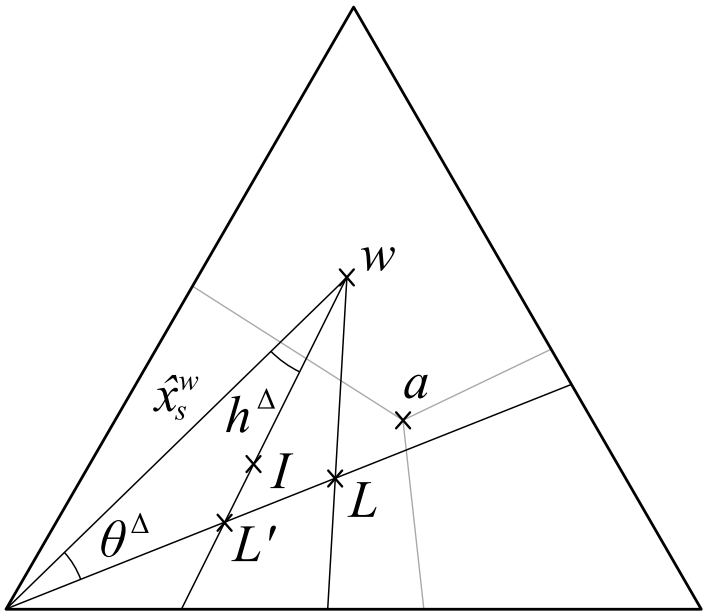

Figure 3.10: A visualisation of tier 1 calculation of L'.

It is possible that more than one of the booleans I_{mr}, I_{mg} and I_{mb} may be true (= 1). In this case it does not matter which of these regions is selected as they will have the same result.

The following conditions asserted in equations 3.46 and 3.47 then form the basis of tier 2. These calculate whether or not the colour L lies on an angle with $\hat{x}$ between the angles of the apex a and the colour I.

$$\frac{a_h^{\hat{x}} \div I_h^{\hat{x}}}{|a_h^{\hat{x}} \div I_h^{\hat{x}}|} = \frac{a_h^{\hat{x}} \div L_h^{\hat{x}}}{|a_h^{\hat{x}} \div L_h^{\hat{x}}|} \tag{3.46}$$

$$|a_h^{\hat{x}} \div I_h^{\hat{x}}| \geq |a_h^{\hat{x}} \div L_h^{\hat{x}}| \tag{3.47}$$

If these assertions are found to be true then we can determine that the colour L could have originally had the same chromatic properties as the colour I and so:

$$L_s^{w'} = I_s^w \tag{3.48}$$

$$L_h^{w'} = I_h^w \tag{3.49}$$

This is illustrated in Figure 3.11. If either of assertions in equations 3.46 and

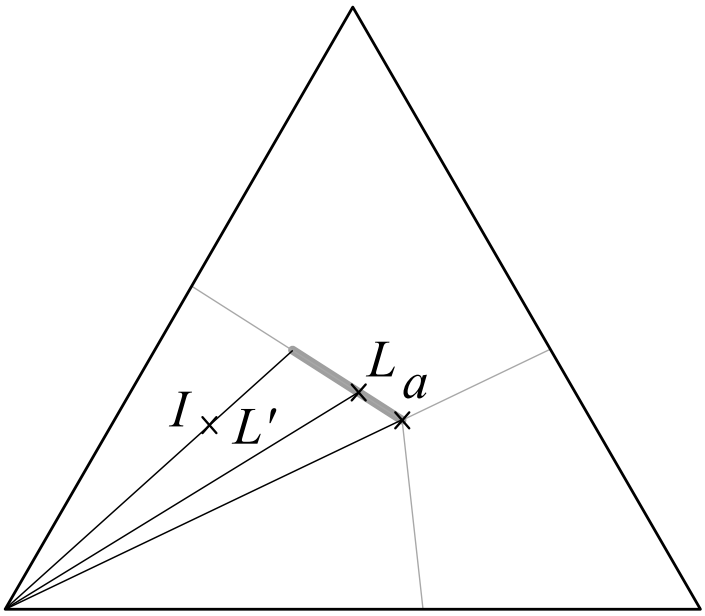

Figure 3.11: A visualisation of tier 2 calculation of L'.

3.47 are false then the method drops down to tier 1. This will then require up to two iterations to determine the correct region to use in equation 3.40 as there is no way to determine this beforehand.

Tier 3 The third and final tier is the most simple. Any colour that has all three colour channels at the maximum value, i.e. $L_{rgb} = a = \{R_{lim}, G_{lim}, B_{lim}\}$, could have been originally sourced from any colour on the chromatic plane. As such the formula is:

$$L_s^{w'} = I_s^w \tag{3.50}$$

$$L_h^{w'} = I_h^w \tag{3.51}$$

3.7 Proposed Models and Techniques

To reiterate and summarise the contributions of this work, the following section will bring together all of the proposed methods from the previous sections.

3.7.1 Signal Linear RGB

Signal Linear RGB is a trichromatic space in which the signal noise from the source sensor, such as a camera, is uniform across the entire space. By modelling the internal settings of the camera such as white balance, exposure and gain it can maintain linearity with a noise distribution of one unit per standard deviation. When converting from a raw RGB source to the proposed SLRGB the resulting space is standard so any models or applications utilising it will not need to be altered when used for other cameras, other than for the initial calibration.

3.7.2 Planar HLS

The two proposed planar measures of hue and saturation along with the commonly used additive luminance can be combined to form the Planar HLS colour model. Planar HLS is unique in that it does not distort the RGB cube but just applies a new coordinate space to it. This makes calculating differences much more robust and linear over the space. With the inclusion of a white balance method that does not disrupt linearity, this space can be used reliably in a variety of environments. Figure 3.12 shows how the axes of Planar HLS relate to the trichromatic axes of RGB with coloured object point clouds shown.

3.7.3 Spherical HLS

The two proposed spherical measures of hue and saturation along with the Euclidean distance luminance measure form the Spherical HLS colour model. While computationally more complex than Planar HLS, the use of a spherical colour system means that the chromatic plane always remains perpendicular to the luminance axis. This means that axes in this model better align to object colour shifts, resulting in better measures for image analysis. Figure 3.13 shows how the axes of Spherical HLS relate to the trichromatic axes of RGB with coloured object point clouds shown.

Spherical HLS also uses rotationally applied white balance which is an effective way to adjust the position of the achromatic axis. It has the advantage of not distorting the space in any way, therefore preserving signal

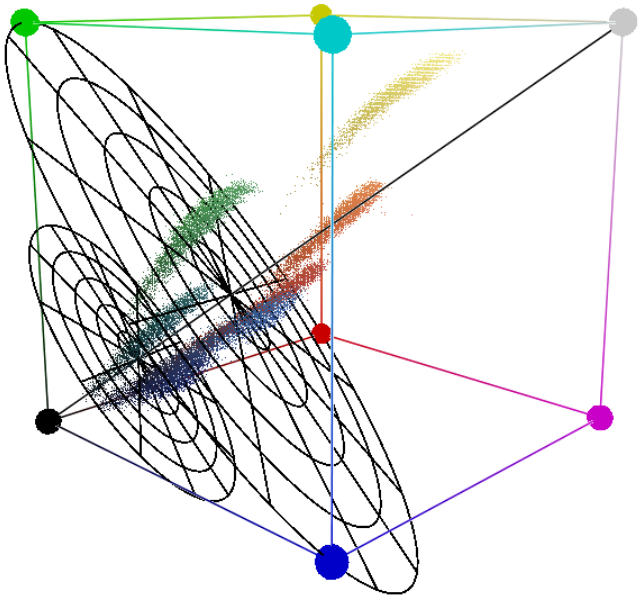

Figure 3.12: The Planar HLS colour axes within the RGB colour space with coloured object point clouds.

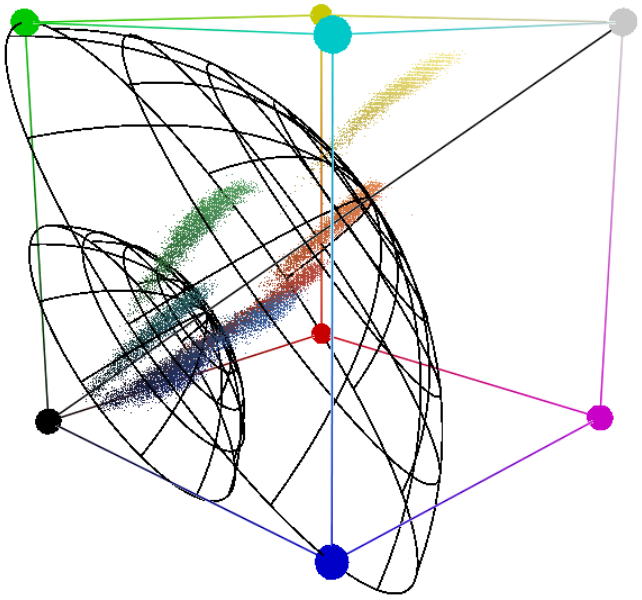

Figure 3.13: The Spherical HLS colour axes within the RGB colour space with coloured object point clouds.

linearity and any other spatial information. By calculating the angle and the direction from the white vector, Rodrigues' rotation formula rotates the entire space. While this can be computationally expensive, this operation can be performed efficiently on modern CUDA supported GPUs which are optimised for these types of computations.

The main limitation of this method as opposed to channel scaling is that objects do not necessarily have consistent chromatic properties under different illuminants. This is because channel scaling closely matches the way colours change under varying illuminants and colours corrected this way will generally retain their original appearance. However when signal linearity is an important factor, the rotational approach is better, although a channel scaled reference can always be used for colour correspondence under different lighting conditions.

Additionally, an RGB sensor cannot completely predict an object's appearance under any illuminant as it is only an approximation of a complete spectral distribution as discussed in Section 2.1. Peaks of specific wavelengths in the light source or in the reflectance properties of the object can cause small to vast differences in apparent colour, even to the human eye.

3.7.4 Minimum Weighted Colour Comparison

The proposed Minimum Weighted Colour Comparison (MWCC) allows a non-uniform coordinate space to make relatively uniform comparisons. It does this by applying a weight calculated from the axes on which the colour component depends upon for scale. There are two primary cases where this method needs to be applied.

In colour models with purity based chromatic planes, the luminance becomes a predicting factor of colour space distortion. With the proposed PHLS, SHLS and prior nRGB colour models this value directly correlates with the changes in chromatic scale, whereas in prior models such as HLS and HSV, distortions are more complex and so luminance is a less accurate predictor. This weight component can be applied to any comparisons made between components on the chromatic plane such as saturation, hue or nRGB components.

All polar colour models exhibit distortion around the centre of the chromatic plane, and so hue differences need to be made based on circumference distances rather than angular difference. Calculation of the circumference c of a circle needs only the radius r:

$$c = 2\pi r \tag{3.52}$$

This equation shows that the distance made around a circle is proportional to the radius of the circle, as 2π is constant. With proportionality not important the only factor needed is the radius, which in the case of a polar colour space is saturation.

If proportionality is important in either case then a constant factor can be included to scale the difference to a level similar in scale to the original measures. To summarise this colour comparison technique, the weight can be calculated using the l luminance and s saturation, found by:

$$w = \begin{cases} ls & if \text{ purity } and \text{ hue} \\ l & if \text{ purity} \\ s & if \text{ hue} \\ 1 & otherwise \end{cases} \tag{3.53}$$

This is a generalised way of viewing the MWCC weight calculation, purity referring to whether the colour model uses a purity based chromatic plane, and hue referring to whether or not the component being weighted is a measure of angular hue.

To better understand this, an example of how it would be applied to three different colour models will be discussed. For the HSI colour model when calculating the difference between two hue values, the weight used would simply be s. This is because in this model luminance does not effect the level of noise present in the hue values measured. Differences between saturation values would have a weight of 1 as there is no noise variation dependent on any other channel. The proposed SHLS colour model would require a weight of ls when calculating differences between hues and a weight of l for differences of saturation. The noise dependence of luminance means that using l to scale differences gives more stable results. The non-polar

model nRGB can also use the MWCC technique. As it is a purity based colour space, when differencing any of the three chromatic values a weight of l can be used, where l is the magnitude or $R+G+B$ from the unnormalised space.

These weights are then used during colour comparison with the minimum weight being multiplied by the calculated difference. This helps to calculate differences with a higher level of linearity in non-uniform colour models.

3.7.5 Gamut Limit Invariant Colour Model

The proposed Gamut Limit Invariant colour model allows for improved robustness in illumination invariant colour comparisons when colours exceed the limits of the camera. This model stores colour information in a coordinate system which has invariants to illumination and gamut limit clipping. These can be used to estimate how close a colour with one, two or all three colours clipped could have been in the hue and saturation dimensions of the PHLS and SHLS colour models. Depending on the number of channels clipped a different estimation strategy is employed, called tier 1, tier 2 and tier 3 estimations.

The GLI colour model consists of a set of global data and individual pixel data. The global data applies to the entire frame, describing the angles and distances relative to the white balance vector and the apex (the RGB colour space upper limits). These only change if either the white balance or the apex shift. The pixel data consists of four boolean descriptors and up to two angular values. The descriptors specify the regions of the colour space in which the colour resides, including which colour components of red, green or blue are proportionately closest to the limits of the colour space and whether or not the colour has reached these limits. The angular values describe the angle made between these primary colours red, green or blue, which is an invariant to tier 1 channel clipping.

No other previous research has estimated clipped colours in this way. Omer and Werman (2003) recognise this shift and present a method to track the changes in the colour as a line as opposed to modelling and predicting it. Where this approach is weak is when specular reflections are visible and

colour can no longer be modelled as a line. As the GLI colour model computes estimates in polar colour models it has the advantage of having invariants to shadow/shading and specular illumination effects.

Chapter 4

Experimental Methodology

4.1 Goals

The following chapter describes four experiments to test the linearity of the proposed methods and models against those in prior research. The proposed methods are:

- Signal Linear RGB Colour Model (SLRGB)
- Planar HLS Colour Model (PHLS)
- Spherical HLS Colour Model (SHLS)
- Minimum Weighted Colour Comparison (MWCC)
- Gamut Limit Invariant Colour Model (GLI)

While MWCC is included in both the PHLS and SHLS colour models, this method can be applied to many of the previous models. Both SLRGB and MWCC will be tested with any prior colour models that support them to test their applicability to other models and to help make comparisons between prior models and PHLS and SHLS independent of these models/methods.

4.2 RGB Linearisation

4.2.1 Aim

This experiment aims to determine the relationship between the signal noise levels of camera input with various camera settings. It is important to know

how the internal settings of the camera affect the signal linearity when calculating the transformation for the linear RGB space. While the inclination would be to keep these settings fixed, the fact that they affect the image before quantisation means that proper utilisation can increase the quality of the data received. When moving between differently lit environments, a better combination of exposure time, gain and white balance can be found by either the automatic camera functions, or by manual adjustments to these settings by the host application or the user. To ignore these settings would result in an inflexible application unable to make the best use of the capabilities of the camera.

To determine the full signal linearity of the camera, an experiment is conducted which aims to determine the relationship between signal linearity and changes in exposure time, gain and white balance settings. Using this information we can quantify the changes and take them into account when linearising the RGB image from the camera. This will enhance the SLRGB colour space so that it remains linear across any adjustments to the camera properties.

This methodology aims to provide a general way to derive a set of formulae to convert from RGB to SLRGB for any given camera. While every camera will require a different transformation to achieve this, the method presented here may not be the only way to build it. This method is a proof of concept more than a practical solution. It is not within the scope of this work to provide a more automatic solution to calibrating individual cameras for the SLRGB colour space.

4.2.2 Data Set

The medium used for this experiment will be video captured from a PlayStation Eye camera. This camera source is ideal for these purposes as one of its main purposes on the PlayStation console is for computer vision. The camera enables adjustments of exposure and gain, and individual red, green, blue adjustments for white balance. These techniques can be applied to different camera makes and models, although in the case of white balance many cameras use a colour temperature based single value to adjust this.

The videos used are stationary recordings of various static scenes exhibiting a range of colours and shades. By using videos recorded in this way we can measure noise levels of individual pixels which should physically remain at fixed levels without the presence of noise. Because of the impossibility of achieving a completely motionless camera and scene, pixels were excluded from evaluation which existed on or around high frequency regions otherwise known as edges. These pixels can vary greatly in detected colour when small movements affect the position of the edges even at a sub pixel level. The remaining pixels are only affected in a minor way by these changes as their neighbouring pixels have an insignificant difference in colour.

These sequences were captured using different white balance, gain and exposure settings on the camera providing separate sets of signal linearity information which correspond to these settings. These sequences are 500 frames each with 17 unique camera configurations in total, all recorded under the same conditions but with different camera settings. Figure 4.1 shows a set of single frames from four of the plasticine video sequences.

4.2.3 Method of Evaluation

As previously discussed, when detecting light to build an image of the scene, a colour camera uses separate colour sensors to detect the red, green and blue intensities at any given location. Each colour sensor is separate and distinct within the camera so it can be assumed that the signal noise is also independent for each sensor. Also, because each set of colour sensors for a given colour channel are almost identical, the assumption is made that each set of sensors (red, green and blue) will exhibit very similar noise properties.

For this experiment each valid pixel is measured across all 500 frames for each sequence, resulting in an average intensity for each colour channel and a standard deviation describing the width of the noise distribution. These values are then combined with all those from other sequences consisting of the same camera properties. The resulting set of standard deviation values are then ordered according to average brightness forming a plot of the signal noise level at each brightness for each channel.

Using these plots, the relationship between changes in signal noise and

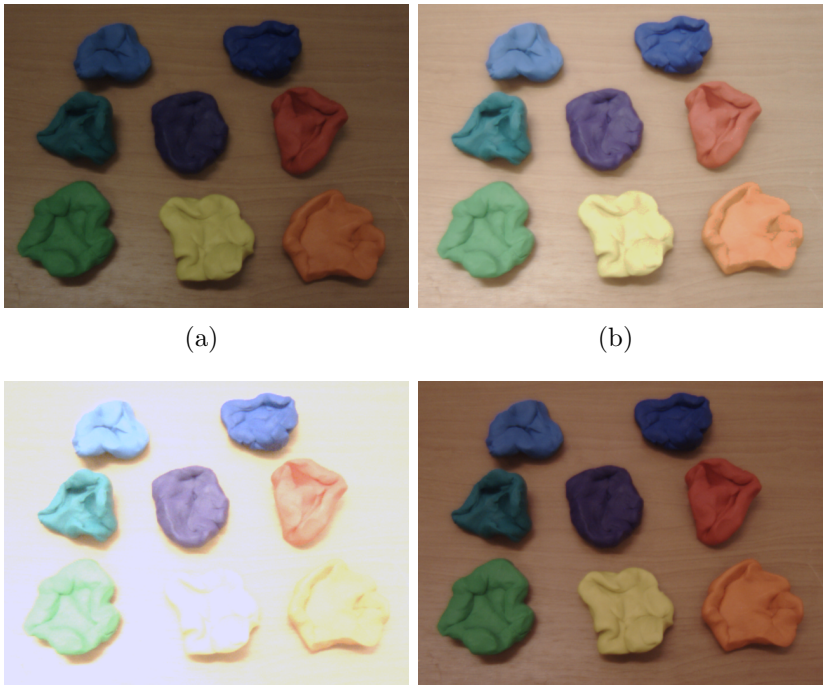

(a) (b)

(c) (d)

Figure 4.1: A frame from the video sequence of plasticine shapes, (a) shows the sequence under standard settings with (b) showing increased exposure time, (c) showing increased gain and (d) showing red shifted white balance.

each of these camera properties can be estimated so that it can be extrapolated later to maintain identical signal noise level under any configuration. The accuracy of this model is then tested on a set of video sequences containing a scene not used for the model derivation.

4.3 Transformation Linearity

4.3.1 Aim

This experiment aims to comprehensively evaluate current and proposed colour measures for transformation linearity. Each of the colour measures transform the original linear space in some way, which often alters the noise distribution in the space, especially when polar coordinates are used. An ideal colour measure for computer vision would represent one of the three decorrelated axes and maintain uniform noise across the space when comparing colours.

4.3.2 Data Set

To evaluate transformation linearity, a synthetic image with simulated Gaussian noise is used rather than real video for two reasons. First, most common scenes only have a narrow distribution of colours contained in them, and most cameras do not detect the full gamut of colours. It is almost impossible to evaluate the complete space using such incomplete information and limited data at high saturations. To get the widest gamut possible using a camera, a palette image would have to be introduced which is a synthetic addition itself and so does not completely solve this problem. Secondly, by evaluating the colour spaces based on data that is known to have uniform noise, the problem of achieving signal linearity in the RGB space is completely separated out from that of maintaining linearity when transforming to a decorrelated space. Figure 4.2 shows one of the test images used containing evenly spaced colours across the entire RGB space.

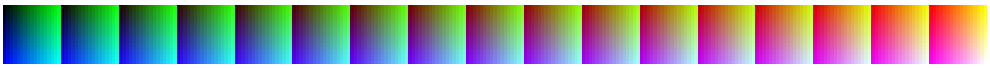

Figure 4.2: An even distribution of colours in the RGB colour space.

4.3.3 Models/Methods Evaluated

The colour models being evaluated in this experiment have been broken up into their individual components or colour measures. This is so that they can be evaluated independently of their parent model. This is an advantage because it means that individual components can be found to be good measures even if the parent model overall is not. Unfortunately when comparing measures in a known linear space, measures based on human perception will be at a disadvantage because they distort the source space to fit human perceptive differences. These types of models often have better results than those fixed to the raw RGB from a camera because cameras are designed with human vision in mind. However, this experiment is working from a controlled linear source model. This is to simulate the effects of SLRGB, or any other transformation of the RGB space into a signal linear one.

The colour components being evaluated have been divided into four distinct categories. The first category is measures of luminance, which are all those that attempt to measure the brightness or power of the light, perceived, physical or otherwise. These include:

- Luma (YUV_Y)
- CIE Lab_L
- CIE Luv_L
- HLS_L
- HSV_V
- Additive (PHLS_L, HSI_I)
- Euclidean (SHLS_L)

The second category includes all of the hue components from various prior models and proposed methods. Many of these measures will result in identical values but have been included for completeness. These include:

- LCH_H^{lab}
- LCH_H^{luv}
- HLS_H
- PHLS_H
- SHLS_H
- HSI_H
- IHLS_H

The third category includes all of the saturation components from various prior models and proposed methods. This is the most varied category and can be split again into two subcategories:

- Chroma
  - LCH_C^{lab}
  - LCH_C^{luv}
  - HSI_S
  - max-min
  - L1 norm
  - L2 norm
- Purity
  - LCH_S^{luv}
  - HLS_S

  - HSV_S
  - $PHLS_S$
  - $SHLS_S$

Lastly, non polar colour models are in the final category. These colour models can be further divided into two subcategories:

- Trichromatic
  - RGB
  - CIE XYZ
- Chromatic Plane
  - nRGB
  - YUV
  - CIE Lab
  - CIE Luv
  - Opponent

While MWCC is already applied to the PHLS and SHLS colour comparisons, it can also be applied to all colour components which converge. To evaluate the effectiveness of MWCC all components from the category hue, the subcategory purity of saturation and the nRGB colour model will be tested with and without MWCC.

4.3.4 Method of Evaluation

To create the test image, the RGB palette image from Figure 4.2 is duplicated 500 times with each having random Gaussian noise applied to each channel, creating 500 frames of noisy video. The sequence is then transformed using each of the colour components being evaluated, including an average image of the sequence $\mu(x, y)$. Using the appropriate difference calculations, the

standard deviation $\sigma(x, y)$ is then calculated for each pixel in the transformed sequence $c(x, y)$ over all 500 frames:

$$\sigma(x, y) = \sqrt{\frac{1}{500} \sum_{i=1}^{500} (c(x, y)_i - \mu(x, y))^2} \tag{4.1}$$

The result is a standard deviation representing the noise in the evaluated measure for each colour present in the original palette image. By analysing this data we can determine how uniform noise is for a given colour measure when calculated directly from an RGB space with uniform noise itself.

4.4 Pixel Classification

4.4.1 Aim

This experiment aims to evaluate current and proposed colour measures for signal linearity on captured video. Because captured camera data does not always conform to the modelled expectations, it is important to test the linearity of the measures with real video as input. By classifying pixels from a set of simple coloured objects using minimum thresholds for each, the uniformity of these minimum thresholds indicates the uniformity of colour comparisons across the space.

4.4.2 Data Set

The medium used for this experiment will be video captured from a PlayStation Eye camera. The video used is a stationary recording of a group of plasticine shapes each consisting of a different colour, shown previously in Figure 4.1. These shapes represent objects in a scene which, at least on the surface, are made up of primarily the same substance. The shapes have the same chromatic properties across their surfaces, but because of large variations in shape and texture of the surface they appear highly varied to the camera. This allows the evaluation of illumination invariance in particular.

4.4.3 Models/Methods Evaluated

In this experiment, all of the components previously evaluated in Section 4.3 will be evaluated again with some notable additions. Since this experiment is based on real camera data, the SLRGB colour model can be used to linearise the source colour space. The SLRGB colour model is used as a condition in this experiment, with evaluations being done using both the RGB and SLRGB colour models as a base colour model. While this will not necessarily be of benefit to the human perceptual CIE models, as previously discussed, they will be included in both forms for completeness.

In the previous experiment the GLI colour model was not evaluated because it models how colours shift when excess light is received by the camera. This experiment can evaluate the use of GLI, by using video sequences recorded with different gain settings. By increasing gain brightness is increased, shifting colours out of the colour range of the camera. GLI is tested with both PHLS and SHLS measures to determine if it provides any improvement on these models.

4.4.4 Method of Evaluation

This experiment aims to determine the minimum thresholds necessary in a colour space to correctly classify most of an object. To determine this we must first create a ground truth classification to compare against. Figure 4.3 shows a combined ground truth mask for each of the different coloured objects in the video. A large region within each object was selected which included varying shades of the object. The minimum threshold is determined to be the minimum range sufficient to classify 95% of the pixels within the mask only. This number was chosen as it represents two standard deviations from average colour. The thresholding is insufficient to exclude many of the pixels outside the coloured object because only one colour component of a model is evaluated at a time. This is acceptable as it allows analysis of each component individually, checking for consistency of threshold ranges between coloured objects. Using the thresholds from each of the components of each model, the complete models can be evaluated for their discriminative power from the rest of the scene. A more traditional ROC analysis was

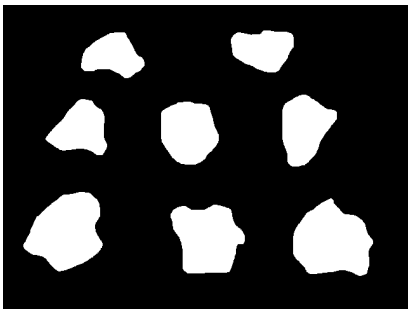

Figure 4.3: The plasticine colour shape mask image.

considered but was determined to be unsuitable for this evaluation. This is because what we evaluating is not the general classification success, which would favour wider tolerances. What we aim to discover is how general a single classification scheme can be made for a range of differently coloured objects and how much discriminative power this provides. To extract this information from a ROC analysis would require test images which cannot be created sufficiently without synthesising them.

Chapter 5

Results

5.1 RGB Linearisation

The following section covers the results found from the RGB linearisation process to form the Signal-Linear RGB colour model. The first part evaluates how changes in hardware based white balance affect the signal noise on a camera. This is followed by the effect of changes in exposure settings. Evaluating changes in gain concludes the investigation of the three camera parameters. The final part evaluates how these are combined with overall linearisation information to maintain linearity of signal noise under changes to these settings due to automatic or manual processes.

5.1.1 White Balance

The first camera parameter investigated is white balance. Many cameras have a simplified one dimensional white balance, usually corresponding to the colour temperature of the light source. Some cameras allow for a higher level of control by using two parameters to describe white balance, using normalised colours to reduce the number of colour parameters from three to two. The camera used in these experiments allows for the ability to specify white balance using three parameters; red, green and blue. This is useful as while it allows the greatest level of control, it also provides the most information about the transformations applied to the image. It also means that it is likely that the effects of each parameter are localised to their respective channels only.

To verify this and to determine the relationship between the camera white balance parameters $w_{\{r,g,b\}}$ the signal noise was measured for each colour channel with different white balance configurations. The initial white balance

$w_{\{r,g,b\}} = \{50, 50, 120\}$ was the white balance from the camera's automatic adjustments. Each parameter was then increased by 20%, followed by an increase of 40% of the original. This allows for a range of balanced and imbalanced settings to be tested, although the limitations of testing with every configuration of the three parameters meant that only three levels for each could be used. These 500 frame videos were then analysed for noise in each pixel and each channel, resulting in three mean intensities and standard deviations for each pixel. This data was then reordered by intensity for each channel with any duplicate intensities averaged.

Figures 5.1, 5.2 and 5.3 shows this standard deviation data for the colour channels; red, green and blue respectively. Each series is labelled with the parameters in red-green-blue format, with parentheses surrounding the parameters which correspond to the channel graphed. From the graphs shown it can be seen that in all cases, noise is unaffected by changes in the parameters of the other channels. This empirically confirms the assertion that each white balance parameter only affects one of each of the colour channels. This allows us to simplify any linearisation formula to only require one of these parameters rather than three.

From this data a function can be estimated to find correspondence between the noise distributions at different white balances. The function used by the camera for this transformation is determined by employing a genetic algorithm, which is used to search out a formula that closely describes the shift in noise observed when altering the white balance. The genetic algorithm software package Eureqa, was used for this. Using its default settings to derive a set of possible solutions and selecting the most appropriate solution. It was found that using the following function to transform the standard deviation data, the datasets would correspond with an R-squared value of 0.960481:

$$f_w(w) = \frac{1}{1 + 0.0240785w} \tag{5.1}$$

This works for all three colour channels in an identical way, bringing all channels to the same level. This adjustment can be seen in Figure 5.4, where all curves closely align every channel and every white balance parameter

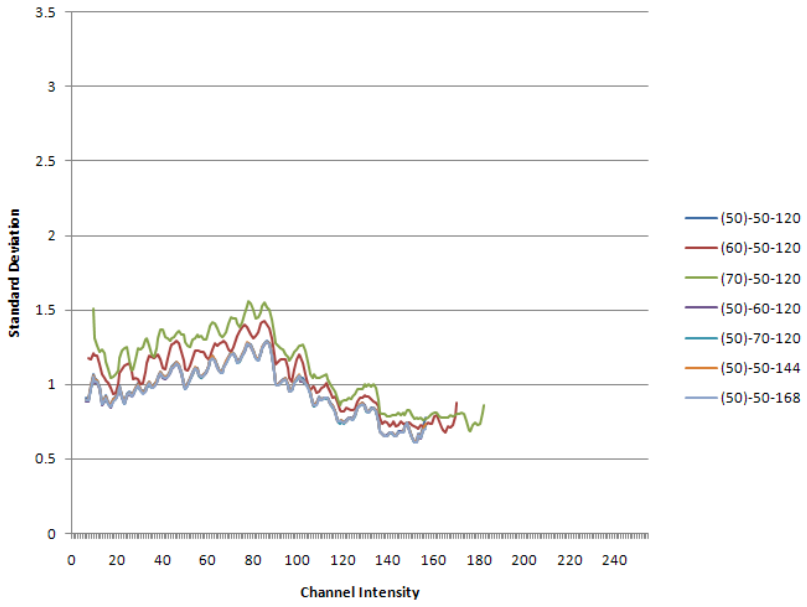

Figure 5.1: Standard deviation of the measured signal noise in the red channel at different camera white balance settings, with each data series labelled in the format (w_r)-w_g-w_b.

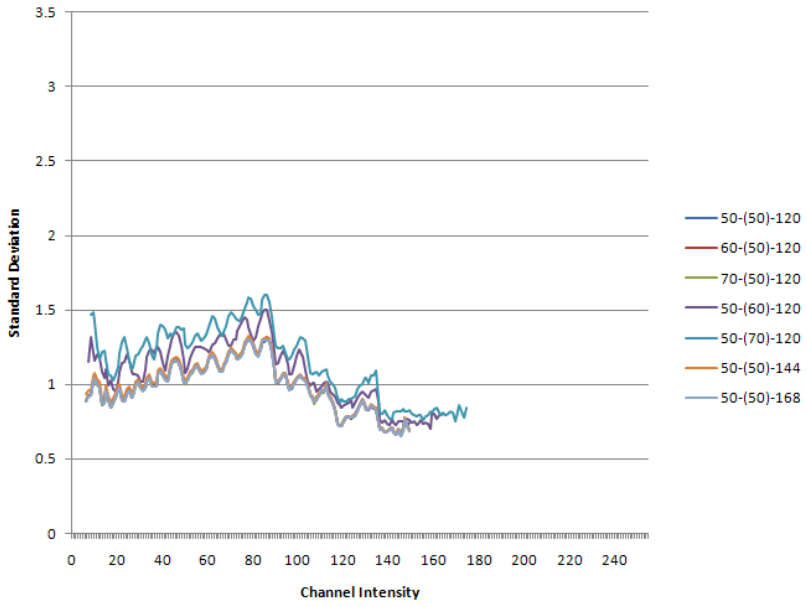

Figure 5.2: Standard deviation of the measured signal noise in the green channel at different camera white balance settings, with each data series labelled in the format w_r-(w_g)-w_b.

Figure 5.3: Standard deviation of the measured signal noise in the blue channel at different camera white balance settings, with each data series labelled in the format w_r-w_g-(w_b).

setting.

5.1.2 Exposure

The second camera parameter tested was exposure. This adjusts the elapsed time the photo sensitive chip inside the camera is receiving light in each frame of video. So while increasing exposure time allows for a higher sensitivity to lower light levels, it also increases the level of motion blur in moving scenes. In this experiment we used video at three different exposure settings; 150, 300 and 450 in the camera's units, which correspond in this case to 50Hz, 25Hz and 12.5Hz refresh rates respectively. These settings are selected specifically because they are synchronised with the frequency of the light source which is 50Hz. When the camera exposure is deviated from these intervals, a visible flickering of the video occurs caused by frames being captured at different stages of the light's emission cycle.

The signal noise was measured and collated using the same method as in section 5.1.1 resulting in a noise mapping for each channel relative to

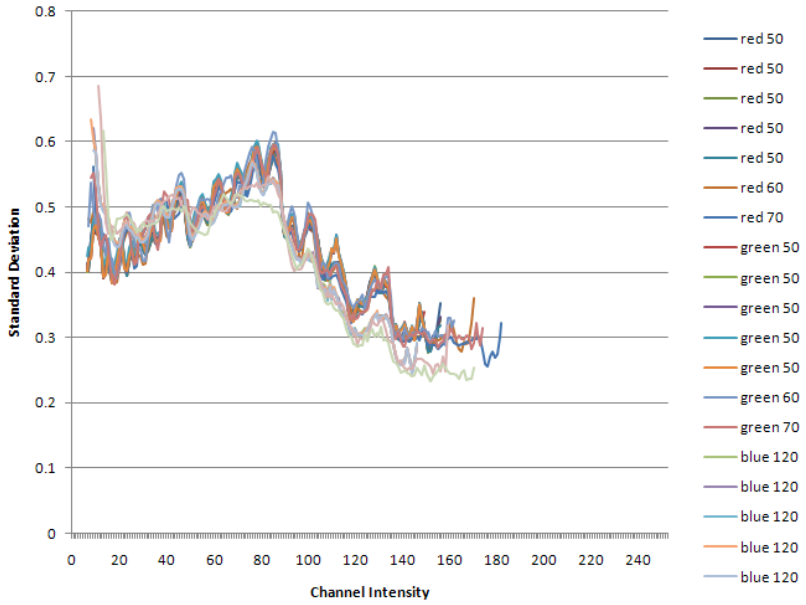

Figure 5.4: Corrected signal noise at different white balance settings.

intensity. Figures 5.5, 5.6 and 5.7 show how these mappings shift as exposure is changed for each of the colour channels; red, green and blue respectively. What can be seen from these graphs is that in terms of noise at a given intensity, nothing changes when the exposure parameter is altered. This means that nothing needs to be done to the received image to correct for exposure. There is an expected increase in the mean intensity when exposure is increased because a longer exposure means more light is received by the camera. However the primary concern is to correct linearity, so this shift is unimportant.

It can also be observed in the graphs that there is a sharp increase in noise at the higher intensities when exposure is increased. It is believed that the reason for this is because the photo sensors in the camera have an optimal range. When the exposure is too long the sensors get over saturated with light and become less accurate. Usually the exposure is set to avoid reaching these limits in conjunction with gain to position the optimal sensor range within the limits of the 24 bit numbering system.

The function therefore to calculate the correspondence between noise data

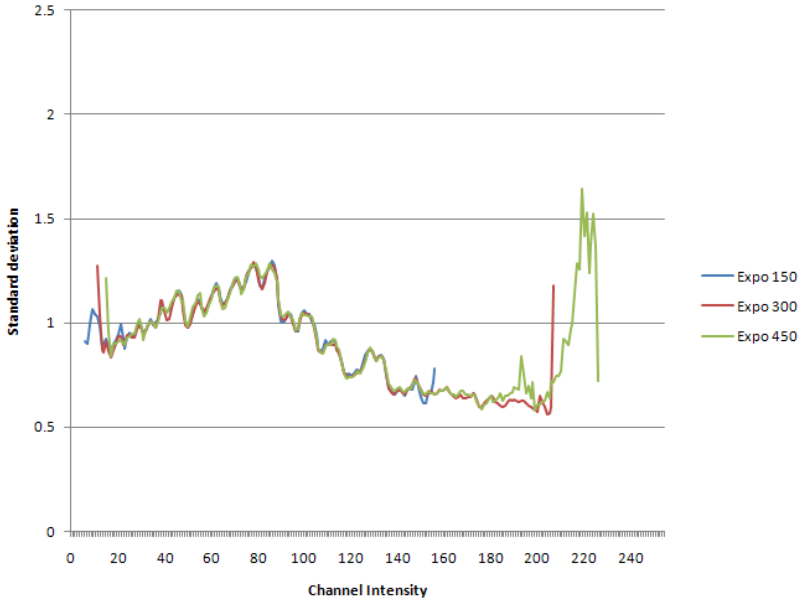

Figure 5.5: Standard deviation of the measured signal noise in the red channel at different camera exposure settings.

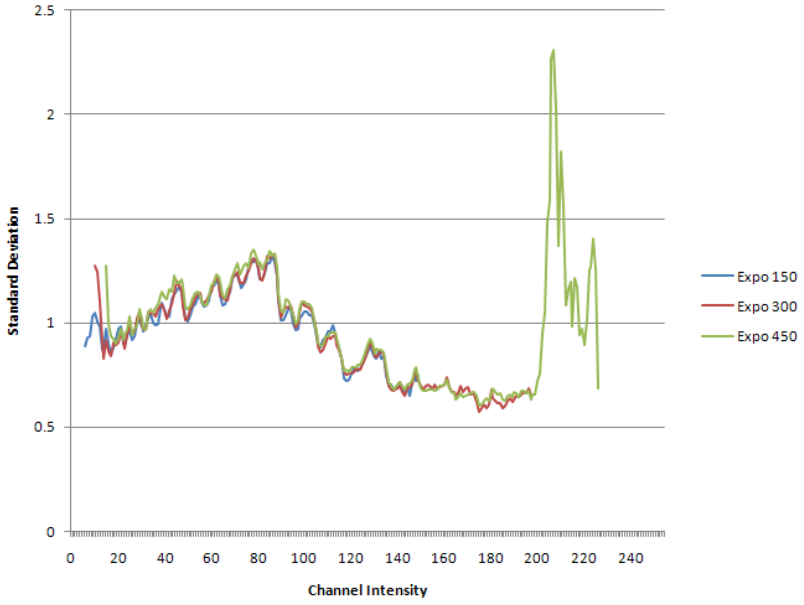

Figure 5.6: Standard deviation of the measured signal noise in the green channel at different camera exposure settings.

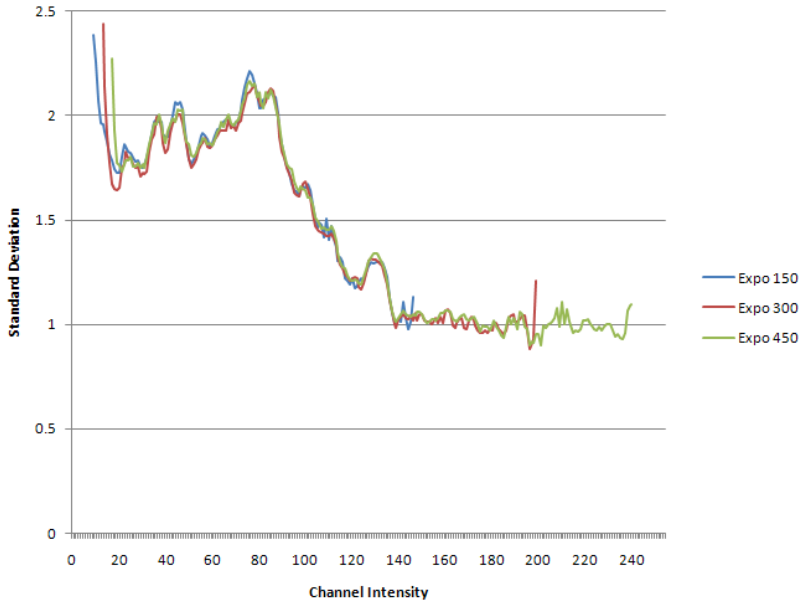

Figure 5.7: Standard deviation of the measured signal noise in the blue channel at different camera exposure settings.

for changes to exposure is simply:

$$f_e(e) = 1 \tag{5.2}$$

Since no changes are necessary the function of exposure factor is the constant 1. While this does not have any effect on the transformation, it is still useful to model as it may not be the same for all cameras.

5.1.3 Gain

The final camera parameter tested was gain. Gain is an adjustment in scale of the image data before it undergoes quantisation. The primary use of gain is to fit the ranges of intensities observed into the three 8 bit channels transmitted to the computer. By fitting the data well, minimal important information is lost when this conversion takes place. This is why gain adjustments should not be performed after receiving the images from the camera, because by this stage the accuracy is already lost. In this experiment we used video at eight different gain settings; 0, 10, 20, 30, 40, 50, 60 and 70. These gain

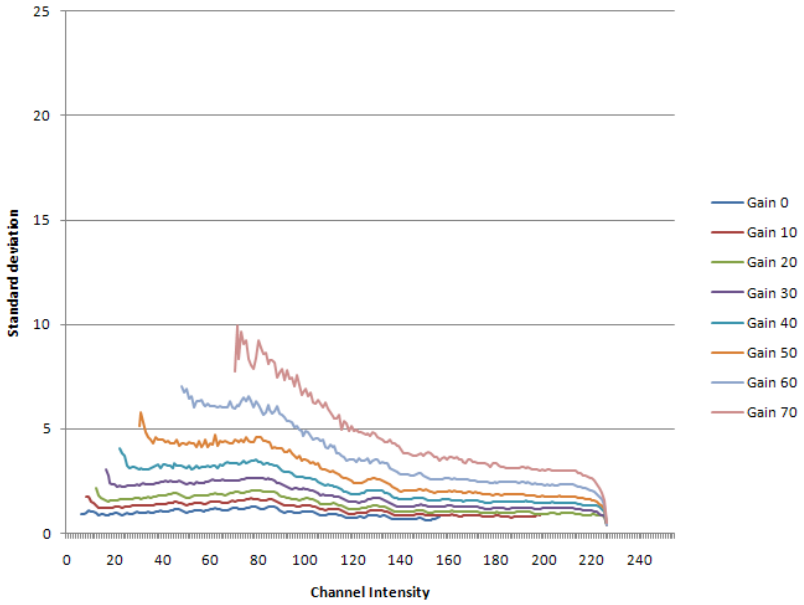

Figure 5.8: Standard deviation of the measured signal noise in the red channel at different camera gain settings.

settings cover the complete range of values provided by the camera and have no specific units.

The signal noise was measured and collated again using the same method as in Section 5.1.1 resulting in a noise mapping for each channel relative to intensity. Figures 5.8, 5.9 and 5.10 show how these mappings vary as gain is changed for each of the colour channels; red, green and blue respectively. What these graphs illustrate is that as camera gain is increased the noise observed at each intensity is also increased. This observation is consistent with the rationale that gain scales the intensities after detection, suggesting that signal noise would also be scaled in this transformation. The sudden drops seen at the higher intensities indicate the boundaries of the colour space. When these limits are approached, the noise level significantly reduces as they begin to be clipped to intensities closer to the average intensity.

The function used by the camera for this transformation is determined by employing a genetic algorithm, which is used to search out a formula that closely describes the shift in noise observed when altering gain. What was found was that the gain transformation required the use of the intensity to

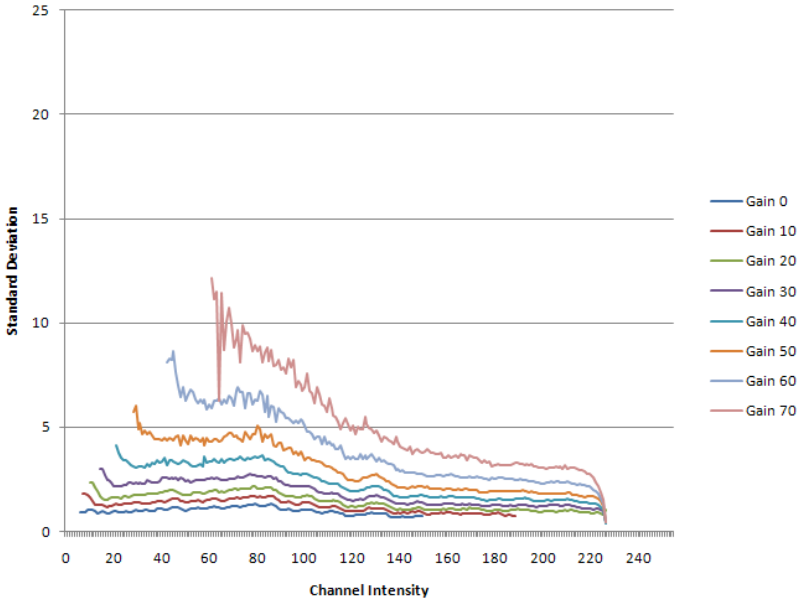

Figure 5.9: Standard deviation of the measured signal noise in the green channel at different camera gain settings.

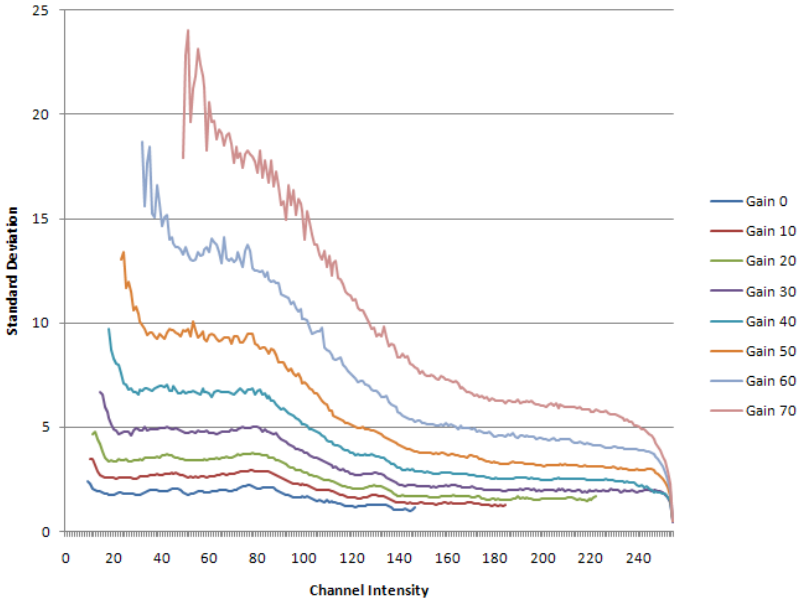

Figure 5.10: Standard deviation of the measured signal noise in the blue channel at different camera gain settings.

properly correlate between gain settings. The following function was found to be a close approximation to the camera gain transformation, where g refers to the gain parameter and i to the intensity of a pixel:

$$f_g(g,i) = \frac{\frac{8256.54}{(g-0.0375127)} + 64120.3g + gi^2 - 105.892i^2 - 348.631g^2 - 2822390}{-105.892i^2 - 3042490} \tag{5.3}$$

This function is camera dependent but not colour channel dependent, being the same for the red, green and blue channels.

5.1.4 Linearisation

The final experiment aims to determine the overall linearity function for the camera after the camera parameters have been corrected for, and all of the noise levels equalised. When corrected, this will result in all of the noise distributions averaging around 1, indicating that every intensity level of every channel will have a standard deviation of approximately 1. The distributions shown in previous sections show that the noise level shifts considerably across the RGB space, peaking at around 80.

All three colour channels are fit together for the reason that if they were each given unique curves, this would cause colour ratio shifts across the space. When analysing a colour object in a scene, under good conditions with no specular reflection, it should maintain the same ratio of R:G:B despite changes in shadow or shading. If each colour channel was transformed differently to the others, these relationships between red, green and blue would also shift with changes in intensity. When all three channels use the same function for transformation, despite shifts in overall colour ratio, any colour ratios that matched in the original RGB colour space will also match in the transformed colour space.

Such a relationship was estimated by employing a genetic algorithm as used for white balance and gain. This was used to search out a formula that fit the curve of the data:

$$f_l(i) = 0.306594 + \frac{130.441}{-9.50227i + e^{0.0650091i} + 1127.6} \tag{5.4}$$

This transformation closely follows the overall variation of the changes in noise without over fitting to localised minima and maxima. Figure 5.11 shows how this linearity curve lies in relation to the curves of the corrected three channels of the base video settings.

Combined, this allows the estimation of the noise for a channel intensity under given camera parameters:

$$f(i, w, e, g) = \frac{f_l(i)}{f_w(w) f_g(g, i) f_e(e)} \tag{5.5}$$

While this in itself is useful, the primary aim is to have a colour space in which this curve is always equal to 1, meaning there is no variation in noise across the entire colour space. Otherwise, when converting to illumination invariant colour spaces, even more complex calculations would need to be made to estimate noise correctly. To achieve this aim, the colour space needs to be distorted by stretching or compressing the space at specific points to change the variation of the signal. To do this, the integral of the inverse function in equation 5.5 is used to rearrange intensities from the camera into a signal uniform spacing. A Riemann sum is used to approximate this integral, with a transformed intensity i' being transformed from i as follows:

$$i' = \sum_{n=1}^{i} \frac{1}{f(i, w, e, g)} \tag{5.6}$$

By transforming the RGB space in this way before any image processing, all certainties in all directions of the three dimensional space will be approximately equal. The following Figures 5.12, 5.13 and 5.14 show the results from the white balance, exposure and gain experiments respectively. They are all run with the same data, but first transformed using equation 5.6. Aside from the spikes at the limits of the colour ranges, the linearisation is successful at averaging signal noise at 1. These spikes are believed to be present for two reasons. The first, dips are believed to be the result of measuring standard deviation in close proximity to a limits of the colour space, after clipping from a wider colour space within the camera. The second, large values are believed to be due to light levels exceeding the sensors capability but falling

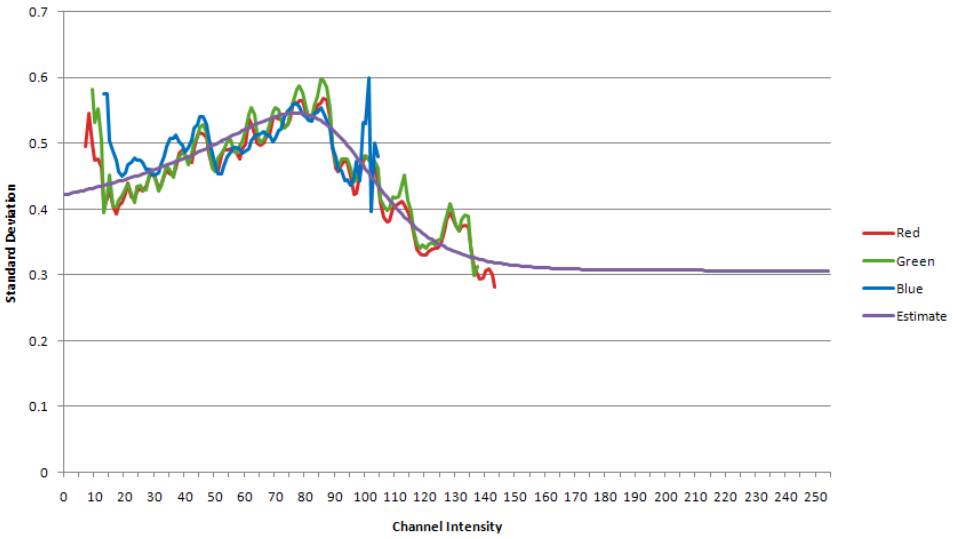

Figure 5.11: The linearity curve estimation in relation to the curves of the adjusted three channels of the base video settings of white balance$_{\{r,g,b\}} = \{50, 50, 120\}$, gain $= 0$ and exposure $= 150$.

within the clipped colour space transmitted by the camera. Gain is the most problematic with lower intensities under higher levels of gain exhibiting much larger fluctuations of the detected noise.

Overall, the linearisation of signal noise was successful with the Signal Linear RGB colour space having an approximately uniform noise with a standard deviation of 1 over the space. Experiments in Section 5.3 test the performance of SLRGB for pixel classification with images captured from the camera. These measure the improvements this transformation provides compared to using the RGB information from the camera directly.

5.2 Transformation Linearity

In the following section the results for the transformation linearity experiment are presented. This compares various colour models as transforms from a linear space. By measuring noise levels on each component from an image with artificial uniform Gaussian noise, we can determine the level to which each space maintains the linearity of noise. This simulates the end result of converting to the SLRGB space when configured perfectly. Avoiding possible

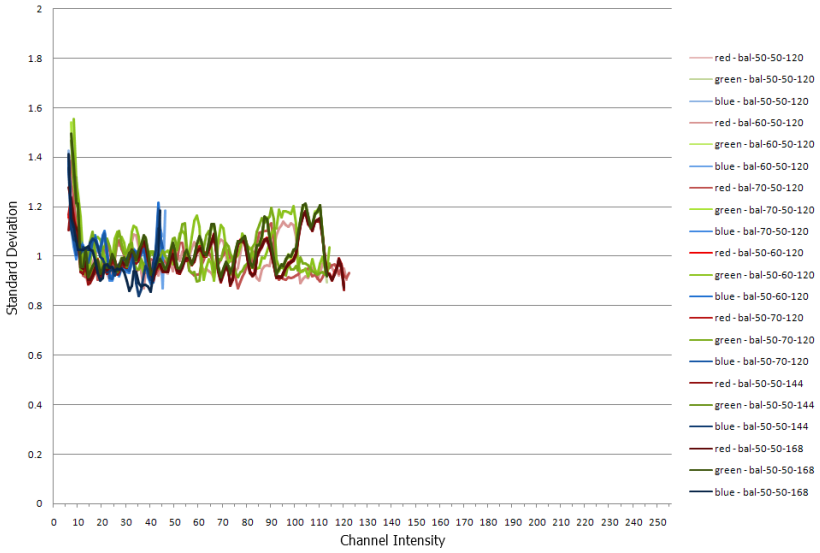

Figure 5.12: Standard deviation of the linearised signal noise in all channels at different camera white balance settings.

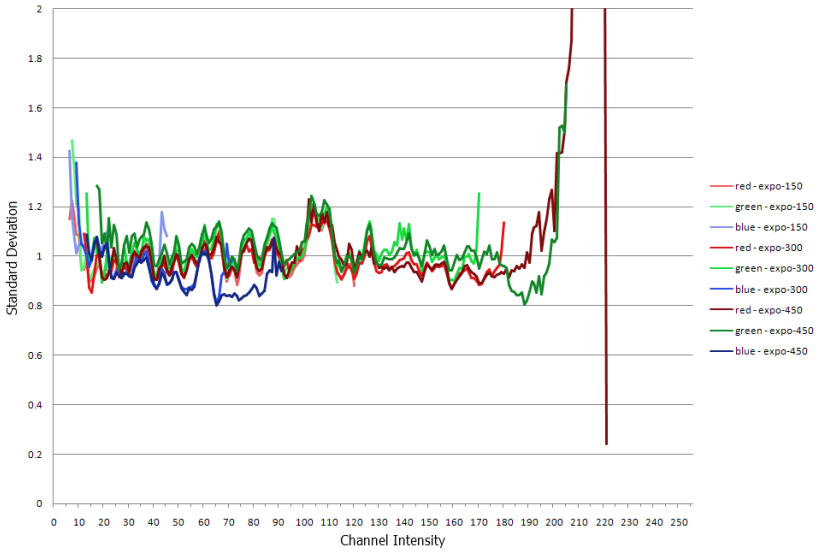

Figure 5.13: Standard deviation of the linearised signal noise in all channels at different camera exposure settings.

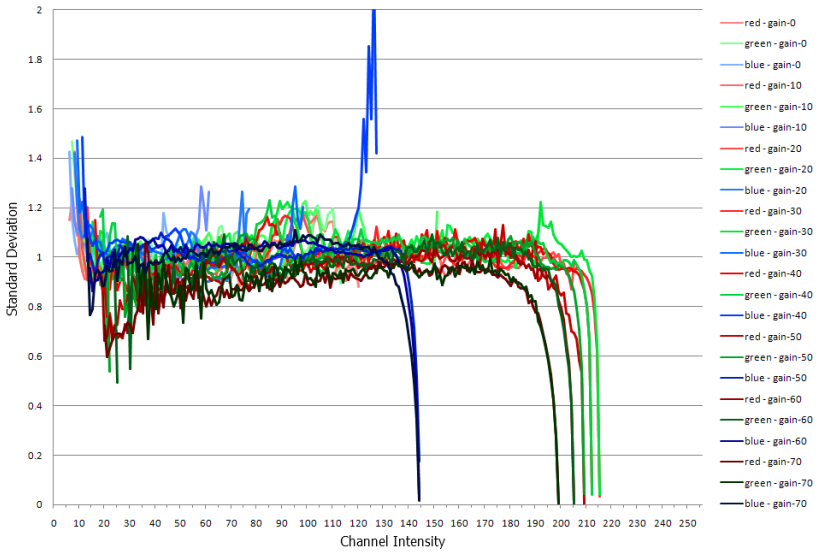

Figure 5.14: Standard deviation of the linearised signal noise in all channels at different camera gain settings.

inaccuracies from the SLRGB transformation allows the evaluation of colour transforms to be independent of the source model's noise distribution. The image used for this contains evenly spaced colours covering the entire RGB space before noise is applied.

The results of this are presented in two forms. The first is an image containing the standard deviations of the noise for each pixel from the base image shown in Figure 4.2. These are scaled so that the average standard deviation is half way between white and black. This ensures the most important information is visible and allows for simple comparison between the colour model components. The second form is a normalised interquartile range of the standard deviations calculated for each pixel. This measure best demonstrates the amount of variation within the space of noise, while reducing the effect of outliers caused by unrelated spikes in noise. These might include the drop encountered when noise is restricted by the limits of the colour space.

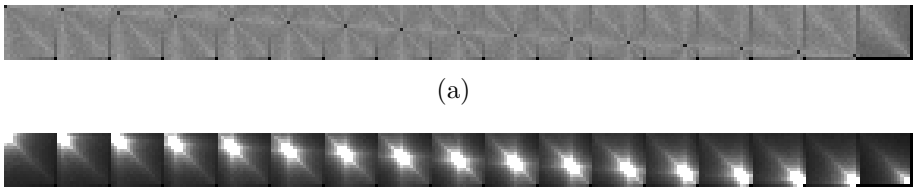

(a)

(b)

Figure 5.15: The normalised standard deviations for each pixel of the source image using the HLS/HSV hue measures (a) weighted using MWCC and (b) unweighted (flat grey indicates no variation in noise while visible changes in pixel brightness indicates variation of noise).

5.2.1 Hue Components

Firstly, all of the hue-type components are investigated and compared. The main issue when comparing hues is that they are represented as angles, and as discussed previously this causes different levels of signal noise depending on saturation. MWCC attempts to correct this by translating angular differences into arc lengths, using the saturation and luminance measures to calculate the radial distance of each colour. The amount of difference this makes to linearity of the space is substantial as can be seen in Figure 5.15. This shows how noise is distributed over the image when using MWCC for HLS/HSV hue differences and when not using this weighting. Figure 5.16 shows how each of the hue measures improve when MWCC is used, with every measure seeing improvement from this weighting.

Comparison is done between each of the hue measures using MWCC. This allows for each transformation's linearity preserving properties to be compared more directly. An ideal interquartile range of zero is not possible because the random noise used for each pixel will have a slightly different standard deviation due to probability. This better reflects noise from a real camera and since every measure was run at the same time, each method was subject to identical noise. Another reason perfect linearity is not possible is because of the circular space. That is, we measure hue difference as a distance around the circular space and because of this, the line is curved to varying degrees depending on the distance from the origin. At low saturations the curve has a much larger difference from a straight lined alternative. Straight

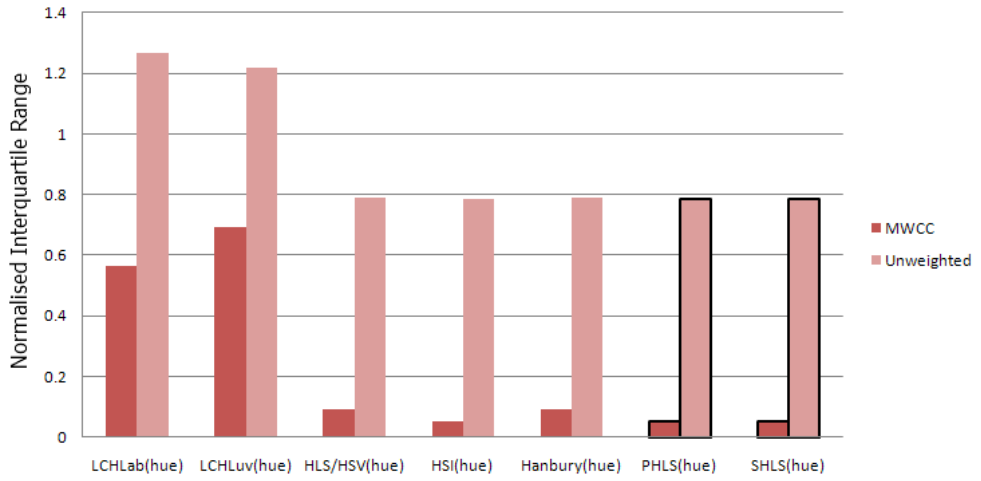

Figure 5.16: Normalised interquartile range of image noise standard deviation for each of the hue measures when weighted using MWCC and without weighting.

line calculations could be made but these would no longer represent accurate differences in hue, which is important in illumination invariance. Using a circular hue measure means small differences where noise is most prevalent the differences are negligible, and with large differences where noise is not an issue, hue changes are calculated much more accurately. For this reason, measures with less invariance will often attain better results as they do not transform the RGB colour space as much, but without decorrelating the measures creating illumination invariants they lack the qualities necessary in situations with real world data.

The graph in Figure 5.17 shows how each of the hue measures performed, showing the normalised interquartile range of the standard deviations across the image. The images in Figure 5.18 show the standard deviations measured at each colour in the image. Clearly LCH_{lab} and LCH_{luv} performed the worst, but this is to be expected for two reasons. First of all they distort the RGB space to better fit human perceptive sensitivities, not taking into account at all the sensitivities of the source. The second reason is that LCH_{lab} and LCH_{luv} sometimes have advantage when working on real camera input because cameras will often be designed to have roughly similar sensitivities to the human eye. This allows these transformations to occasionally gain some

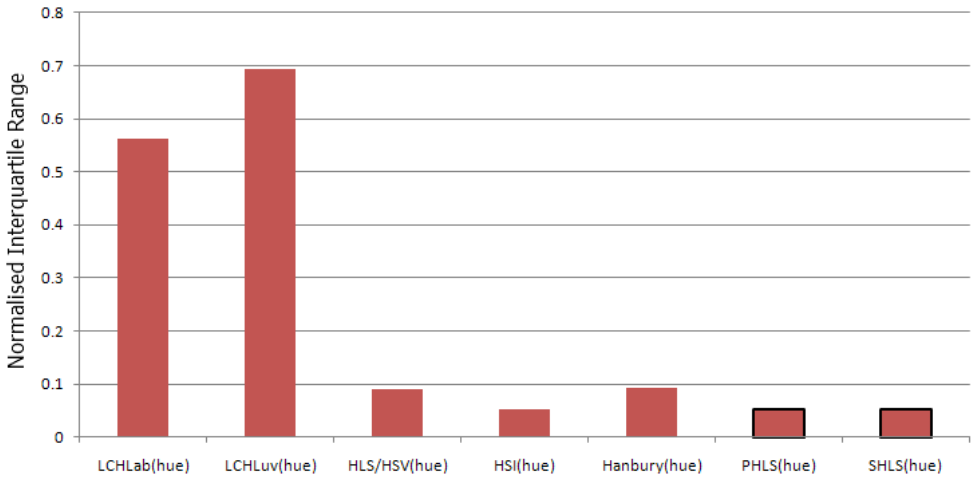

Figure 5.17: Normalised interquartile range of image noise standard deviation for each of the hue measures weighted with MWCC.

advantage in signal linearity when working with real camera data, which in this case it clearly is not. The HLS/HSV and Hanbury measures of hue both perform considerably better than LCH_{lab} and LCH_{luv}, however they are not as uniform as the remaining three. This is because both of these measures distort the chromatic plane from a triangle to a circle, and when using MWCC these distances cause periodic changes in linearity that can be seen in Figures 5.18(c) and 5.18(e). Finally, HSI and the proposed PHLS and SHLS models perform almost equally. This is not surprising as they all take a very similar approach to calculating hue and none of them distort the chromatic plane when making saturation measurements. As can be seen in figures 5.18(d), 5.18(f) and 5.18(g) most of the image consists of evenly distributed noise. It is only really the edges and at the achromatic axis where this noise drops towards zero.

5.2.2 Luminance Components

In this section all of the luminance-type components are investigated and compared. Weighting is not necessary when comparing luminance values because the component is not inherently dependent on the others. For models like CIE Lab the luminance is not linear to the original by design and as

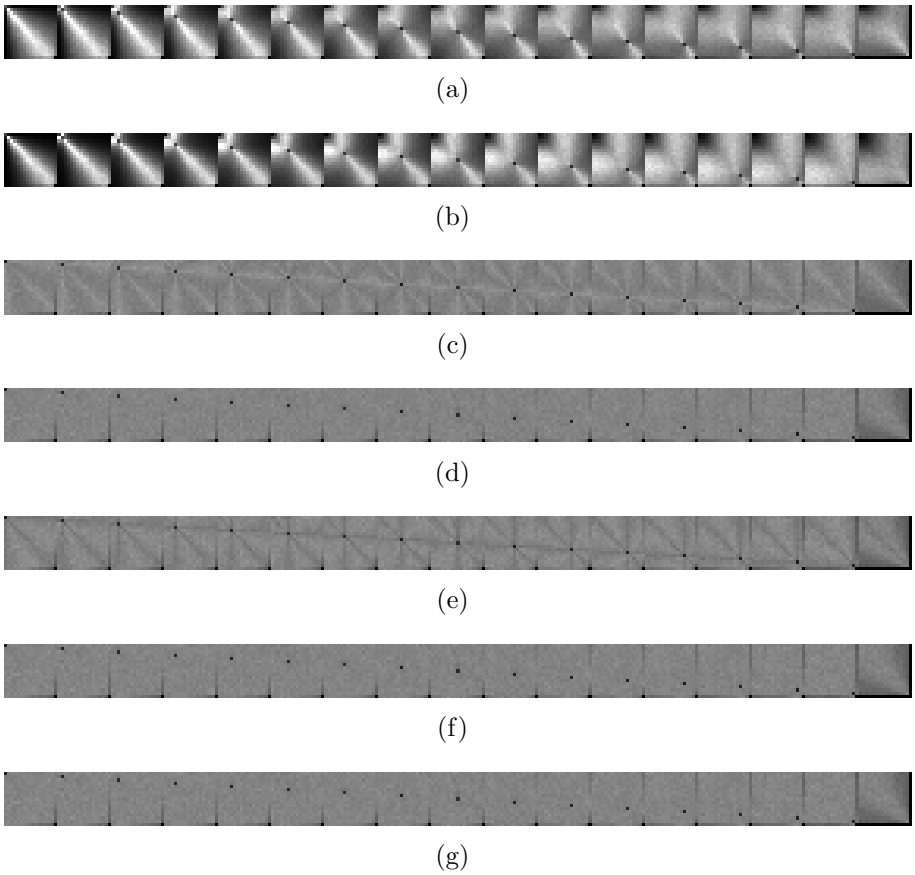

Figure 5.18: The normalised standard deviations for each pixel of the source image using the hue measures weighted using MWCC, (a) LCH_{lab}, (b) LCH_{luv}, (c) HLS/HSV, (d) HSI, (e)Hanbury Hue, (f)PHLS and (g) SHLS (flat grey indicates no variation in noise while visible changes in pixel brightness indicates variation of noise).

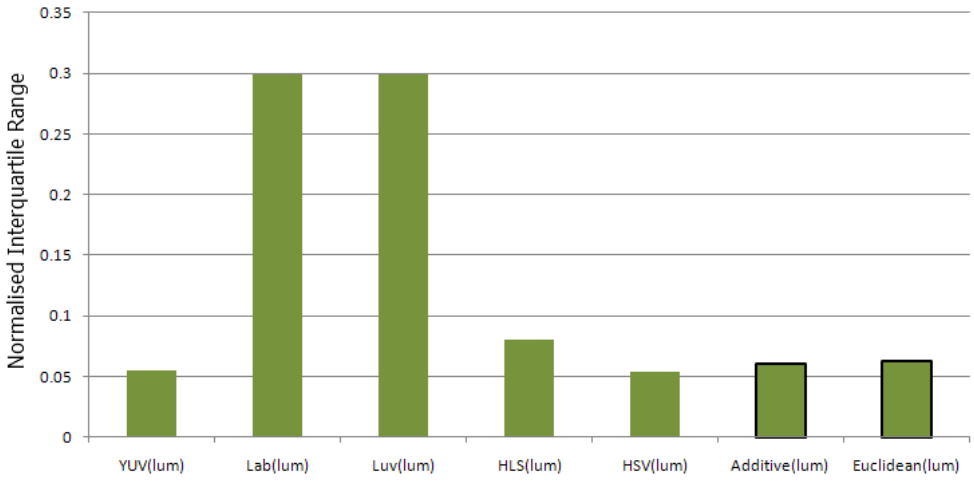

Figure 5.19: Normalised interquartile range of image noise standard deviation for each of the luminance measures.

mentioned in the previous section this may be an unfair comparison. The CIE models are included for completeness and the experiment in Section 5.3 give a better comparison using real camera images.

The graph in Figure 5.19 shows how each of the luminance measures performed, showing the normalised interquartile range of the standard deviations across the image. The images in Figure 5.20 show the standard deviations measured at each colour in the image. CIE Lab and CIE Luv performed the worst at 0.299468 and 0.299468 respectively, but this was expected since they were computed from a linear space. The HLS measures of luminance follows at 0.080006, with the Additive and Euclidean measures coming in at 0.060713 and 0.062196 respectively. The two best measures appear to be YUV and HSV with marginally better results of 0.054361 and 0.05421 respectively. When considering why these methods performed slightly better, their methods of calculation become important.

The YUV luminance measure works by assigning each colour component a weight when averaging them, depending on the component's apparent brightness to the human eye. This means green is given much more weight compared to blue while red sits somewhere in the middle. If the noise applied in this experiment was identical for all three of the components then

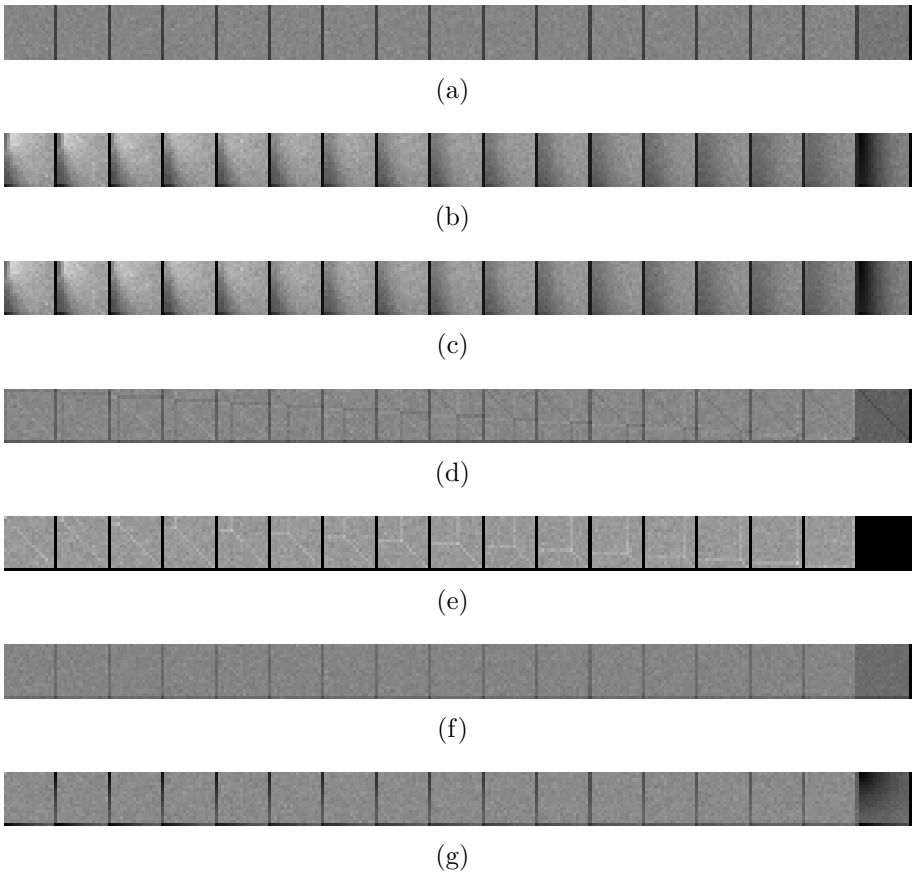

Figure 5.20: The normalised standard deviations for each pixel of the source image using the luminance measures, (a) YUV, (b) CIE Lab, (c) CIE Luv, (d) HLS, (e) HSV, (f) Additive and (g) Euclidean (flat grey indicates no variation in noise while visible changes in pixel brightness indicates variation of noise).

this weighting would have no effect on the linearity calculated. But because real noise was simulated and each component had randomised noise, it is possible for one colour component to receive more noise than the other two, which would either improve or weaken the results of the YUV measure. In this case, same methods were used to measure the linearity of the base RGB colour model which provides an indication of any differences to the noise applied to each of the channels. These results were 0.048956 for red, 0.048016 for green and 0.050594 for blue, coincidentally with green the least noisy and blue the most noisy. This is likely to explain the improvement displayed

by the YUV measure as other than these weightings, it is identical to the Additive method.

The HSV method gets better results for a different reason. This measure of luminance is simply found by taking the maximum of the red, green and blue components for a colour. The marginal improvement it exhibits is because of slightly lower noise due to only using noise from one component at a time. This has the disadvantage of not providing as much information as luminance measures which use all three components, as the contributions of the other two components are ignored.

5.2.3 Saturation Components

In this section all of the saturation type components are investigated and compared. Weighting is not necessary when comparing chroma measures because by their nature they are not dependent on luminance as they already incorporate this information into their interpretation of "colourfulness". Conversely, purity measures can use MWCC for weighting as they are dependent on luminance. Without MWCC, noise greatly increases as luminance is decreased and comparisons are no longer linear. Figure 5.21 shows how each of the purity measures improve when MWCC is used, with every measure unsurprisingly seeing improvement from this weighting. As with the previous components, the CIE models are included for completeness but their performance in this experiment is not necessarily reflective of their performance with real video, and they are evaluated in Section 5.3 which gives a better comparison using real camera images.

Comparing each of the saturation measures directly with each other, using MWCC where applicable, can allow a fair comparison of how well these transformations preserve the linearity of the noise. The graph in Figure 5.22 shows how each of the chroma and purity measures performed, showing the normalised interquartile range of the standard deviations across the image. The images in Figure 5.23 show the standard deviations measured at each colour in the image. LCH_{lab}, LCH_{luv} and LSH_{luv} performed the worst, but it has been previously discussed why this would be the case. Overall, the rest of the chroma measures perform well. Hanbury's Max-Min measure performs

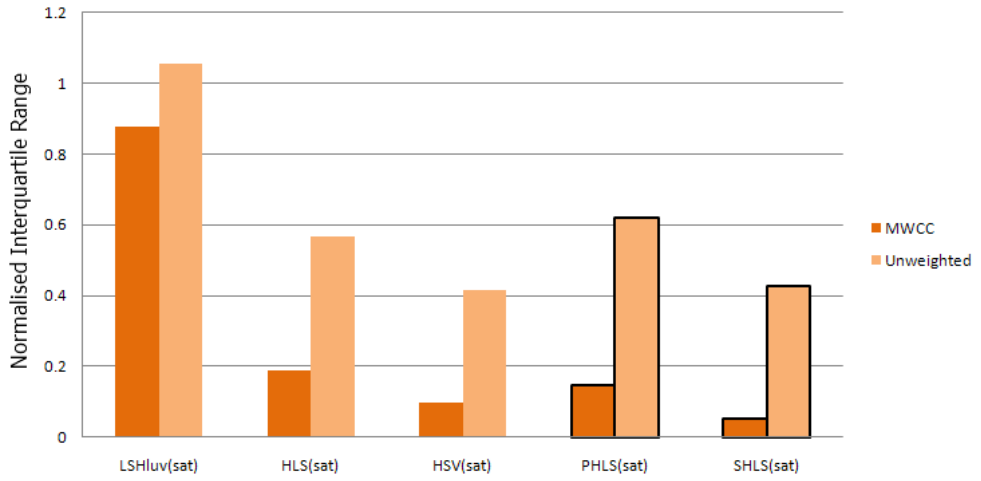

Figure 5.21: Normalised interquartile range of image noise standard deviation for each of the purity measures with and without weighting.

the worst of these due to the fact that it expands the chromatic plane to a circle. While HSI and L2 saturation perform the best at 0.060423. The reason these are identical is because they both measure the direct euclidean distance from the colour to the closest point on the achromatic axis. The main difference between the two being that the HSI formula has parameters for rotational white balancing. The chroma measures were expected to perform better than the purity measures as they do not have to account for a varying coordinate space. However the saturation component of SHLS performs comparably well while using a shadow/shading invariant measure of saturation.

For the purity measures, HLS performs the worst of the non-CIE measures, followed by the PHLS measure. When looking at the noise distribution image for PHLS saturation it becomes clear that it is not completely linear due to the changing shades across the space. Further investigation revealed that this non-linearity is present whenever an illumination invariant (purity based) planar chromatic plane is used. This affects any colour model using a chromatic plane that expands relative to luminance because as saturation increases, a skew is introduced as the angle of the intersection between the luminance and saturation axes becomes more acute. The result of this is

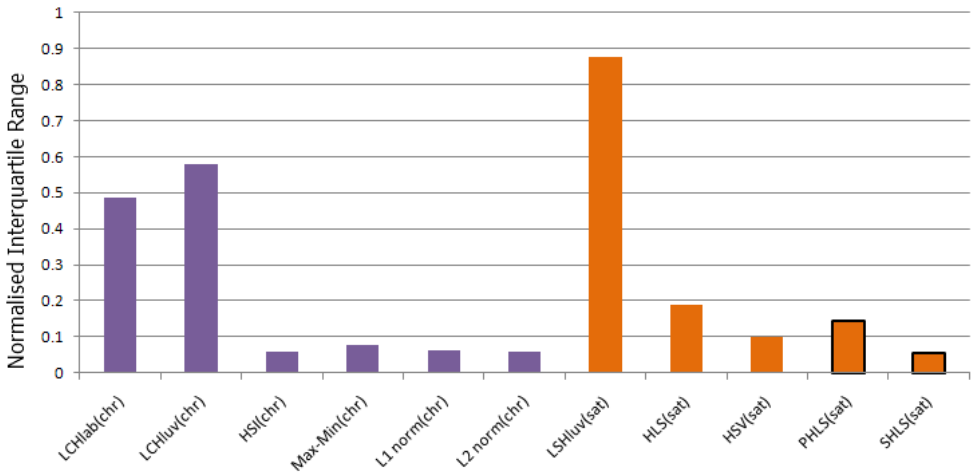

Figure 5.22: Normalised interquartile range of image noise standard deviation for each of the chroma (in purple) and purity (in orange) measures.

a mismatched elliptical region fitting the evenly distributed noise. This is illustrated in Figure 5.24. On the left side a_1 and b_2 show how the saturation and luminance estimates of standard deviation do not fit to the uniform noise of the original space, shown by circles. c_1 shows the region being estimated by this method as an ellipse which becomes further distorted as saturation increases. The SHLS model uses a spherical chromatic plane and so maps saturation as an angle as shown on the right. This means that all of the saturation ranges a_2, b_2 and c_2 lie perpendicular to the chromatic plane, estimating circles which closely match the noise of the linear underlying model.

A solution was found to correct for this by increasing saturation differences based on their distance from the origin, however this was found to be inadequate when white balancing was required. Because of the method of white balancing used with the PHLS colour model, the calculation of this difference correction function becomes much more complex. A rotationally applied white balance could be used but some of the extra complexity required to compare saturation values is still present. This was discovered to also apply to the nRGB colour model making it unsuitable for applications which require linearity but not invariance to specular highlights.

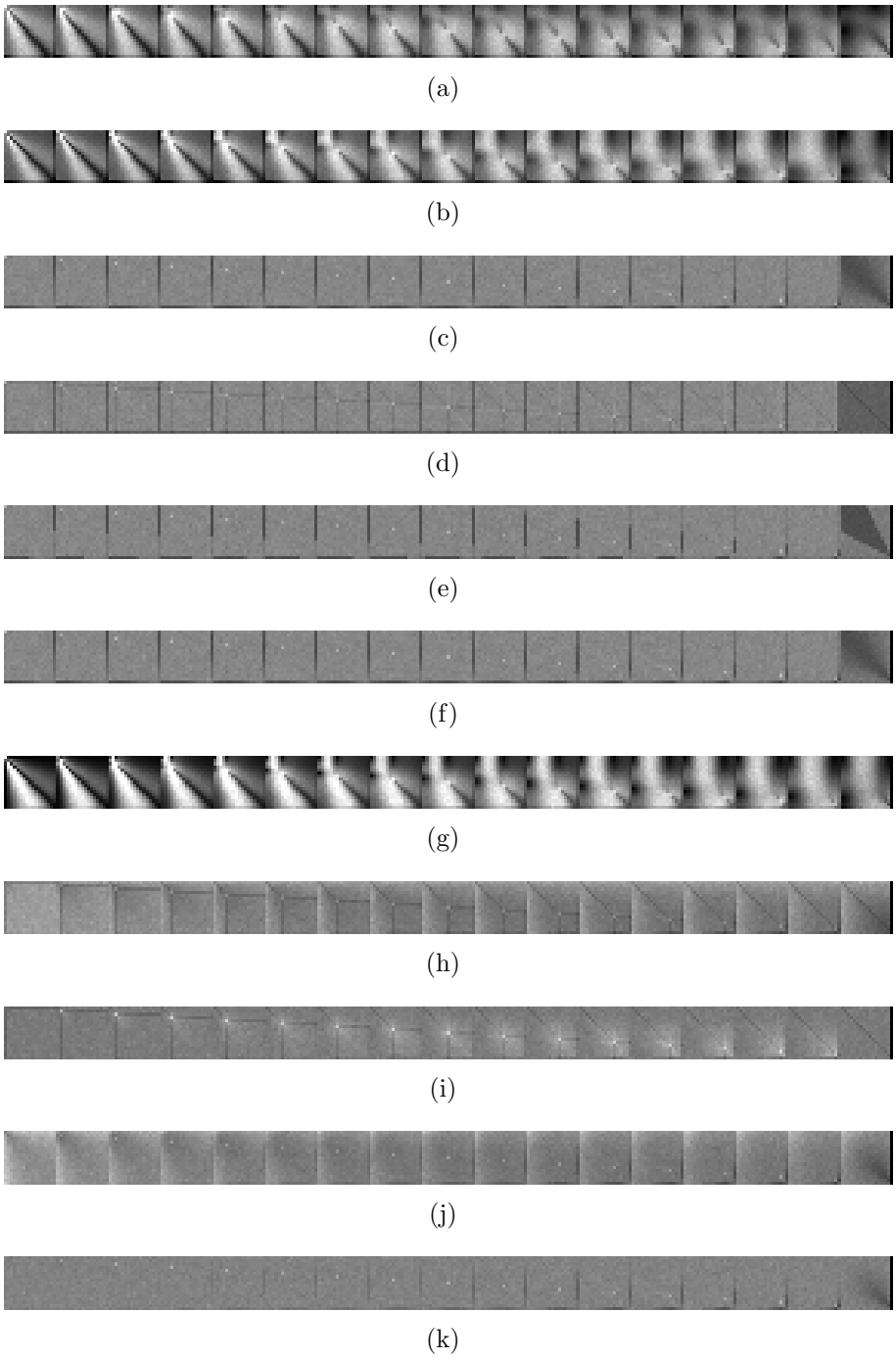

Figure 5.23: The normalised standard deviations for each pixel of the source image using the saturation measures weighted using MWCC, (a) LCH_{lab}, (b) LCH_{luv}, (c) HSI, (d) Max-Min, (e) L1 norm, (f) L2 norm, (g) LSH_{luv}, (h) HLS, (i) HSV, (j) PHLS and (k) SHLS (flat grey indicates no variation in noise while visible changes in pixel brightness indicates variation of noise).

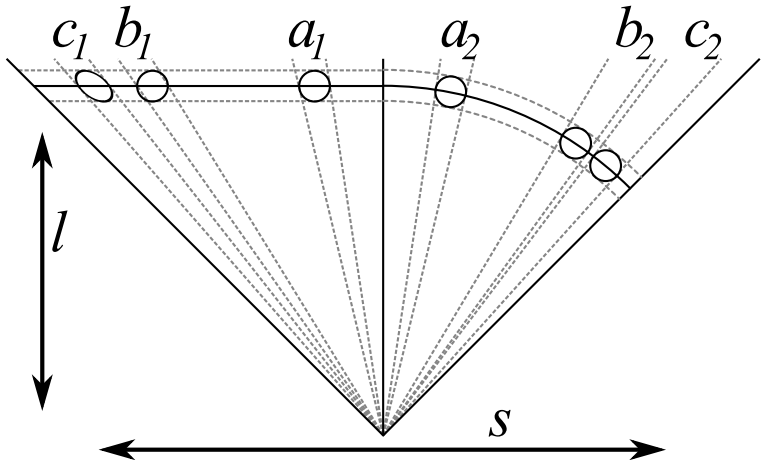

Figure 5.24: The source of non-linearity in planar polar colour models. a_1 and b_1 show the differences from low to high saturations with c_1 showing the actual elliptical region calculated. a_2, b_2 and c_2 show how all of these are equal when using a spherical model.

5.2.4 Non-Polar Models

This section investigates how the invariant colour components hue, luminance and saturation compare to colour components that are not invariant or are only shadow/shading invariant. Figure 5.25 shows the noise distributions measured from the three colour components next to widely used colour models. It is worth noting that the RGB colour model has the best three scores as expected, given this is the source colour model and any transformations from this would only decrease linearity. From this we can gather that the opponent colour model (OOO) performs very well, due to the fact that it is simply a rotation of the RGB colour model. Likewise with the YUV colour model which is also a rotation and distortion aligned to human brightness perception. The only model shown which is shadow/shading invariant but not specular highlight invariant is the nRGB colour model which does not perform well, due to the non-linearity pointed out in the previous section. The CIE colour models perform much worse, the results for the CIE XYZ components suggesting why the other CIE transformations do not perform well, as CIE XYZ is the base model for all of the other CIE models. Figure 5.26 shows the same data but grouped together with the respective colour

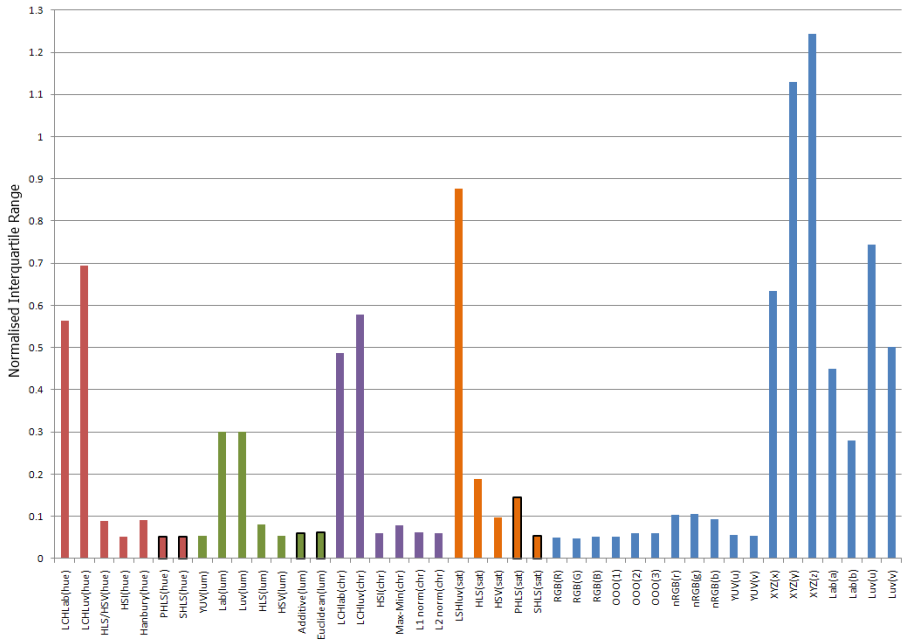

Figure 5.25: Normalised interquartile range of image noise standard deviation for each of the hue, luminance, chroma, purity and non-polar measures.

models. The CIE colour models have been removed in this case to allow for a better view of the data. All of the models have been ordered with Component 1 being hue, Component 2 being luminance and Component 3 being saturation where ever possible. The first four colour models are invariant to specular highlights but not shadow/shading and the last four are either non-invariant or invariant to shadow/shading. Of all of the invariant colour models SHLS performs the best overall and a 30.6% improvement on the next best shadow/shading/specular invariant colour model.

5.3 Pixel Classification

In this section the linearity functions derived in section 5.1 are brought together with the colour models analysed in section 5.3 for pixel classification in real video from a camera. In this video, eight plasticine coloured objects with varying shades and specularities are placed and subsequently classified using each component of each colour model. The aim of this is to determine the

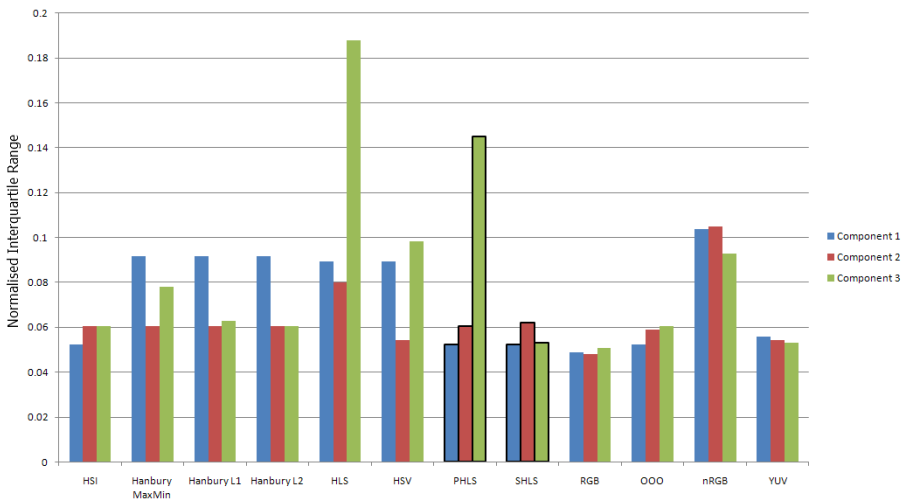

Figure 5.26: Normalised interquartile range of image noise standard deviation for each of the colour models (excluding the CIE colour models).

smallest threshold necessary for each colour component to correctly classify 95% of all eight objects with the minimal waste.

In this experiment we define waste as the difference between the largest and the smallest of the individual object thresholds normalised by the average of all of the thresholds. This metric equates to the proportion of the colour component that would be wasted when classifying an object with the least noise and when using the minimum threshold that will classify all eight of the objects. In this way, an ideal colour component which is uniform across the entire axis would calculate this number to be zero as there would be no difference between the largest and smallest thresholds. Figure 5.27 shows the minimum 95% threshold for each colour object divided by the average of all eight for both the HLS/HSV hue component and for the SHLS hue component. These thresholds represent the variation for that component over the object which could be caused by signal noise or shifts due to shadow, shading, specular highlights and other effects. The best performing colour components have very little difference between the thresholds needed representing the least amount of waste to classify all eight objects. In this case, the thresholds for the SHLS hue component are very close together, indicating a highly linear space with minimal waste.

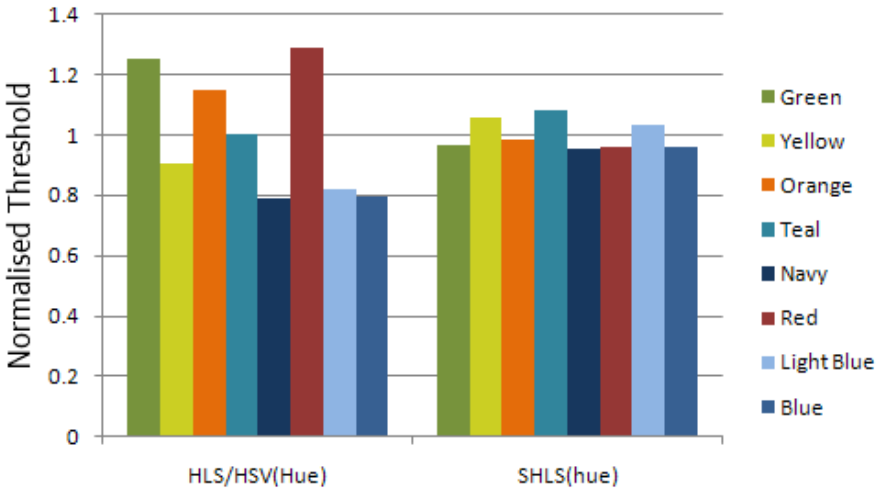

Figure 5.27: The normalised minimum 95% threshold for each colour object using the HLS/HSV hue and the SHLS hue measure.

5.3.1 Hue Components

Hue is the most important component in this experiment because it is invariant to shadow, shading and specular highlights, all of which exist on the objects being classified in the video. This indicates that a successful hue measure will have the lowest threshold range of any of the other components as hue does not vary from any of these lighting effects. Figure 5.28 shows how each of the hue measures perform, showing both results when transforming from both RGB and the proposed SLRGB. In all cases the use of SLRGB reduced the variation of the calculated thresholds with the largest improvements in the HSI, PHLS and SHLS colour models. This is because the white balancing used by these methods preserves signal linearity as it rotates the colour space rather than scaling each colour component by the corresponding component of the white vector. Unlike the previous experiment where white balancing was not necessary, the difference this makes is more apparent. The best two measures of hue were HSI and SHLS in this experiment.

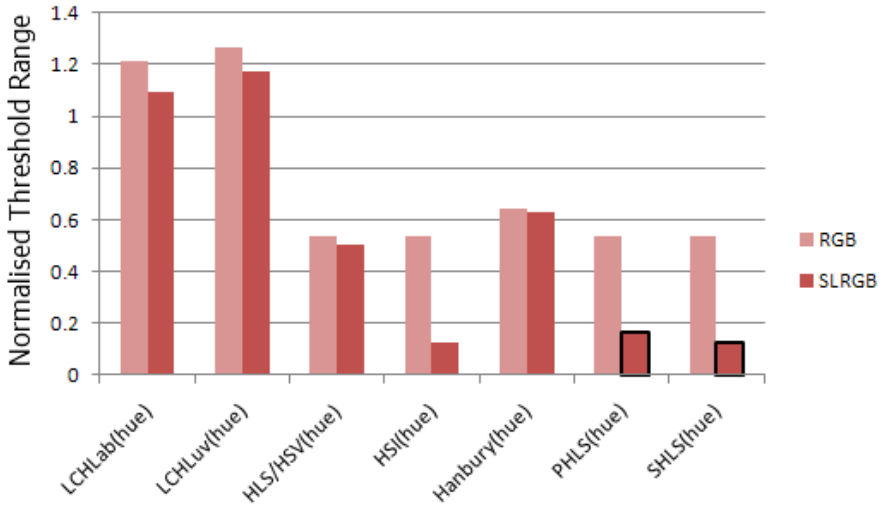

Figure 5.28: Comparison of normalised threshold range for each of the hue measures.

5.3.2 Luminance Components

The luminance component measures of threshold variation have the least importance in this experiment because each individual object will have a different brightness range depending on the reflectance properties of the surface and the shape of the object. As the relationship between the objects colour and the observed colour is multiplicative with the power of the source light, brighter colours will tend to have much wider ranges.

Figure 5.29 shows how these different brightness measures compare to each other. Between different measures of illumination there is relatively little difference between the threshold variations of each. Also there is very little difference between using the RGB and SLRGB colour models because the variation between object luminance distributions is large enough that linearity does not have a significant impact. This suggests that when it comes to colour classification which measure of brightness is relatively unimportant although there are a few other motivations that might be considered when selecting a luminance measure.

The Euclidean luminance component used in the SHLS colour model measures changes in illumination along a vector which matches the direction

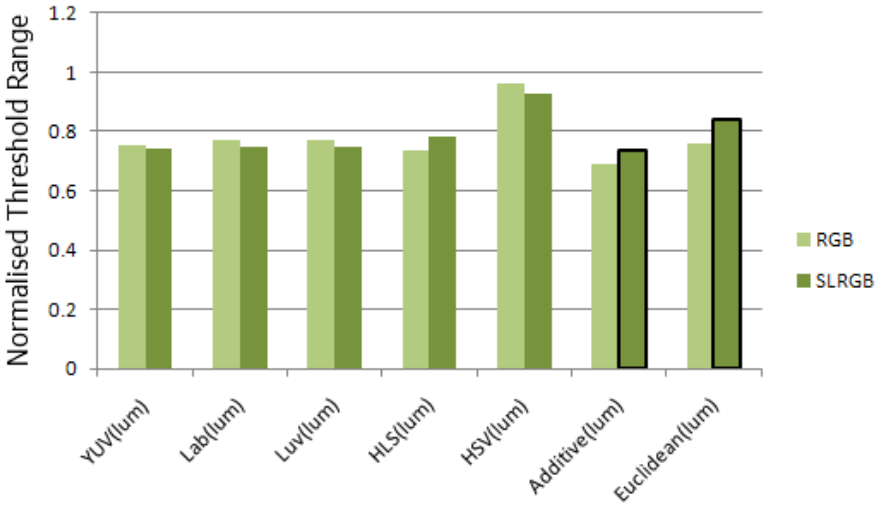

Figure 5.29: Comparison of normalised threshold range for each of the luminance measures.

of the brightness transformation undergone by the object. This makes the Euclidean measure more ideal for measuring luminance changes within an object, such as for internal edges. Additive, HSV and HLS measures have the advantage of reduced computational complexity if performance is an important issue. The YUV, Lab and Luv luminances are useful when taking human factors into consideration and if differences that would be detected by people are the most important. Of these YUV is probably the most suitable if the preservation of signal linearity is to be maintained since the Lab and Luv luminance measures did not perform well in the previous experiment, as shown in Figure 5.19.

5.3.3 Saturation Components

The saturation component measures of threshold variation are useful, however there are some confounding factors which make them not ideal. Because the objects analysed are not free of specular reflection, the purity components will drop when these kinds of reflections occur. Specular reflection is often unrelated to the diffuse reflection properties of an object and is caused more by attributes of the surface which are often called gloss or shine. Because

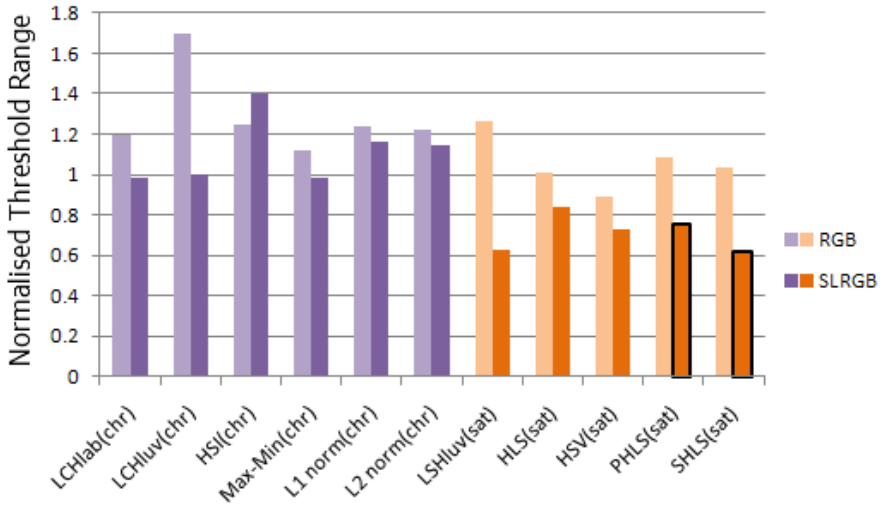

Figure 5.30: Comparison of normalised threshold range for each of the chroma (in purple) and purity (in orange) measures.

all of the objects being analysed are made from plasticine, these surface attributes are kept relatively consistent between objects. This however does not account for other more subtle differences, such as those relating to any impressed textures on the soft surface, or differences in the shape produced.

Figure 5.30 shows how these saturation measures compare to each other, with all of the chroma measures shown in purple on the left and purity measures in orange on the right. There is a clear overall difference between the results for the chroma measures and those measuring purity, with all of the purity measures outperforming chroma measures when SLRGB is used. This is a reversal of the results from the previous experiment shown in Figure 5.22 where chroma measures performed better overall. The reason for this outcome is because this experiment uses real images and complete objects which have varying brightnesses and not just local pixel noise on a single colour. Chroma measures do not match these real illumination effects and so are not suited to this kind of task. A chroma threshold will also be much wider relative to the bounds of the component because of this lack of shadow/shading invariance.

Of the saturation measures, the best performance was achieved from the

LSH_{luv} and the proposed SHLS saturation components. However, due to the large variations in linearity found in the previous experiment, shown in Figure 5.23(g), it is unlikely this performance would be maintained over the whole space. The PHLS saturation component is a little worse than the SHLS counterpart. This could be because of the inherent non-linearity identified in the previous experiment which would cause more saturated objects to exhibit more noise. Also of note is the lack of difference between the measures that use rotational white balancing as opposed to channel scaling. Suggesting that for this component, local noise had less of a contribution to the results, while the ability of the measure to match colour shifts was more important. Specular highlights cause large shifts in the colour towards white, contributing much more difference between objects than signal noise.

5.3.4 Non-Polar Models

This section takes a look at how the invariant colour components hue, luminance and saturation compare to colour components that are not invariant or are only shadow/shading invariant. Figure 5.31 shows the threshold variation results, showing the results for the three colour components next to widely used prior colour models. It shows that the hue measures of HSI and the proposed PHLS and SHLS are much more uniform than any other measure. Figure 5.32 shows this information again with each of the colour models grouped with the results for each of their respective components. This graph only shows the information from the SLRGB case as it showed an improvement overall for almost all of the colour models. The only colour model this was not the case for was the CIE XYZ colour model, but this colour model is the first step when converting to all of the other CIE colour models which saw improvement when using the SLRGB colour model. From this graph we can see that the proposed PHLS and SHLS colour models overall have the least variation of thresholds when classifying a range of different colours. While HSI performs well with hue and luminance the chroma measure it uses is much worse, coupled with the fact that it is not shadow/shading invariant. The nRGB colour model also performs well being the only shadow/shading invariant colour model that does not use a polar coordinate system. This

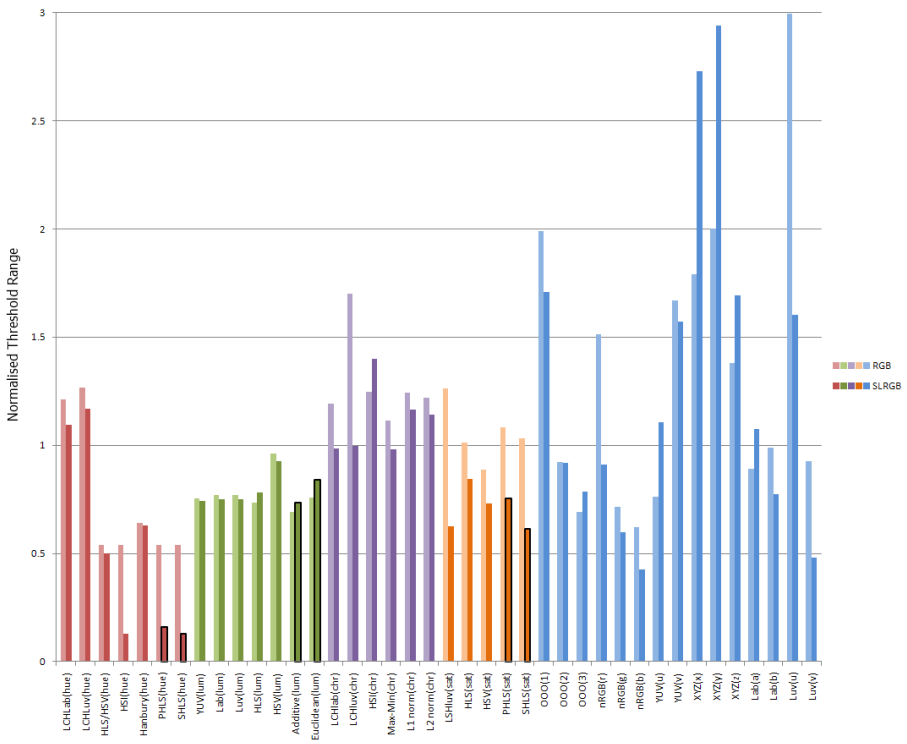

Figure 5.31: Comparison of normalised threshold range for each of the hue, luminance, chroma, purity and non-polar measures.

version also uses MWCC to counter the shift in scale as luminance increases, even though nRGB is the only shadow/shading invariant colour model not to have a luminance component included, although if it were to include one it would be the additive measure.

Using the data gathered from the experiment, the colour models were able to be evaluated further for their discriminative power. The previous variation of thresholds metric provided an insight into how much of the component space was wasted when classifying every colour with a consistent threshold. It does not however indicate how much of the available colour space was required to classify all of these colours. The combination of the three thresholds and an average colour for a component results in a volume which takes up some of the available colour space. The larger this volume is, the more likely it is that volumes containing other colour objects will overlap. This follows on to reason that with larger volumes, less colours can be

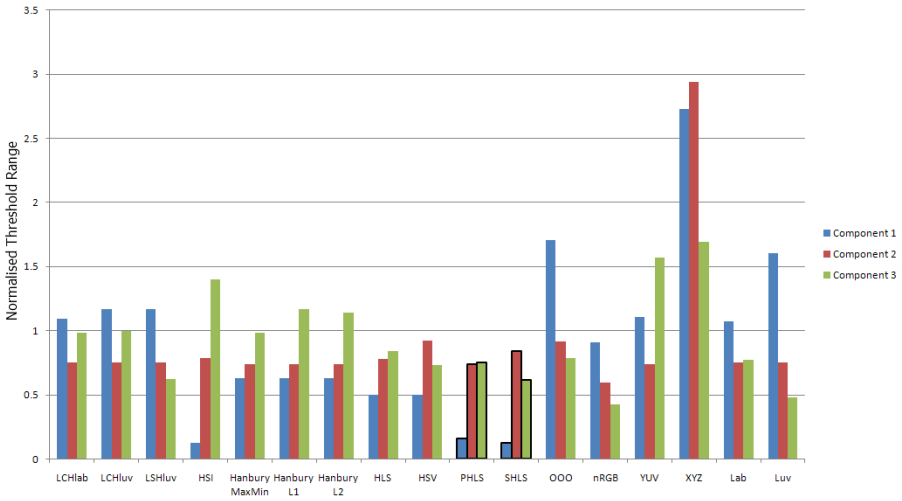

Figure 5.32: Comparison of normalised threshold range for each of the colour models using SLRGB.

classified accurately and need to be spaced further apart. Therefore, the size of this volume important when considering which colour model is best when classifying colour.

To measure this for each colour model, the palette image from a previous experiment shown in Figure 4.2 was classified using the thresholds centred around the average colour for each object. In this way, all colour models used the same averages that the thresholds were originally derived from, while using the widest of the thresholds calculated for each object. What this produces is a binary image describing for each pixel whether or not it was classified as one of the eight objects. As this image contains colours evenly distributed over the available RGB colour space, the proportion of classified pixels relative to the total number of pixels is a close approximation of the volume of the RGB space required for classification for each colour space.

Figure 5.33 shows the percentage of the source RGB colour space that each of the derived colour models occupy when classifying all eight coloured objects. In particular this graph shows the difference that using MWCC makes when classifying colours, with every colour space that can use it seeing a reduction in the total volume used. In all cases the space required dropped by more than 48%, and for the proposed models, PHLS and SHLS, dropped

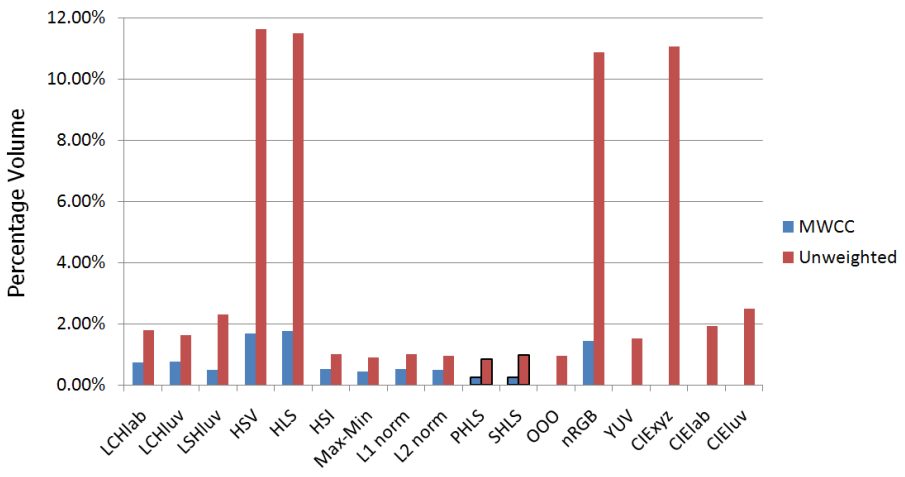

Figure 5.33: Percentage volume of the source RGB colour space used to classify all eight coloured objects with and without MWCC.

significantly more by 69% and 74% respectively.

Figure 5.34 shows only the MWCC data, sorted from the smallest volume to the largest. When viewed this way it can be seen that the two proposed models PHLS and SHLS at 0.26% and 0.25% respectively both perform much better than the next closest model, being one of Hanbury's proposed cylindrical colour models using the Max-Min chroma measure at 0.45%. The Max-Min, LSH_{Luv}, L2 norm, HSI and L1 norm models make up the second group of models, using approximately twice as much space as the proposed models. Only one in this group, LSH_{Luv} has a shadow/shading invariant chromatic plane, while the other three (nRGB, HSV and HLS) performed the worst.

By occupying less of the available colour space to classify colour objects, the proposed colour models have greater discriminative power when differentiating between colours. It does this by essentially shrinking areas of increased noise so that their noise levels are comparable to low noise areas. This allows thresholds to be reduced resulting in less waste when classifying areas of low noise which normally would use the higher tolerances required for high noise areas. In a tracking problem this may be the difference between a moving object becoming untrackable over a similarly coloured background, or detecting a camouflaged animal in a detailed forest scene. Figures 5.35, 5.36

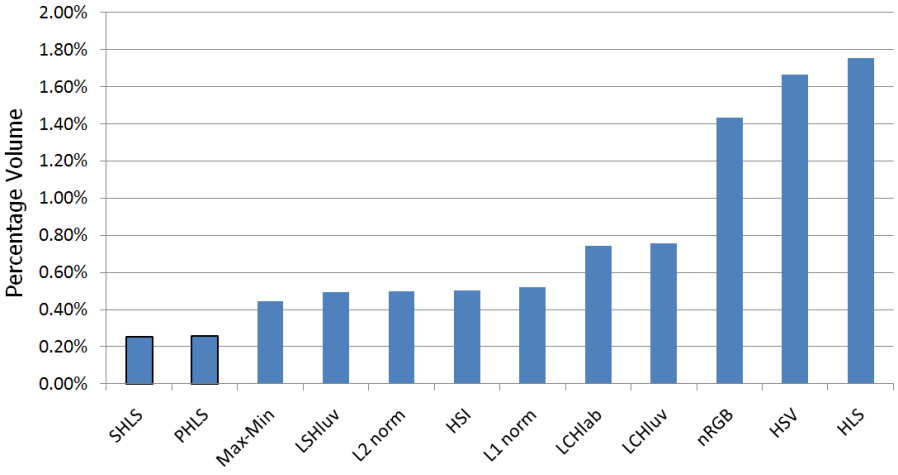

Figure 5.34: Ordered percentage volume of the source RGB colour space used to classify all eight coloured objects with MWCC.

and 5.37 show this in practice. Using the original video of the eight coloured objects, these images show the classification results when the largest of the eight thresholds are used. In the images, any white pixels are due to multiple objects being classified to that pixel. Accordingly, images with less white pixels have less overlapping thresholds between objects. The best three colour models were HSI shown in Figure 5.35(c), PHLS shown in Figure 5.37(d) and SHLS shown in Figure 5.37(e). These show that the proposed PHLS and SHLS colour models classifies the objects just as well as the HSI colour model while using half of the colour space volume to do it.

5.3.5 Gamut Limit Invariance

In this section the effect of using the proposed Gamut Limit Invariant (GLI) colour model with the proposed PHLS and SHLS colour models. The GLI colour model estimates the correct values for hue and saturation when the true colours are out of gamut. Typically gamut clipping causes colours to change from their original hue and saturations, making tasks such as pixel classification problematic. To measure the improvements when using this, the methodology of the pixel classification experiment is used but is done at multiple levels of camera gain. This brightens the image within the camera,

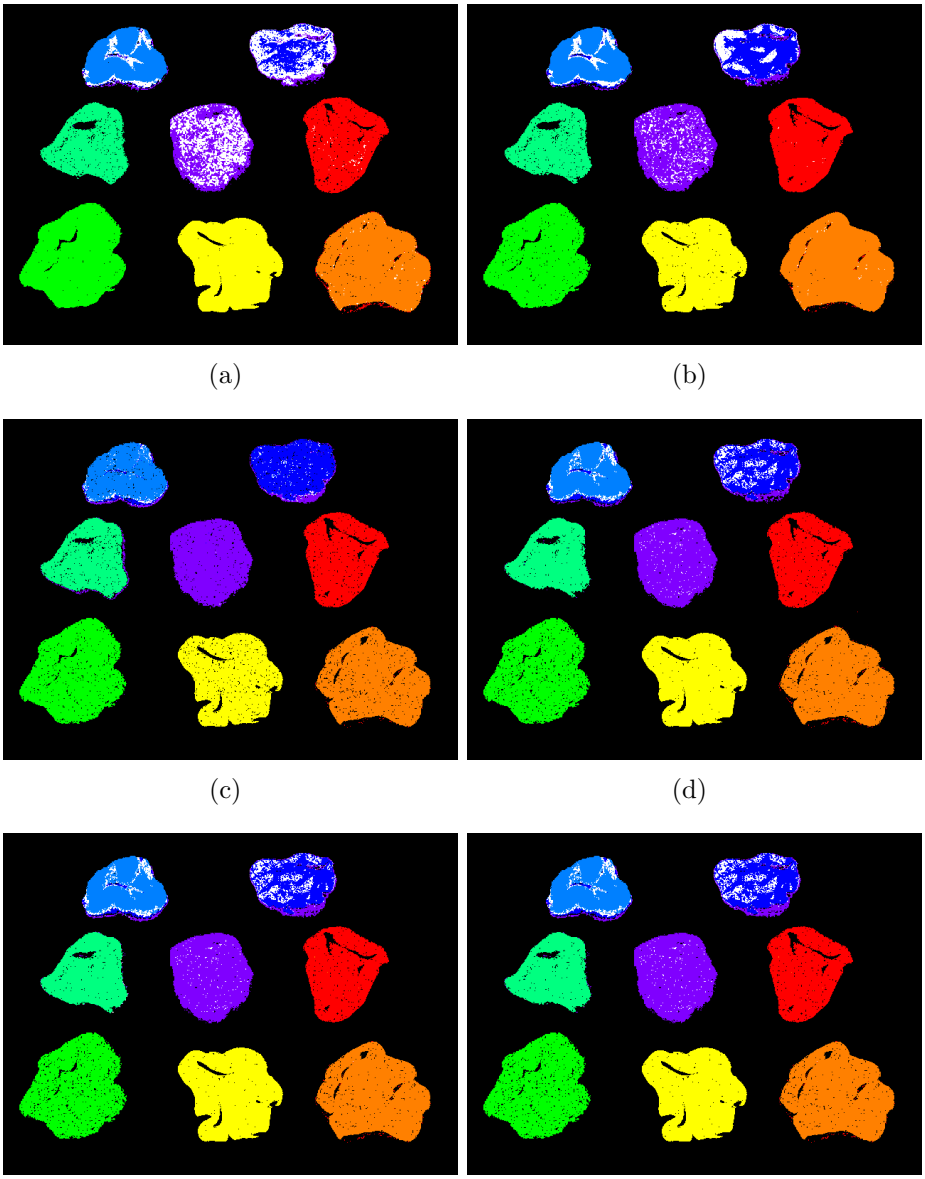

(a) (b) (c) (d) (e) (f)

Figure 5.35: Complete pixel classification using the widest threshold for all objects with chroma based models. Black pixels denote no classification and white pixels denote multiple objects classified. (a) LCH_{lab}, (b) LCH_{luv}, (c) HSI, (d) Max-Min, (e) L1 norm and (f) L2 norm.

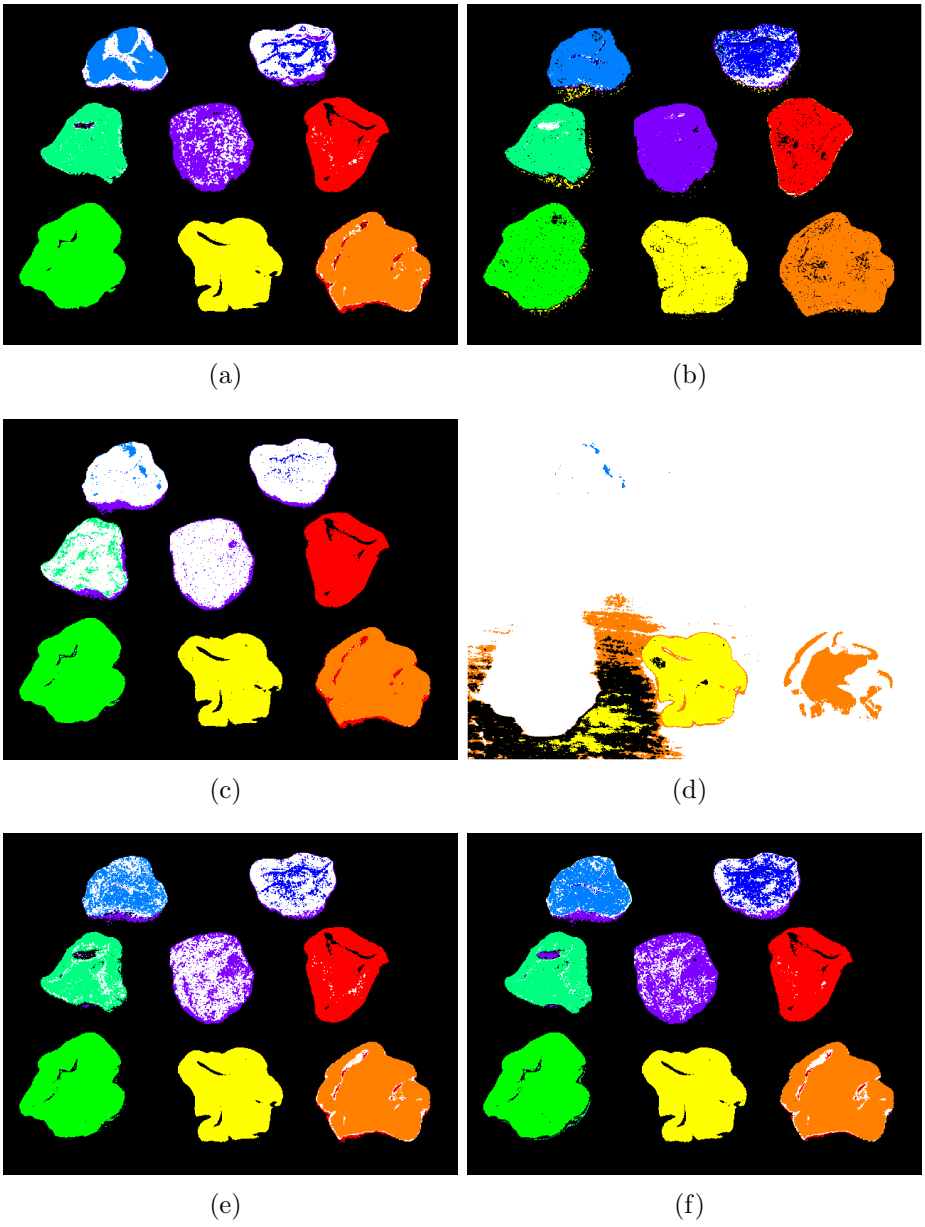

(a) (b) (c) (d) (e) (f)

Figure 5.36: Complete pixel classification using the widest threshold for all objects with non-polar models. Black pixels denote no classification and white pixels denote multiple objects classified. (a) OOO, (b) nRGB, (c) YUV, (d) CIEXYZ, (e) CIELab and (f) CIELuv.

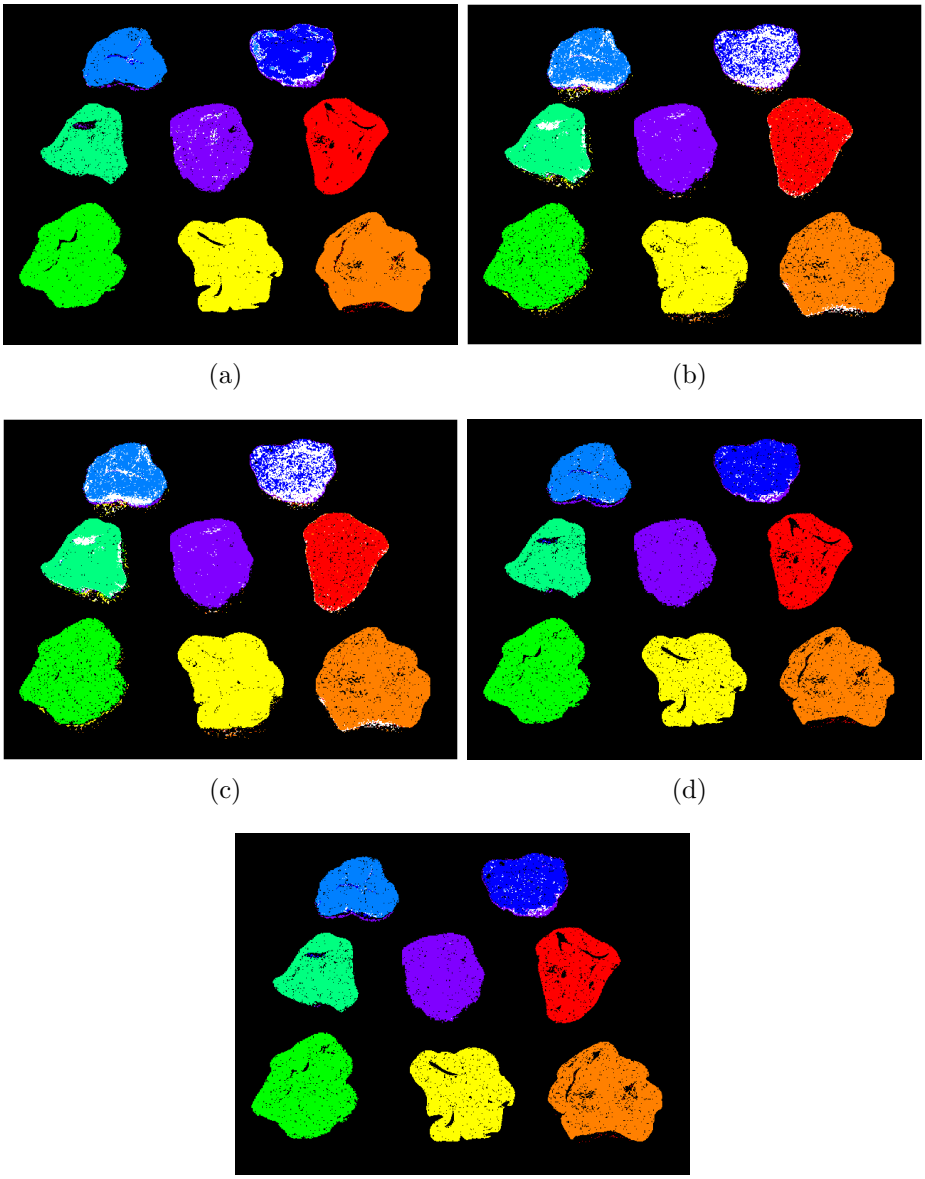

(a) (b) (c) (d) (e)

Figure 5.37: Complete pixel classification using the widest threshold for all objects with purity based models. Black pixels denote no classification and white pixels denote multiple objects classified. (a) LSH_{luv}, (b) HSV, (c) HLS, (d) PHLS and (e) SHLS.

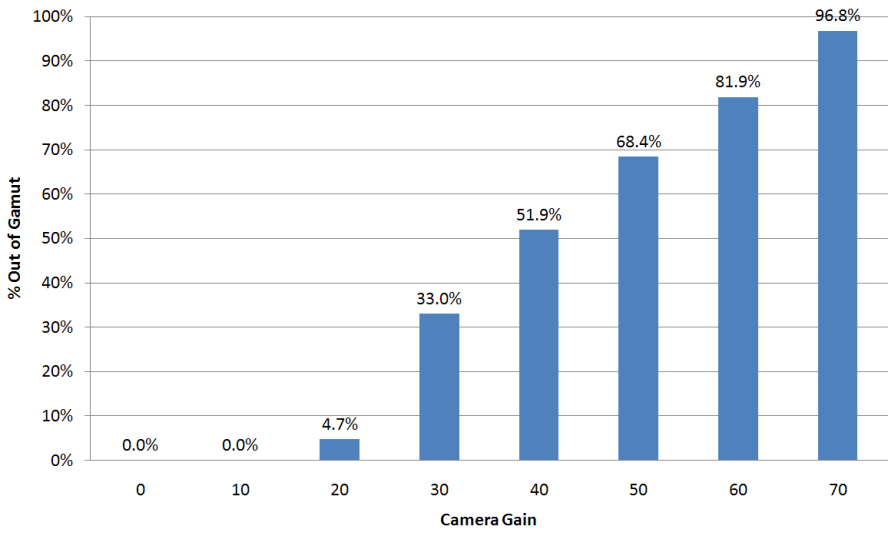

Figure 5.38: Percentage of the classification regions at the limits of the gamut at each camera gain setting.

with the brightest pixels being clipped to fit in to the 24 bit RGB space. Figure 5.38 shows the percentage of the masked classification region that is at the limits of the gamut for each camera gain setting. This covers a large range, ranging from no clipping and very little clipping to almost every pixel clipped by the gamut.

The results showed a reduction in the thresholds required for both hue and saturation when GLI was used with PHLS and SHLS. Figure 5.39 shows the percentage reduction in total threshold size when using GLI for all eight classification colours. At the first two camera gain settings there is no change in the thresholds used as there are no pixels classified which have been clipped by the limited gamut. This shows the greatest improvements for the hue measures, with the level of improvement showing a similar trend to the gamut figures. The saturation measures do not perform as well or as consistently but always show an improvement, with the SHLS measure performing much better than PHLS at two of the gain levels.

Figure 5.40 shows a comparison between the normalised total thresholds with and without GLI for the hue measures of PHLS and SHLS. While the standard colour models show increased thresholds when the number of out

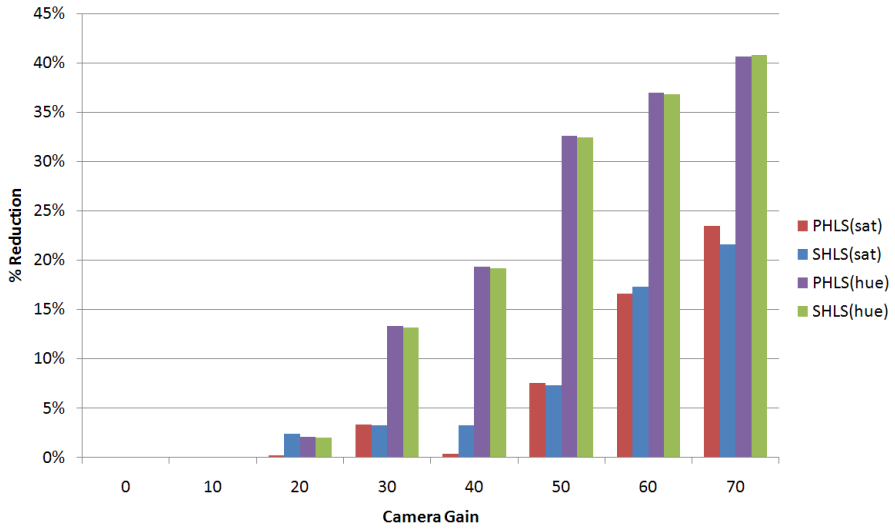

Figure 5.39: Percentage reduction in total threshold size when using GLI for all eight classification colours.

of gamut pixels is increased, using GLI these thresholds deviate to a much lower degree. The drop in thresholds at the camera gain level of 70 is likely due to 96.8% of classified pixels being out of gamut as shown in Figure 5.38. At this level, many of the objects will be completely out of gamut being classified using only these colours, reducing some of the width required for a threshold.

Figure 5.41 shows a comparison between the normalised total thresholds with and without GLI for the saturation measures of PHLS and SHLS. These improvements are much more marginal, because of the much more hue-centric approach used when calculating GLI colour differences.

5.4 Summary of Results

The results presented in this chapter have shown consistently that the proposed techniques and models have performed consistently better in most circumstances or on par than with those currently available. The SLRGB colour model linearises the signal noise present in the camera even under changes to the camera settings of white balance, exposure and gain. This linear model has shown to improve results of the pixel classification experiment for almost

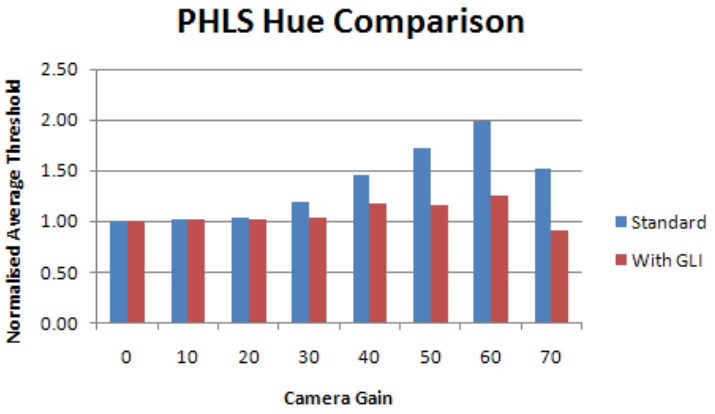

(a)

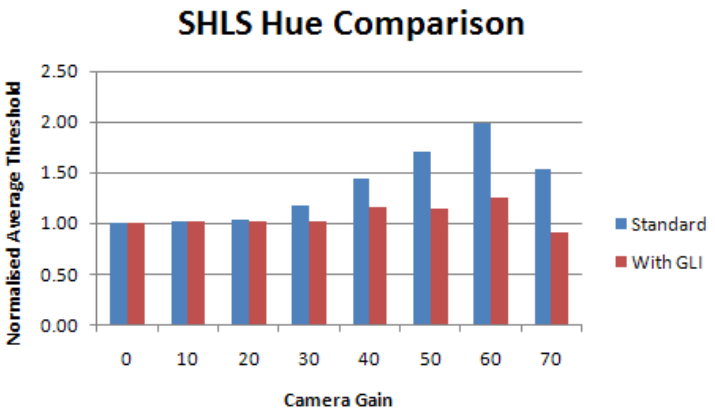

(b)

Figure 5.40: Comparison between the normalised total thresholds with and without GLI for hue measures of (a) PHLS and (b) SHLS.

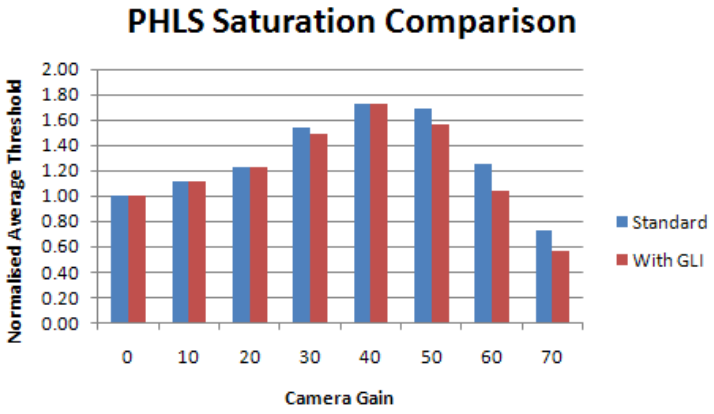

(a)

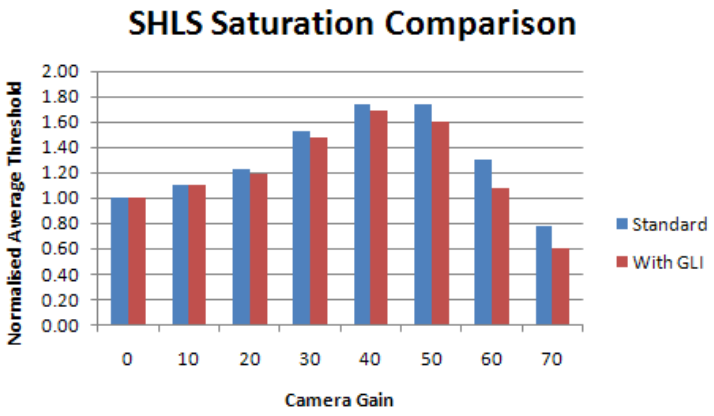

(b)

Figure 5.41: Comparison between the normalised total thresholds with and without GLI for saturation measures of (a) PHLS and (b) SHLS.

all colour models.

Similarly the MWCC technique has shown to unanimously improve results in the transformation linearity experiment, providing significant improvements to colour comparisons in purity based and/or polar based colour models. It was also shown that it greatly reduces the volume of the colour space required for successful classification.

The PHLS colour model while found to be not completely linear in the transformation linearity experiment, performed strongly when used for pixel classification. The SHLS colour model remained competitive in every experiment, performing as well as or much better than every other model, most of which do not share its feature set. The GLI colour model adds gamut limit invariance to the PHLS and SHLS colour models and was shown to improve classification results when pixels became clipped by the gamut.

Table 5.1 shows a summary of all of the colour models tested in the transformation linearity and pixel classification experiments, comparing their features. Object linearity describes the results of the pixel classification experiment and the ability of the colour model to classify an object with linear thresholds.

Table 5.1: Colour model features

Measure	Shadow, Shading	Specular Highlights	Shadow, Shading & Specular	Transformation Linearity	White Balance Linearity	Object Linearity	Gamut Limit Invariance
RGB	-	-	-	✓	-	-	-
Opponent(OOO)	-	-	-	✓	-	-	-
nRGB	✓	-	-	-	-	-	-
YUV	-	-	-	✓	-	-	-
CIE XYZ	-	-	-	-	-	-	-
CIE Lab	-	-	-	-	-	-	-
CIE Luv	-	-	-	-	-	-	-
LCH_{Lab}	-	✓	✓	-	-	-	-
LCH_{Luv}	-	✓	✓	-	-	-	-
HSI	-	✓	✓	✓	✓	-	-
Hanbury MaxMin	-	✓	✓	-	-	-	-
Hanbury L1	-	✓	✓	-	-	-	-
Hanbury L2	-	✓	✓	-	-	-	-
LSH_{Luv}	✓	✓	✓	-	-	-	-
HLS	✓	✓	✓	-	-	-	-
HSV	✓	✓	✓	-	-	-	-
PHLS	✓	✓	✓	-	✓	✓	-
SHLS	✓	✓	✓	✓	✓	✓	-
PHLS + GLI	✓	✓	✓	-	✓	✓	✓
SHLS + GLI	✓	✓	✓	✓	✓	✓	✓

Chapter 6

Conclusion

The results show that the proposed colour models outperformed all prior colour models in achieving the goal of this research which was to enable the most accurate information possible for processing colour images by maintaining uniform signal noise and decorrelating dimensions to the reflective properties of light.

The Signal Linear Red Green Blue (SLRGB) colour model exhibited uniform noise across the space even under changes of camera settings. The model is derived for an individual camera and its success evaluated, consistently providing improvements to colour models utilising it.

The Planar Hue Luminance Saturation (PHLS) colour model demonstrated a relatively low computational cost polar colour model invariant to shadow, shading and specular highlights, with near linear axes. The combination of some of the best elements of the HLS, HSI and nRGB colour models, this model is evaluated and is a strong improvement on other colour models. Requiring the second lowest volume of colour space (to the proposed SHLS model) for complete object classification, it is determined to have better discriminative power than any previous model.

The Spherical Hue Luminance Saturation (SHLS) colour model is a polar colour model invariant to shadow, shading and specular highlights, with strongly linear axes. Using a spherical coordinate system, the model consistently outperforms the other invariant colour models on linearity and performing strongly against less invariant models. Requiring the lowest volume of colour space for complete object classification, it is determined to have better discriminative power than any other model, using almost half as much colour space as the next best non-proposed model.

The Minimum Weighted Colour Comparison (MWCC) technique is a

method of comparing colours represented in models with converging axes. This has been shown to greatly improve linearity for comparisons in hue and purity based saturation measures, with significant reductions in the amount of colour space required to classify the test objects in all cases.

The Gamut Limit Invariant (GLI) colour model, a novel colour model used to estimate the possible true values of a colour that has been clipped by a limited gamut. This model has been shown to provide some improvement in pixel classification when significant portions of the image exceed gamut limitations.

A set of novel experimental methodologies were presented that can be used to measure important aspects of colour models such as linearity, allowing comparison between colour models with different scales and limits.

The primary emphasis of this thesis has been on acquiring the most information possible when processing colour images. The approach that was taken was not to enhance the data in any way but to transform the data such that important information would be inherent, especially when comparing colours. This important information falls into two main categories; noise properties and object properties. Making this information inherent in the data involves three key transformations:

- **Signal linearity** makes noise inherent by adjusting the image data so that noise is uniform over the entire space, further extending this by adjusting noise to always have a variance of one unit.

- **Illumination invariance** makes object properties inherent by isolating the effects of light reflection into separate channels of data making light information accessible but independent.

- **Gamut limit invariance** further increases illumination invariance by counteracting colour shifts caused by gamut clipping making object colours identifiable even when some of the colour information is lost.

In this research these key requirements for colour models were identified and discussed, including how current models and solutions meet or fail to meet these requirements. A collection of new colour models and techniques were proposed and evaluated including; the Signal Linear Red Green

Blue (SLRGB) colour model, the Planar Hue Luminance Saturation (PHLS) colour model, the Spherical Hue Luminance Saturation (SHLS) colour model, the Minimum Weighted Colour Comparison (MWCC) and the Gamut Limit Invariance (GLI) colour model.

The results of these evaluations demonstrated that the proposed colour models/methods outperformed all prior colour models:

- **SLRGB** The Signal Linear Red Green Blue colour space is a linearisation of inconsistently noisy RGB data. It is important to achieve the first of the three key transformations, signal linearity. By measuring signal noise at different camera settings, signal noise was modelled as a function of detected intensity and camera white balance, gain and exposure settings. When noise was measured after linearisation it was shown to have an approximately consistent standard deviation of one, even subject to changes of the camera settings. Further experiments demonstrated that this proposed model consistently provided improvements to linearity compared to RGB when used as a basis for other colour models.

- **PHLS and SHLS** The Planar and Spherical Hue Luminance Saturation colour models are new polar representations of colour which achieve the second of the three key transformations, illumination invariance, while unlike previous models, they also maintain the signal linearity achieved by SLRGB.

  The transformation linearity experiment showed that the SHLS colour model was had the least variation in noise across the entire space of all of the polar colour models. When conducting this experiment a non-linearity became apparent in the PHLS saturation measure, causing noise to increase for highly saturated colours. This effect is inherent in all planar purity based chromatic plane colour models, but because the only others are HLS and HSV which are highly non-linear this is not apparent in them.

  The pixel classification experiment showed that the PHLS and SHLS colour models both outperform all of the other tested colour models for

both linearity of required thresholds and total colour space volume used for classification. To successfully classify 95% of pixels for all coloured objects using only one set of thresholds the PHLS and SHLS used only 0.26% and 0.25% of the entire colour volume, with the next best being significantly higher at 0.45%.

The SHLS colour model outperforms the PHLS colour model in almost all experiments, although only usually by a small margin. The saturation measure of PHLS reduces the colour models linearity making it less suitable for vision applications. However the PHLS colour model is computationally simpler making the choice between the two likely dependent on the application.

- **MWCC** The Minimum Weighted Colour Comparison technique used to achieve linear colour comparisons in the PHLS and SHLS colour models can be broadly applied to other colour models with converging axes. The transformation linearity experiment showed that MWCC was to provide significant improvements to linearity when comparing hue values and purity values. Because of these improvements specifically for purity measures allowed them to be compared at the same level as chroma measures which are not susceptible to these shifts in linearity. The pixel classification experiment showed that MWCC also significantly reduces the required volume for classification in all cases.

- **GLI** The Gamut Limit Invariant colour model represents colours so that out of gamut colours can have their possible true values estimated for colour comparisons invariant of the limits of the colour gamut. Tested with different levels of gamut clipping, the GLI colour model reduced the need for wider thresholds when colours are clipped by the gamut. The hue and saturation thresholds required in all cases was reduced, with hue exhibiting the greatest improvements.

6.1 Future Work

This section discusses the future directions for the research presented in this thesis:

- **Camera linearisation utility** This would run through the experiments described to calculate the correct conversion from RGB for a given camera to SLRGB. Other techniques will be utilised such as refining the model as the application runs or using other research to calculate linearity information from still images if necessary. This utility would greatly improve the applicability of the SLRGB colour model making it hardware independent.

- **PHLS, SHLS and GLI conversion optimisations** The proposed colour models were designed with accuracy as the primary motivation. With the colour models now clearly defined, optimisations will be made to increase calculation speed while paying special attention not to lose the important information.

- **GLI colour extrapolation** The GLI colour model allows for out of gamut colours to be estimated based on a matching colour to determine if there is any similarity. An algorithm will be designed to use neighbouring unclipped colours to estimate the true colours of clipped colours. This will result in an image with a larger sensor range than possible with the camera hardware.

References

Agarwal, V., Abidi, B., Koschan, A. and Abidi, M.: 2006, An overview of color constancy algorithms, *Journal of Pattern Recognition Research* **1**(1), 42–54.

Alter, F., Matsushita, Y. and Tang, X.: 2006, An intensity similarity measure in low-light conditions, *in* A. Leonardis, H. Bischof and A. Pinz (eds), *ECCV (4)*, Vol. 3954 of *Lecture Notes in Computer Science*, Springer, pp. 267–280.

Anderson, H., Garcia, E. and Gupta, M.: 2007, Gamut expansion for video and image sets, *Image Analysis and Processing Workshops, International Conference of* **0**, 188–191.

Arend, L. and Reeves, A.: 1986, Simultaneous color constancy, *J. Opt. Soc. Am. A* **3**(10), 1743–1751.

Barnard, K.: 1999, Color constancy with fluorescent surfaces, *IS&T/SID Seventh Color Imaging Conference: Color Science, Systems and Applications*, The Society for Imaging Science and Technology, Springfield, Va., pp. 257–261.

Barnard, K. and Finlayson, G.: 2000, Shadow identification using colour ratios, *in IS&T/SID 8th Colour Imaging Conference: Colour Science, Systems and Appl*, pp. 97–101.

Barnard, K., Finlayson, G. and Funt, B.: 1996, Colour constancy for scenes with varying illumination, *Computer Vision and Image Understanding* **65**, 311–321.

Barnard, K. and Funt, B.: 1999, Investigations into multi-scale retinex, *Color Imaging in Multimedia*, Technology, (Wiley), pp. 9–17.

Berwick, D. and Lee, S. W.: 1998, A chromaticity space for specularity, illumination color- and illumination pose-invariant 3-D object recognition, *Proc. of the Int. Conf. on Computer Vision*, IEEE, pp. 165–170.

Blackwell, K. T. and Buchsbaum, G.: 1988, Quantitative studies of color constancy, *J. Opt. Soc. Am. A* **5**(10), 1772–1780.

Brainard, D. H. and Wandell, B. A.: 1986, Analysis of the retinex theory of color vision, *J. Opt. Soc. Am. A* **3**(10), 1651–1661.

Bruce, J., Balch, T. and Veloso, M.: 2000, Fast and inexpensive color image segmentation for interactive robots, *In Proceedings of IROS-2000*, pp. 2061–2066.

Buck, S. L., Knight, R. F. and Bechtold, J.: 2000, Opponent-color models and the influence of rod signals on the loci of unique hues, *Vision Research* **40**(24), 3333 – 3344.

Chen, H.-C., Chien, W.-J. and Wang, S.-J.: 2004, Contrast-based color image segmentation, *Signal Processing Letters, IEEE* **11**(7), 641–644.

CIE: 1932, *Commission internationale de l'Eclairage proceedings, 1931*, Cambridge University Press, pp. 19–29.

Comaniciu, D. and Meer, P.: 1997, Robust analysis of feature spaces: color image segmentation, *Computer Vision and Pattern Recognition, 1997. Proceedings., 1997 IEEE Computer Society Conference on*, pp. 750 –755.

Demarty, C.-H. and Beucher, S.: 1998, Color segmentation algorithm using an hls transformation, *ISMM '98: Proceedings of the fourth international symposium on Mathematical morphology and its applications to image and signal processing*, Kluwer Academic Publishers, Norwell, MA, USA, pp. 231–238.

Erbay, F., Turgay, E. and Akar, G.: 2011, Color super resolution in HSV domain, *Signal Processing and Communications Applications (SIU), 2011 IEEE 19th Conference on*, pp. 1064 –1067.

Evans, A. N. and Liu, X. U.: 2006, A morphological gradient approach to color edge detection, *IEEE Transactions on Image Processing* **15**(6), 1454–1463.

Femiani, J. and Razdan, A.: 2009, Interval HSV: Extracting ink annotations, *Computer Vision and Pattern Recognition, 2009. CVPR 2009. IEEE Conference on*, pp. 2520 –2527.

Finlayson, G.: 1995, Color constancy in diagonal chromaticity space, *Computer Vision, 1995. Proceedings., Fifth International Conference on*, pp. 218 –223.

Finlayson, G. D., Hordley, S. D. and Drew, M. S.: 2002a, Removing shadows from images, *ECCV '02: Proceedings of the 7th European Conference on Computer Vision-Part IV*, Springer-Verlag, London, UK, pp. 823–836.

Finlayson, G. D., Hordley, S. D. and Drew, M. S.: 2002b, Removing shadows from images using retinex, *Color Imaging Conference*, IS&T - The Society for Imaging Science and Technology, pp. 73–79.

Geusebroek, J., van den Boomgaard, R., Smeulders, A. and Dev, A.: 2000, Color and scale: The spatial structure of color images, *6th European Conference on Computer Vision*, pp. 331–341.

Gevers, T. and Smeulders, A.: 1999, Color-based object recognition, *Pattern Recognition* **32**(3), 453–464.

Gijsenij, A. and Gevers, T.: 2007a, Color constancy by local averaging, *Image Analysis and Processing Workshops, 2007. ICIAPW 2007. 14th International Conference on*, pp. 171–174.

Gijsenij, A. and Gevers, T.: 2007b, Color constancy using image regions, *ICIP*, Vol. 3, pp. 501–504.

Glenn, J. J. and Killian, J. T.: 1940, Trichromatic analysis of the munsell book of color, *J. Opt. Soc. Am.* **30**(12), 609–616.

Guo, H., Guo, P. and Liu, Q.: 2005, Mean shift-based edge detection for color image, *Neural Networks and Brain, 2005. ICNN&B '05. International Conference on*, Vol. 2, pp. 1118–1122.

Hanbury, A.: 2002, The taming of the hue, saturation and brightness colour space, *In Proceedings of the 7th CVWW*, pp. 234–243.

Hanbury, A.: 2008, Constructing cylindrical coordinate colour spaces, *Pattern Recogn. Lett.* **29**(4), 494–500.

Hanbury, A. and Serra, J.: 2001, Mathematical morphology in the HLS colour space, *Proceedings of the British Machine Vision Conference 2001*, BMVA, pp. 451–460.

Hanbury, A. and Serra, J.: 2003, Colour image analysis in 3d-polar coordinates, *Pattern Recognition*, pp. 124–131.

Hill, B., Roger, T. and Vorhagen, F. W.: 1997, Comparative analysis of the quantization of color spaces on the basis of the cielab color-difference formula, *ACM Trans. Graph.* **16**(2), 109–154.

Hordley, S. D.: 2006, Scene illuminant estimation: Past, present, and future, *Color Research & Application* **31**(4), 303–314.

Kelly, K. L., Gibson, K. S. and Nickerson, D.: 1943, Tristimulus specification of the munsell book of color from spectrophotometric measurements, *J. Opt. Soc. Am.* **33**(7), 355–375.

Lam, E.: 2005, Combining gray world and retinex theory for automatic white balance in digital photography, *Consumer Electronics, 2005. (ISCE 2005). Proceedings of the Ninth International Symposium on*, pp. 134 – 139.

Lam, H.-K., Au, O. and Wong, C.-W.: 2004a, Automatic white balancing using adjacent channels adjustment in rgb domain, *Multimedia and Expo, 2004. ICME '04. 2004 IEEE International Conference on*, Vol. 2, pp. 979 –982 Vol.2.

Lam, H.-K., Au, O. and Wong, C.-W.: 2004b, Automatic white balancing using standard deviation of rgb components, *Circuits and Systems, 2004. ISCAS '04. Proceedings of the 2004 International Symposium on*, Vol. 3, pp. III – 921–4 Vol.3.

Lambert, P. and Carron, T.: 1999, Symbolic fusion of luminance-hue-chroma features for regionsegmentation, *Pattern Recognition* **32**(11), 1857–1872.

Larson, G.: 1998, Overcoming gamut and dynamic range limitations in digital images, *Color Imaging Conference, Scottsdale, Arizona*.

Lastra, A., Pretto, A., Tonello, S. and Menegatti, E.: 2007, Robust color-based skin detection for an interactive robot, *AI*IA '07: Proceedings of the 10th Congress of the Italian Association for Artificial Intelligence on AI*IA 2007*, Springer-Verlag, Berlin, Heidelberg, pp. 507–518.

Levkowitz, H. and Herman, G.: 1993, GLHS: A generalized lightness, hue, and saturation color model, *Graphical Models & Image Processing* **55**(4), 271–285.

Lin, J.: 2006, An automatic white balance method based on edge detection, *Consumer Electronics, 2006. ISCE '06. 2006 IEEE Tenth International Symposium on*, pp. 1 –4.

Lin, S., Gu, J., Yamazaki, S. and Shum, H.-Y.: 2004, Radiometric calibration from a single image, *Computer Vision and Pattern Recognition, 2004. CVPR 2004. Proceedings of the 2004 IEEE Computer Society Conference on*, Vol. 2, pp. II–938 – II–945 Vol.2.

Lin, S. and Zhang, L.: 2005, Determining the radiometric response function from a single grayscale image, *Computer Vision and Pattern Recognition, IEEE Computer Society Conference on* **2**, 66–73.

Liu, K.-C. and Chou, C.-H.: 2007, Perceptual contrast estimation for color edge detection, *Systems, Signals and Image Processing, 2007 and 6th*

EURASIP Conference focused on Speech and Image Processing, Multimedia Communications and Services. 14th International Workshop on, pp. 86–89.

Luo, M. R., Cui, G. and Rigg, B.: 2001, The development of the CIE 2000 colour-difference formula: CIEDE2000, *Color Research & Application* **26**(5), 340–350.

Marchant, J. A. and Onyango, C. M.: 2000, Shadow-invariant classification for scenes illuminated by daylight, *J. Opt. Soc. Am. A* **17**(11), 1952–1961.

Matas, J., Marik, R. and Kittler, J.: 1994, Illumination invariant colour recognition, *In Proceedings of the British Machine Vison Conference*, BMVA Press, pp. 469–479.

Matsushita, Y. and Lin, S.: 2007, Radiometric calibration from noise distributions, *CVPR*, pp. 1–8.

Omer, I. and Werman, M.: 2003, Image specific color representation, *Color and Photometric Methods in Computer Vision, IEEE International Workshop on* .

Qian, D., Toker, J. and Bencuya, S.: 1997, An automatic light spectrum compensation method for ccd white balance measurement, *Consumer Electronics, IEEE Transactions on* **43**(2), 216 –220.

Rizzi, A., Gatta, C. and Marini, D.: 2002, Color correction between gray world and white patch, *Human Vision and Electronic Imaging VII* **4662**(1), 367–375.

Shafer, S. A.: 1992, Using color to separate reflection components, *Color* pp. 43–51.

Shafique, K. and Shah, M.: 2004, Estimation of the radiometric response functions of a color camera from differently illuminated images, *in Proceedings of the IEEE International Conference on Image Processing*, pp. 24–27.

Sharma, G. and Trussell, H. J.: 1997, Digital color imaging, *IEEE Transactions on Image Processing* **6**, 901–932.

Sharma, G., Wu, W. and Dalal, E. N.: 2005, The CIEDE2000 color-difference formula: implementation notes, supplementary test data, and mathematical observations, *Color research and application* **30**(1), 21–30.

Shashua, A.: 1997, On photometric issues in 3d visual recognition from a single 2d image, *International Journal of Computer Vision* **21**, 99–122.

Sigal, L., Sclaroff, S. and Athitsos, V.: 2003, Skin color-based video segmentation under time-varying illumination, *IEEE Transactions on Pattern Analysis and Machine Intelligence* **26**, 862–877.

Takamatsu, J. and Matsushita, Y.: 2008, Estimating camera response functions using probabilistic intensity similarity, *Computer Vision and Pattern Recognition, IEEE Computer Society Conference on* **0**, 1–8.

Takamatsu, J., Matsushita, Y. and Ikeuchi, K.: 2008, Estimating radiometric response functions from image noise variance, *European Conference on Computer Vision, In Proceedings of*, pp. IV: 623–637.

Terrillon, J.-C. and Akamatsu, S.: 2000, Comparative performance of different chrominance spaces for color segmentation and detection of human faces in complex scene images, *Proc. of the12th Conf. on Vision Interface (VI '99)*, pp. 180–187.

Terrillon, J.-C., Fukamachi, H., Akamatsu, S. and Shirazi, M. N.: 2000, Comparative performance of different skin chrominance models and chrominance spaces for the automatic detection of human faces in color images, *FG '00: Proceedings of the Fourth IEEE International Conference on*

Automatic Face and Gesture Recognition 2000, IEEE Computer Society, Washington, DC, USA, p. 54.

van de Weijer, J., Gevers, T. and Geusebroek, J.-M.: 2005, Edge and corner detection by photometric quasi-invariants, *IEEE Transactions on Pattern Analysis and Machine Intelligence* **27**(4), 625–630.

van de Weijer, J., Gevers, T. and Smeulders, A.: 2006, Robust photometric invariant features from the color tensor, *IEEE Trans. Image Processing* **15**(1), 118–127.

Yang, C. and Kwok, S.: 2000, Gamut clipping in color image processing, *Image Processing, 2000. Proceedings. 2000 International Conference on*, Vol. 2, pp. 824–827 vol.2.

Zeng, H.: 2005, Color encoding for gamut extension and bit-depth extension, *in* C.-S. Li & M. M. Yeung (ed.), *Society of Photo-Optical Instrumentation Engineers (SPIE) Conference Series*, Vol. 5637 of *Society of Photo-Optical Instrumentation Engineers (SPIE) Conference Series*, pp. 6–13.

Zickler, T., Mallick, S., Kriegman, D. and Belhumeur, P.: 2006, Color subspaces as photometric invariants, *Computer Vision and Pattern Recognition, 2006 IEEE Computer Society Conference on*, Vol. 2, pp. 2000 – 2010.